

CHRISTOPH HEIL, BSc

**Strong Coupling Expansion  
for the Bose-Hubbard  
and the Jaynes-Cummings  
Model**

**MASTER THESIS**

For obtaining the academic degree  
Diplom-Ingenieur

Master Programm of  
Technical Physics



**Technische Universität Graz**

Supervisor:

Univ.-Prof. Dipl.-Phys. Dr.rer.nat. Wolfgang von der Linden  
Institut für Theoretische Physik – Computational Physics

Graz, September 2010



# Abstract

Quantum information theory and quantum computing has attracted a lot of interest in the scientific world recently and one was searching for simple models with whom one can on the one hand, describe the physics easily but on the other hand can use to perform quantum computations.

Two systems that are very interesting in this regard are the Bose-Hubbard model and the Jaynes-Cummings model. The Bose-Hubbard model considers bosons on a lattice of cavities, that can interact with each other and also tunnel from one cavity to the other. The Jaynes-Cummings model takes this thought further and adds to the cavities for the bosons a two-level atomic system at every cavity site. The bosons can therefore not only interact with each other, but also with the two-level atomic systems.

In this work we are going to treat these two systems with the Kato formalism, that promises to be a great method to deal with such physical problems as it uses a diagrammatic approach that can treat such lattice system with extremely low computational efforts compared to other methods. First of all we are going to introduce this new approach with a detailed derivation and also explain how it can be transformed into numerical algorithms to calculate the ground state energy corrections for both systems. Additionally we will also discuss the limitations and possible problems of these algorithms. Actual results obtained with our algorithms will be presented and compared with results from the Variational Cluster Approach.

We are then going to explain how the Kato formalism can be implemented to compute the Mott insulator-superfluid phase boundary for the Bose-Hubbard and the Jaynes-Cummings model.

Additionally, we are also going to introduce a disordered Bose-Hubbard model, for which we will calculate the ground state energy corrections and the Mott insulator-superfluid phase boundary.



# Kurzfassung

Quantum Information Theory und Quantum Computing sind zwei Schlagwörter, die derzeit in der wissenschaftlichen Literatur sehr geläufig sind. Man ist auf der Suche nach Quantensystemen, die sich einerseits leicht beschreiben lassen, sich andererseits aber gut dazu eignen Quanteninformationstheorie und Quantum Computing durchzuführen.

Zwei theoretische Modelle die sich dafür anbieten sind das Bose-Hubbard Modell und das Jaynes-Cummings Modell. Das Bose-Hubbard Modell beschreibt bosonische Teilchen auf einem Gitter aus Bosonenfallen, wobei die Bosonen miteinander wechselwirken und sogar von einer Falle zu einer benachbarten tunneln können. Das Jaynes-Cummings Modell verfolgt diesen Gedanken weiter und führt außerdem ein Zwei-Niveau Atomsystem in jeder Bosonenfalle ein. Somit können die Bosonen nicht nur miteinander interagieren, sondern darüber hinaus noch mit diesen Atomsystemen.

In dieser Arbeit wollen wir diese beiden Modelle mit dem Kato Formalismus untersuchen, der eine hervorragende Methode darstellt, solche physikalische Probleme zu behandeln, da er auf einem diagrammatischen Ansatz beruht mit dem sich solche Gittersysteme mit sehr geringem Rechenaufwand behandeln lassen. Zuerst werden wir die Herleitung dieses Formalismus ausführlich darstellen und außerdem besprechen, wie man ihn numerisch umsetzen kann um die Energiekorrekturen zur Grundzustandsenergie für beide theoretischen Modelle bestimmen zu können. Es werden schließlich Resultate präsentiert, die wir mit unserer Umsetzung des Kato Formalismus erhalten haben und mit Resultaten einer anderen Methode, des Variational Cluster Approaches verglichen.

Als nächstes werden wir besprechen, wie man den Kato Formalismus adaptieren und umschreiben kann, um mit ihm die Phasengrenze zwischen Mottisolator und Suprafluid des Bose-Hubbard und des Jaynes-Cummings Modell zu bestimmen.

Außerdem werden wir Unordnung in das Bose-Hubbard System einführen und wieder diskutieren, wie die Algorithmen adaptiert werden müssen, um die Energiekorrekturen und Phasengrenzen wie zuvor bestimmen zu können.



# Contents

Abstract	iii
Kurzfassung	v
<b>I The Kato Formalism</b>	<b>1</b>
<b>1 The Kato Formalism</b>	<b>3</b>
1.1 Introduction . . . . .	3
1.2 The Greens Function . . . . .	7
1.3 Expansion Series Representations . . . . .	9
1.3.1 Expansion Series Representation of $G(z)$ . . . . .	9
1.3.2 Expansion Series Representation of $\hat{P}$ . . . . .	9
1.3.3 Expansion Series Representation of $\hat{H}\hat{P}$ . . . . .	12
1.3.4 Expressions for the Energy Corrections . . . . .	13
<b>II The Bose-Hubbard Model</b>	<b>17</b>
<b>2 Introduction</b>	<b>19</b>
<b>3 Energy Corrections</b>	<b>21</b>
3.1 Applying the Kato Formalism . . . . .	21
3.2 Graphical Representation . . . . .	22
3.3 Explicit Examples . . . . .	24
3.3.1 Energy Corrections in Second Order . . . . .	24
3.3.2 Energy Corrections in Fourth Order . . . . .	26
<b>4 Numerical Implementation</b>	<b>29</b>
4.1 Constructing the Paths . . . . .	31
4.2 Translational Redundancies . . . . .	33
4.3 Topologically Unique Diagrams . . . . .	36
4.4 Computing the Kato Sequences . . . . .	41
4.5 Assigning the Kato Sequences to Paths . . . . .	43
4.6 Evaluating the Energy . . . . .	44
4.7 Results . . . . .	46

<b>5</b>	<b>Mott Insulator-Superfluid Phase Transition</b>	<b>49</b>
5.1	Introduction . . . . .	49
5.2	Method of Effective Potential . . . . .	50
5.2.1	Power Series Representation . . . . .	52
5.2.2	Developing a Phase Boundary Criterion . . . . .	57
5.3	Consequences for the Kato Formalism . . . . .	61
5.3.1	Changes in the Path Creation and Identification . . . . .	63
5.3.2	Determining $t_c/U$ . . . . .	67
5.3.3	Introducing Disorder to the System . . . . .	74
<b>III</b>	<b>The Jaynes-Cummings Model</b>	<b>81</b>
<b>6</b>	<b>Introduction</b>	<b>83</b>
<b>7</b>	<b>Changes in the Algorithm</b>	<b>89</b>
7.1	Energy Corrections . . . . .	89
7.2	Mott Insulator-Superfluid Phase Transition . . . . .	100
<b>8</b>	<b>Conclusions and Outlook</b>	<b>105</b>
	<b>Acknowledgements</b>	<b>107</b>

**Part I**

**The Kato Formalism**



# Chapter 1

## The Kato Formalism

### 1.1 Introduction

Quantum many-body systems experienced much attention in recent years, because they yield very interesting effects and properties and allow us to improve our knowledge about the quantum mechanical world, which is so different from the world we experience in everyday life. To this end, many different methods have been invented to study such systems, especially at the lower energy range of their spectrum.

#### Density Matrix Renormalization Group (DMRG)

The DMRG was first introduced by [1] in 1992 and is up to this date the method of choice for 1-dimensional quantum systems. Suppose you have a 1-dimensional chain of quantum sites. The Hilbert space of such a system grows exponentially with the size of the chain, it is therefore clear that for large systems a straight forward analytical computation is not feasible. One therefore splits the system in two pieces, which do not need to contain the same amount of sites. Then a trial ground state for the whole system is being suggested, which is then projected into each of the pieces of the chain individually using density matrices. In the subspaces the ground states can now be improved to explain the system better.

The next step is then to extend the first block on costs of the second block and repeat the whole procedure of projecting the new ground state into the two subspaces and so on.

Once the first block has grown to its maximal possible size, the growing procedure is inverted so that the second chain grows on the expense of the first one and so on. This is done until a defined precision has been reached. The DMRG approach has also been extended to be able to treat the time evolution of product matrix states, which are of great interest for quantum computing [2].

### Quantum Monte Carlo (QMC) computations

Another method to deal with the huge Hilbert space of many-body quantum systems is QMC. It is based on the classical Monte Carlo method, that relies on statistics to simulate a system [3]. First of all one needs to define the 'boundaries' of the system, i.e. which variables are to be considered and in what domains are they defined. Secondly, inputs are generated according to a predefined probability distribution and a deterministic simulation of the system is done with these inputs. This is done many times and after each sweep the system is adjusted based on the previous computations until the whole system converges.

QMC now uses the general Monte Carlo method to deal with the multidimensional integrals of a quantum system. With this it is possible to simulate the many-body effects that make the analytical computation of the system's wave function impossible [4].

### Cluster Perturbation Theory (CPT)

The Cluster Perturbation approach is used to treat big quantum systems that are too big for methods like exact diagonalization. The idea behind CPT now is to divide the whole lattice into identical smaller clusters [5, 6]. Then the Greens function is solved for each cluster independently by methods of exact diagonalization, like the Lanczos method for example [7, 8, 9]. The formula for the Greens function, which one gets from CPT, is the lowest order result of a strong coupling perturbation theory. To improve the accuracy of this method one has to consider larger clusters, it does not help to consider higher orders of correction.

### Variational Cluster Approach (VCA)

The Variational Cluster Approach is a further development of CPT. It is a method stemming from the Self Energy Functional Approach (SFA) for fermionic systems [10, 11] that has later been adopted for bosonic systems [12]. This method divides the whole system into smaller clusters too and calculates the Greens function at the stationary point of the grand potential by choosing a variational parameter space [13].

### Kato Formalism

The Kato formalism is quite a unique approach to quantum perturbation theory. In contrast to the Schrödinger-Rayleigh perturbation theory, which is an iterative approach, the Kato formalism provides us with a method to specify specific orders of corrections explicitly, without having to compute all the previous orders of correction [14].

Let's consider a non degenerated system that is composed of an already solved hamiltonian  $\hat{H}_0$  with the eigenstates  $|\psi_i^{(0)}\rangle$  and eigenvalues  $E_i^{(0)}$  and a

perturbation part  $\lambda V$ , where  $\lambda$  is a parameter taking on the values between 0 and 1 and thus determining the strength of the perturbation. With the Schrödinger-Rayleigh approach one first needs to compute the first order energy corrections, which is

$$E_n^{(1)} = \langle \psi_n^{(0)} | V | \psi_n^{(0)} \rangle . \quad (1.1)$$

In other words, the perturbation  $V$  causes the system, that is in the state  $|\psi_i^{(0)}\rangle$  to adopt a higher energy value. Additionally the states  $|\psi_i^{(0)}\rangle$  are, while still being valid quantum states, no longer eigenstates of the whole system due to the perturbation. Therefore, one also has to compute the corrections to the eigenstates, which can be written as

$$|\psi_i^{(1)}\rangle = \sum_{n \neq m} \frac{\langle \psi_n^{(0)} | V | \psi_m^{(0)} \rangle}{E_m^{(0)} - E_n^{(0)}} |\psi_n^{(0)}\rangle . \quad (1.2)$$

With knowledge about the first correction of the eigenstate, we can now calculate the second order energy correction, which looks as follows:

$$E_n^{(2)} = \sum_{n \neq m} \frac{|\langle \psi_n^{(0)} | V | \psi_m^{(0)} \rangle|^2}{E_m^{(0)} - E_n^{(0)}} \quad (1.3)$$

At this point we are able to compute the second order eigenstate correction  $|\psi_i^{(2)}\rangle$ , with which we can then compute the third order energy correction

$$\begin{aligned} E_n^{(3)} = & \sum_{\substack{n \neq m \\ l \neq m}} \frac{\langle \psi_m^{(0)} | V | \psi_n^{(0)} \rangle \langle \psi_n^{(0)} | V | \psi_l^{(0)} \rangle \langle \psi_l^{(0)} | V | \psi_m^{(0)} \rangle}{(E_m^{(0)} - E_n^{(0)}) (E_m^{(0)} - E_l^{(0)})} \\ & - \langle \psi_n^{(0)} | V | \psi_n^{(0)} \rangle \sum_{n \neq m} \frac{|\langle \psi_m^{(0)} | V | \psi_n^{(0)} \rangle|^2}{(E_m^{(0)} - E_n^{(0)})^2} , \end{aligned} \quad (1.4)$$

and so on. But equation (1.4) already shows, that getting to higher order corrections with the Schrödinger-Rayleigh approach is a very tedious endeavor as the work needed increases drastically. Another big disadvantage of this method is, that at higher orders there is a mixing of processes.

Consider a system where bosonic particles 'live' on a regular lattice. In the unperturbed case the particles are confined to their lattice sites, but we can turn on a perturbation that lets the particles hop from one site to another. If you want to treat such a system according to the Schrödinger-Rayleigh perturbation theory the higher orders of the perturbation corrections will consist of processes where different numbers of hopping processes occur on the lattice.

Let's elaborate on this in more detail: Equation (1.1) contains one perturbation term  $V$ , thus there is one hopping taking place, equation (1.3) has

two of these terms, therefor taking into account all perturbations with two hoppings, and so on. But at higher orders it is no longer possible to separate the energy corrections in a way that we have only to consider perturbations with  $n$  hoppings.

This is the point where the Kato formalism gains a huge leverage as it is quite easy to write down any order of correction without having to compute all the previous ones and moreover the  $n^{\text{th}}$  order correction will consist only of perturbation processes with  $n$  hoppings.

In the next few section we will derive the Kato formalism with the general Greens function as a starting point to ensure maximal generality. This derivation is based on [14, 15, 16, 17, 18, 19]. Anyone not directly interested in how one arrives at the determining formulas of the Kato approach can skip this chapter entirely and move on to chapter II, where this new approach is actually being put to work.

## 1.2 The Greens Function

We start out with the Greens function in the complex plane

$$G(z) = \frac{1}{z - \hat{H}}, \quad (1.5)$$

which has poles only along the real axis. For simplicity, we assume a discrete spectrum with eigenstates  $|\psi_i\rangle$ . We therefor have energies  $E_0, E_1, \dots$  and the corresponding projection operators  $\hat{P}_i$  can be written in the following way

$$\hat{P}_i = |\psi_i\rangle\langle\psi_i|. \quad (1.6)$$

The projection operators are orthogonal to each other and the sum of all projection operators has to be 1. In mathematical terms this can be written the following ways

$$\hat{P}_i \hat{P}_j = \delta_{ij} \hat{P}_i \quad (1.7)$$

$$\sum_i \hat{P}_i = \hat{\mathbb{1}}. \quad (1.8)$$

Since  $|\psi_i\rangle$  is an eigenvector of  $\hat{H}$  and  $G(z)$  is a function only dependent on  $\hat{H}$  and  $z$  we can compute the effect of  $\hat{P}_i$  on  $G(z)$

$$G(z) \hat{P}_i = \frac{1}{z - E_i} \hat{P}_i. \quad (1.9)$$

We can therefor construct the function  $G(z)$  by summing over all projection operators, as they span the whole space  $\hat{H}$  is defined on.

$$G(z) = \sum_i G(z) \hat{P}_i \quad (1.10)$$

$$= \sum_i \frac{\hat{P}_i}{z - E_i} \quad (1.11)$$

On the other hand we can describe  $\hat{P}_i$  as a function of  $G(z)$ : Each eigenvalue of  $\hat{H}$  is a simple pole of  $G(z)$  and its residuum is the corresponding projection operator, or rather

$$\hat{P}_i = \frac{1}{2\pi i} \oint_{\Gamma_i} G(z) dz, \quad (1.12)$$

where  $\Gamma_i$  is a closed contour in the complex plane, that includes  $E_i$  and no other eigenvalue of  $\hat{H}$ . Generally speaking, if  $\Gamma$  is a closed contour that contains a couple of eigenvalues but does not touch or 'cross' one, then we

can write it as a sum of the projection operators that belong to the energies enclosed by  $\Gamma$

$$\hat{P}_\Gamma = \frac{1}{2\pi i} \oint_\Gamma G(z) dz \quad (1.13)$$

$$= \sum_{E_i \in \Gamma} \hat{P}_i . \quad (1.14)$$

In other words,  $\hat{P}_\Gamma$  is the projector into the subspace spanned by the eigenvectors corresponding to the eigenvalues included in  $\Gamma$ . Now we want to calculate the effect of  $\hat{P}_\Gamma$  on  $\hat{H}$

$$\hat{H} \hat{P}_\Gamma = \hat{H} \frac{1}{2\pi i} \oint_\Gamma G(z) dz \quad (1.15)$$

$$= \frac{1}{2\pi i} \hat{H} \oint_\Gamma G(z) dz \quad (1.16)$$

$$= \frac{1}{2\pi i} \oint_\Gamma \left( \mathbb{1} + \hat{H} G(z) \right) dz . \quad (1.17)$$

In the last step we used that  $\oint_\Gamma dz = 0$ . Now, according to the definition of  $G(z)$ , as specified in equation (1.5), we have

$$(z - \hat{H})G(z) = \mathbb{1} , \quad (1.18)$$

which can be rewritten to

$$\mathbb{1} + \hat{H}G(z) = zG(z) . \quad (1.19)$$

And finally we can state a closed explicit expression for the effect of  $\hat{P}_\Gamma$  on  $\hat{H}$  in form of a closed contour integral

$$\hat{H} \hat{P}_\Gamma = \frac{1}{2\pi i} \oint_\Gamma zG(z) dz . \quad (1.20)$$

## 1.3 Expansion Series Representations

### 1.3.1 Expansion Series Representation of $G(z)$

We consider a hamiltonian that can be split in two parts. A part  $\hat{H}_0$ , whose eigenvalues can be calculated exactly and a part  $\lambda V$  that represents a perturbation to  $\hat{H}_0$ .

$$\hat{H} = \hat{H}_0 + \lambda V , \quad (1.21)$$

where  $\lambda$  is the usual smallness parameter in Schrödinger perturbation theory. We can therefor write for the complete Greens function

$$G(z) = \frac{1}{z - \hat{H}_0 - \lambda V} , \quad (1.22)$$

but we can also define a Greens function  $G_0(z)$ , that is only a function of the unperturbed hamiltonian

$$G_0(z) = \frac{1}{z - \hat{H}_0} . \quad (1.23)$$

Combining equation (1.22) with equation (1.23) leads to

$$G^{-1} = (G_0^{-1} - \lambda V) \quad (1.24)$$

$$\begin{aligned} G &= (G_0^{-1} - \lambda V)^{-1} \\ &= G_0(\mathbb{1} - \lambda V G_0)^{-1} . \end{aligned} \quad (1.25)$$

Hence we can write  $G$  as a series expansion in powers of  $V$  of the form

$$G = \sum_{n=0}^{\infty} \lambda^n G_0(V G_0)^n . \quad (1.26)$$

### 1.3.2 Expansion Series Representation of $\hat{P}$

Next we determine the power series of  $\hat{P}_a$ , which shall be the projector on an exact eigenstate. According to (1.13) we have

$$\hat{P}_a = \frac{1}{2\pi i} \oint_{\Gamma_a} G(z) dz , \quad (1.27)$$

where  $\Gamma_a$  is a closed contour containing only the energy  $E_a$ . Later on we have given a more precise definition. Inserting the power series of  $G$ , as specified

in equation (1.26) we obtain

$$\hat{P}_a = \frac{1}{2\pi i} \oint_{\Gamma_a} \left( G_0 + \sum_{n=1}^{\infty} \lambda^n G_0 (V G_0)^n \right) dz \quad (1.28)$$

$$= \frac{1}{2\pi i} \oint_{\Gamma_a} G_0 dz + \sum_{n=1}^{\infty} \frac{1}{2\pi i} \oint_{\Gamma_a} \lambda^n G_0 (V G_0)^n dz . \quad (1.29)$$

If  $\Gamma_a$  also contains the unperturbed ground state energy  $E_a^{(0)}$  but no other eigenvalues of  $\hat{H}_0$ , then the first contribution is equal to  $\hat{P}_0$  and we can simplify the expression (1.29)

$$\hat{P}_a = \hat{P}_0 + \sum_{n=1}^{\infty} \frac{1}{2\pi i} \oint_{\Gamma_a} \lambda^n G_0 (V G_0)^n dz . \quad (1.30)$$

To make any progress at this point we first have to take a closer look at the Greens function again. We expand  $G_0(z)$  in a Taylor series about  $z = E_a^{(0)}$ , the unperturbed ground state energy enclosed by the contour  $\Gamma_a$ :

$$\begin{aligned} G_0(z) &= \frac{1}{z - \hat{H}_0} \\ &= \frac{1}{z - \hat{H}_0} \hat{P}_0 + \frac{1}{z - \hat{H}_0} \hat{Q}_0 \\ &= \frac{1}{z - E_a^{(0)}} \hat{P}_0 + \frac{1}{z - \hat{H}_0} \hat{Q}_0 , \end{aligned} \quad (1.31)$$

where we used the abbreviation  $\hat{Q}_0 = \hat{\mathbb{1}} - \hat{P}_0$ . Now we write the factor  $(z - \hat{H}_0)^{-1}$  as a series

$$\begin{aligned} \frac{1}{z - \hat{H}_0} &= \frac{1}{z - E_a^{(0)} + E_a^{(0)} - \hat{H}_0} \\ &= \frac{1}{E_a^{(0)} - \hat{H}_0} \cdot \frac{1}{1 + \frac{z - E_a^{(0)}}{E_a^{(0)} - \hat{H}_0}} \\ &= \frac{1}{E_a^{(0)} - \hat{H}_0} \sum_{k=0}^{\infty} (-1)^k \left( \frac{z - E_a^{(0)}}{E_a^{(0)} - \hat{H}_0} \right)^k \\ &= \sum_{k=1}^{\infty} (-1)^{k-1} \frac{(z - E_a^{(0)})^{k-1}}{(E_a^{(0)} - \hat{H}_0)^k} \end{aligned} \quad (1.32)$$

and insert this expression in equation (1.31)

$$G_0(z) = (z - E_a^{(0)})^{-1} \hat{P}_0 + \sum_{k=1}^{\infty} (-1)^{k-1} \frac{(z - E_a^{(0)})^{k-1}}{(E_a^{(0)} - \hat{H}_0)^k} \hat{Q}_0 . \quad (1.33)$$

Finally this can be squeezed into a more compact expression so that we have a very compact series representation for the unperturbed Greens function:

$$G_0(z) = \sum_{k=0}^{\infty} (-1)^{k-1} (z - E_a^{(0)})^{k-1} S_k \quad (1.34)$$

$$S_k := \begin{cases} -\hat{P}_0 & \text{for } k = 0 \\ \frac{\hat{Q}_0}{(E_a^{(0)} - \hat{H}_0)^k} & \text{otherwise} \end{cases} \quad (1.35)$$

After we have managed to write down a series expansion for  $G_0(z)$  we want to concern ourselves again with the projection operator  $\hat{P}$ . To this end we rewrite equation (1.30)

$$\hat{P} = \hat{P}_0 + \sum_{n=1}^{\infty} \lambda^n A_n \quad (1.36)$$

with the substitution

$$A_n := \frac{1}{2\pi i} \oint_{\Gamma_a} G_0(VG_0)^n dz . \quad (1.37)$$

$\hat{P}_0$  is quite a trivial part in this equation, so in order to break equation (1.36) down to a more readable form we are going to deal with  $A_n$ . In the first step we are going to plug in the series expression for the Greens function  $G_0$ , which we already obtained in the previous section (equation (1.34)). As only the factor  $(z - E_a^{(0)})$  is a function of  $z$ , we can write everything else outside the integral. As  $G_0$  is a sum from  $k = 0$  to  $k = \infty$  and we have to multiply  $G_0(VG_0)^n$  we end up with a sum over all possible  $k_n$  that result from the multiplication of the two sums.

$$A_n = \sum_{k_1, k_2, \dots, k_{n+1}} \left( (-1)^{\sum_n k_n - (n+1)} S_{k_1} V S_{k_2} V \dots V S_{k_{n+1}} \cdot \underbrace{\frac{1}{2\pi i} \oint_{\Gamma_a} (z - E_a^{(0)})^{\sum_n k_n - (n+1)} dz}_{\delta(\sum_n k_n - n - 1 = -1)} \right) \quad (1.38)$$

The closed contour integral along the curve  $\Gamma_a$  has a very simple solution; it takes the form of an delta distribution that has only non-vanishing contributions where  $\sum_n k_n - n - 1 = -1$ , i.e.  $\sum_n k_n = n$  holds true

$$A_n = - \sum_{k_1, k_2, \dots, k_{n+1}} S_{k_1} V S_{k_2} V \dots V S_{k_{n+1}} \delta\left(\sum_n k_n = n\right) . \quad (1.39)$$

As the delta distribution singles out only those terms of the sum which have non negative integers  $k_1, \dots, k_{n+1}$  for whom

$$\sum_{i=1}^{n+1} k_i = n \quad (1.40)$$

applies, we can write

$$A_n = - \sum_{\{k_{n+1}\}}^{(n)} S_{k_1} V S_{k_2} V \cdots V S_{k_{n+1}} , \quad (1.41)$$

where  $\sum_{\{k_{n+1}\}}^{(n)}$  is a sum over all those combinations discussed before. With this, we can go back to equation (1.36) and can finally write down our series expression for the projection operator

$$\hat{P} = \hat{P}_0 - \sum_{n=1}^{\infty} \lambda^n \sum_{\{k_{n+1}\}}^{(n)} S_{k_1} V S_{k_2} V \cdots V S_{k_{n+1}} . \quad (1.42)$$

### 1.3.3 Expansion Series Representation of $\hat{H}\hat{P}$

Next we repeat these considerations for  $\hat{H}\hat{P}$ , starting out from equation (1.20)

$$(\hat{H} - E_a^{(0)})\hat{P}_a = \frac{1}{2\pi i} \oint_{\Gamma_a} z G(z) dz . \quad (1.43)$$

Using equation (1.11) this can be written as

$$(\hat{H} - E_a^{(0)})\hat{P}_a = \frac{1}{2\pi i} \oint_{\Gamma_a} (z - E_a^{(0)}) G(z) dz . \quad (1.44)$$

Now we plug in our series expansion for the Greens function, as stated in formula (1.26)

$$(\hat{H} - E_a^{(0)})\hat{P}_a = \frac{1}{2\pi i} \oint_{\Gamma_a} (z - E_a^{(0)}) \sum_{n=0}^{\infty} \lambda^n G_0 (V G_0)^n dz , \quad (1.45)$$

and with a simple reorganization we end up with

$$(\hat{H} - E_a^{(0)})\hat{P}_a = \sum_{n=0}^{\infty} \lambda^n \frac{1}{2\pi i} \oint_{\Gamma_a} (z - E_a^{(0)}) G_0 (V G_0)^n dz . \quad (1.46)$$

This expression resembles the one for  $A_n$  in the previous section quite closely, so we use the same argumentation as we used to get from equation (1.37) to equation (1.41)

$$\begin{aligned}
 (\hat{H} - E_a^{(0)})\hat{P}_a &= \sum_{n=0}^{\infty} \lambda^n \sum_{k_1, k_2, \dots, k_{n+1}} \left( (-1)^{\sum_i k_i - n - 1} S_{k_1} V S_{k_2} \cdots V S_{k_{n+1}} \right. \\
 &\quad \left. \cdot \underbrace{\frac{1}{2\pi i} \oint_{\Gamma_a} (z - E_a^{(0)})^{\sum_i k_i - n - 1 + 1} dz}_{\delta(\sum_i k_i - n = -1)} \right) \\
 (\hat{H} - E_a^{(0)})\hat{P}_a &= \sum_{n=0}^{\infty} \lambda^n \sum_{\{k_{n+1}\}}^{(n-1)} S_{k_1} V S_{k_2} \cdots V S_{k_{n+1}} . \tag{1.47}
 \end{aligned}$$

For  $n = 0$  the constraint  $\sum_{i=0}^n k_i = n - 1$  cannot be fulfilled and hence the sum over  $n$  starts with  $n = 1$  and by putting  $E_a^{(0)}\hat{P}_a$  at the other side of the equation we finally have our series expression for  $\hat{H}\hat{P}_a$

$$\hat{H}\hat{P}_a = E_a^{(0)}\hat{P}_a + \sum_{n=1}^{\infty} \lambda^n \sum_{\{k_{n+1}\}}^{(n-1)} S_{k_1} V S_{k_2} \cdots V S_{k_{n+1}} . \tag{1.48}$$

For the following discussion it is advantageous to use the following shorter notation

$$\hat{H}\hat{P}_a = E_a^{(0)}\hat{P}_a + \sum_{n=1}^{\infty} \lambda^n B_n \tag{1.49}$$

with

$$B_n = \sum_{\{k_{n+1}\}}^{(n-1)} S_{k_1} V S_{k_2} \cdots V S_{k_{n+1}} . \tag{1.50}$$

### 1.3.4 Expressions for the Energy Corrections

We are now almost at a point where we can write down a closed expression for the energy corrections, but before that let's go through the first two factors  $B_n$  to see how they look like and to get an impression of what we are dealing with.

- The first order term  $B_1$  reads like

$$B_1 = \sum_{k_1, k_2}^{(0)} S_{k_1} V S_{k_2} . \tag{1.51}$$

As the only two valid indices that fulfill constraint (1.40) are  $k_1 = 0$  and  $k_2 = 0$ , we have

$$B_1 = S_0 V S_0 \quad (1.52)$$

which, according to equation (1.35), is

$$B_1 = \hat{P}_0 V \hat{P}_0 . \quad (1.53)$$

- The second order contribution reads

$$B_2 = \sum_{k_1, k_2, k_3}^{(1)} S_{k_1} V S_{k_2} V S_{k_3} . \quad (1.54)$$

There are 3 choices now for  $\{k_1, k_2, k_3\}$ , which are  $(0, 0, 1)$ ,  $(0, 1, 0)$ ,  $(1, 0, 0)$ , leading to

$$B_2 = S_0 V S_0 V S_1 + S_0 V S_1 V S_0 + S_1 V S_0 V S_0 \quad (1.55)$$

$$= \hat{P}_0 V \hat{P}_0 V \frac{\hat{Q}_0}{z - \hat{H}_0} + \hat{P}_0 V \frac{\hat{Q}_0}{z - \hat{H}_0} V \hat{P}_0 + \frac{\hat{Q}_0}{z - \hat{H}_0} V \hat{P}_0 V \hat{P}_0 . \quad (1.56)$$

If the first order correction vanishes, which can easily be achieved by a spectral shift, then  $\hat{P}_0 V \hat{P}_0 = |\psi_a\rangle E_a^{(1)} \langle \psi_a| = 0$  and only the term in the middle is retained.

For the case of a non degenerate eigenvalue we arrive at a very compact formula for the energy correction of a system. The degenerate generalization can be found in [17, page 202]. Starting out from the eigenvalue equation  $\hat{H} \hat{P}_a = E_a \hat{P}_a$  and employing  $\text{Tr} \hat{P}_a = \text{Tr} \hat{P}_0 = 1$  we end up with

$$E_a = \text{Tr}(\hat{H} \hat{P}) = E_a^{(0)} + \sum_{n=1}^{\infty} \lambda^n \text{Tr}(B_n) . \quad (1.57)$$

So the  $n$ -th order energy correction reads

$$\Delta E_a^{(n)} = \lambda^n \sum_{\{k_{n+1}\}}^{(n-1)} \text{Tr} \left( S_{k_1} V S_{k_2} \cdots V S_{k_{n+1}} \right) . \quad (1.58)$$

Each of the terms  $B_n$  contains at least once a term  $\hat{P}_0$ , i.e.  $B_n$  has the structure  $B_n = M \hat{P}_0 N$ , with some operators  $M$  and  $N$ . Due to the cyclic invariance of the trace, we can get to a structure like

$$\Delta E_a^{(n)} = \langle \psi_a^0 | N M | \psi_a^0 \rangle . \quad (1.59)$$

This is nothing else than the expectation value of the operators  $NM$  for the unperturbed ground state  $|\psi_a^0\rangle$ . Alternatively, there is Bloch's expression for the  $n^{\text{th}}$  order energy correction and with this we finally arrive at our Kato equation for the energy correction of the  $n^{\text{th}}$  order.

$$\Delta E_a^{(n)} = \sum_{\{k_{n-1}\}}^* \langle \psi_a | V S_{k_1} V S_{k_2} \cdots V S_{k_{n-1}} V | \psi_a \rangle \quad (1.60)$$

along with the constraints

$$\sum_{k=1}^s \alpha_k \geq s \quad \text{for } s = 1, 2, \dots, (n-2) \quad (1.61)$$

$$\sum_{k=1}^{n-1} \alpha_k = n - 1. \quad (1.62)$$

We will now use this approach to calculate the energy corrections for the Bose-Hubbard model in 1, 2 and 3 dimensions and for the Jaynes-Cummings model as well. Additionally we are going to show, how the Kato-Bloch formalism can be adjusted and altered to calculate other properties of these system, as will be demonstrated for the Mott insulator-superfluid phase transition.

### 1.3. EXPANSION SERIES REPRESENTATIONS

---

## Part II

# The Bose-Hubbard Model



# Chapter 2

## Introduction

The Bose-Hubbard model is used to describe bosonic particles in a lattice at very low temperatures [20] and has been treated with many different methods, including the mean-field method [21], DMRG [22, 23, 24, 25], QMC [26, 27, 28, 29] and strong-coupling methods [30, 31], therefor constituting a perfect testing ground for our method. Additionally, the Kato formalism has also been used by [18] to treat the Bose-Hubbard model. The hamiltonian for this system can be written as:

$$\hat{H} = \frac{U}{2} \sum_i \hat{n}_i(\hat{n}_i - 1) - \sum_{i,j} t_{i,j} \hat{a}_i^\dagger \hat{a}_j - \sum_i \mu_i \hat{n}_i \quad (2.1)$$

- In the first term,  $U$  stands for the interaction energy of several particles at the same site and  $\hat{n}_i$  is the particle number operator of site  $i$ . Simply put, as soon as there is more than one particle at site  $i$  this term yields a positive contribution to the overall energy of the system.
- The second term describes the hopping processes that take place on the lattice. The annihilation operator  $\hat{a}_j$  takes away one particle from site  $j$  and the creation operator  $\hat{a}_i^\dagger$  increases the particle number of site  $i$  by one, i.e. one particle hops from site  $j$  to site  $i$ . The hopping parameter  $t_{i,j}$  defines the 'strength' of this process.
- The last term in our hamiltonian accounts for a confining potential of the lattice given by the chemical potential  $\mu_i$  at the site  $i$ .

For further analysis we choose a system in which hopping only occurs between nearest neighbors and in which the chemical potential is the same for each site. These constraints lead to a simplified hamiltonian reading

$$\hat{H} = \frac{U}{2} \sum_i \hat{n}_i(\hat{n}_i - 1) - t \sum_{\langle i,j \rangle} \hat{a}_i^\dagger \hat{a}_j - \mu \hat{N} . \quad (2.2)$$

---

Here  $\langle i, j \rangle$  means that the sum only takes nearest neighbor sites  $i$  and  $j$  into account and  $\hat{N} = \sum_i \hat{n}_i$ . Additionally we split our hamiltonian into a part  $\hat{H}_0$  for which the eigenvalue equation is already solved and a hopping part  $\hat{H}_t$  which has to be treated perturbatively.

$$\begin{aligned}
\hat{H} &= \hat{H}_0 + \hat{H}_{hop} \\
\hat{H}_0 &= \frac{1}{2} \sum_i \hat{n}_i (\hat{n}_i - 1) - \frac{\mu}{U} \hat{N} \\
\hat{H}_{hop} &= -\frac{t}{U} \sum_{\langle i, j \rangle} \hat{a}_i^\dagger \hat{a}_j
\end{aligned} \tag{2.3}$$

For large potentials of the lattice the hopping parameter  $t/U$  vanishes, i.e. no hopping between sites occurs. In this case, only  $\hat{H}_0$  has to be considered. The ground state of our  $\hat{H}_0$ , where each of the  $N$  sites in our lattice is occupied with  $g$  bosons can be constructed with the well known Fock-states:

$$|\mathbf{g}\rangle = \prod_i \frac{(\hat{a}_i^\dagger)^g}{\sqrt{g!}} |0\rangle \tag{2.4}$$

The smaller the lattice potential gets, the more likely hopping processes will occur, thus the perturbation term  $\hat{H}_{hop}$  will influence the behavior of our system more and more.

# Chapter 3

## Energy Corrections

### 3.1 Applying the Kato Formalism

In order to calculate the ground state energy of this perturbed system, we make use of the Kato formalism. The big advantage of this approach, as has already been said, lies in the fact that it yields closed expressions for every order of correction, in contrast to the iterative approach of the Schrödinger-Rayleigh perturbation theory. One constraint of this approach as we will use it here is that the eigenstates must not be degenerated.

As the derivation in the previous chapter was quite lengthy and complicated, the most important formulas will be rewritten here at the beginning to avoid skipping back and forth through the chapters, allowing for a more fluent read.

The  $n^{\text{th}}$  order energy correction for the Bose-Hubbard model ground state energy can be written as:

$$\Delta E_g^{(n)} = \sum_{\{k_{n-1}\}} \langle \mathbf{g} | V S_{k_1} V S_{k_2} \dots V S_{k_{n-1}} V | \mathbf{g} \rangle \quad (3.1)$$

The index  $\{k_{n-1}\}$  means that the sum runs over all possible sequences of  $k_{n-1}$  which satisfy the following requirements:

$$\sum_{l=1}^s k_l \geq s \quad \text{for } s = 1, 2, \dots, n-2 \quad (3.2)$$

$$\sum_{l=1}^{n-1} k_l = n-1 \quad (3.3)$$

The variables  $V$  and  $S_k$  stand for the following terms:

$$V = -\frac{t}{U} \sum_{\langle i,j \rangle} \hat{a}_i^\dagger \hat{a}_j \quad (3.4)$$

$$S_k = \begin{cases} -|\mathbf{g}\rangle\langle\mathbf{g}| & \text{for } k = 0 \\ \sum_{i \neq g} \frac{|\mathbf{i}\rangle\langle\mathbf{i}|}{\left(E_g^{(0)} - E_i^{(0)}\right)^k} & \text{otherwise} \end{cases} \quad (3.5)$$

The energies  $E_i^{(0)}$  are the unperturbed energies, which can be computed by evaluating  $\hat{H}_0$  using the state  $|\mathbf{i}\rangle$

$$\begin{aligned} E_i^{(0)} &= \langle \mathbf{i} | H_0 | \mathbf{i} \rangle \\ &= \sum_k n_k \left( \frac{n_k - 1}{2} - \frac{\mu}{U} \right). \end{aligned} \quad (3.6)$$

Obviously the unperturbed ground state energy can be written as:

$$E_g^{(0)} = Ng \left( \frac{g-1}{2} - \frac{\mu}{U} \right) \quad (3.7)$$

Another notation for the energy correction, which we will be using in chapter 5 about the Mott insulator-superfluid phase transition is

$$\begin{aligned} \Delta E_g &= \sum_{n=1}^{\infty} E_g^{(2n)} \\ &= \sum_n \alpha^{(2n)}(g) \left( \frac{t}{U} \right)^n, \end{aligned} \quad (3.8)$$

whose derivation will be explained in section 3.3, as it will be more comprehensible at that time.

## 3.2 Graphical Representation

In order to understand exactly how the Kato formalism can be used to compute the energy corrections for the Bose-Hubbard model we take a step back and look closely at equation (3.1). Each of the single  $V$ -terms represents a hopping process that can be pictured graphically as single paths on a lattice. Let's consider for example a small, two dimensional square lattice where we number the sites consecutively for the ease of reference.

A hopping term  $\hat{a}_5^\dagger \hat{a}_4$  could in this graphical representation be drawn as an arrow starting at site 4 and ending at site 5 (red arrow in figure 3.1);  $\hat{a}_6^\dagger \hat{a}_3$  as an arrow pointing from site 3 to site 6 (blue arrow in figure 3.1). To calculate

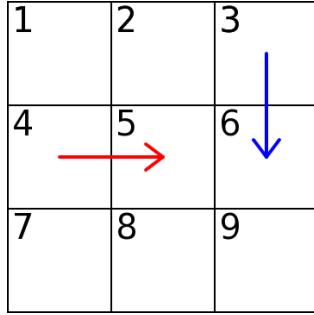


Figure 3.1: Two possible hopping processes on a square lattice.

the  $n^{\text{th}}$  energy correction of an infinitely big lattice one would need to consider every possible configuration that can be constructed out of  $n$  hopping processes. As we are dealing with an infinite lattice this would of course not be a feasible approach, so we will reduce the number of configurations that have to be considered drastically. For that we take a second look at equation (3.1), more precisely we take a look at the combination of  $VS_kV$ .  $S_k$  for  $k \neq 0$  is a linear combination of all states  $|\mathbf{i}\rangle$  that are not equal to the ground state weighted with a function of the unperturbed energies (equation (3.5)).  $V$  stands for a specific hopping process, i.e. from site  $i$  to site  $j$  (equation (3.4)). Thus, the combination becomes

$$VS_kV = \sum_{i \neq g} \frac{V|\mathbf{i}\rangle\langle\mathbf{i}|V}{\left(E_g^{(0)} - E_i^{(0)}\right)^k} \quad \text{for } k \neq 0. \quad (3.9)$$

Going back to our graphical description this means that the  $S_k$  link the single perturbation terms. As each of these 'chains' starts with our ground state  $|\mathbf{g}\rangle$  and ends with the ground state  $|\mathbf{g}\rangle$  too, they actually have to be closed paths in order to result in a non vanishing contribution to the energy.

This simplifies our situation a lot as we no longer have to take every possible combination of hopping processes on our lattice into account, but only those that result in closed paths. (It also means of course that there will be no contributions of the energy with an odd number of hopping processes.)

To state these facts even clearer we will explicitly look at the energy contributions in second and fourth order.

### 3.3 Explicit Examples

#### 3.3.1 Energy Corrections in Second Order

There is only one sequence  $\{k_n\}$  that meets the constraints of equation (3.2) and (3.3), which results in the following energy correction:

$$\begin{aligned}\Delta E_g^{(2)} &= \langle \mathbf{g} | V S_1 V | \mathbf{g} \rangle \\ &= \sum_{i \neq g} \frac{\langle \mathbf{g} | V | \mathbf{i} \rangle \langle \mathbf{i} | V | \mathbf{g} \rangle}{E_g^{(0)} - E_i^{(0)}}\end{aligned}\quad (3.10)$$

which matches the expression of the second order energy correction of the Schrödinger-Rayleigh perturbation theory. If we bear on a single site we can draw every one of these paths in our two dimensional lattice from before (figure 3.2).

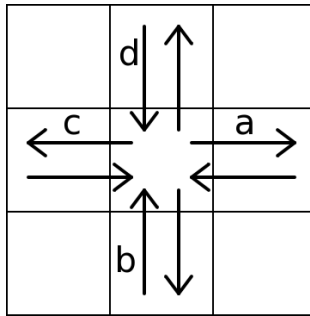


Figure 3.2: All possible closed paths in second order with the same origin.

As the model we are investigating at the moment has a uniform chemical potential and a hopping parameter that is the same for all sites, it is translationally invariant. Because of that it is sufficient to consider only topologically different paths whose contributions to the energy then get multiplied by the number of their appearance, i.e. their multiplicity.

Another fact worth mentioning is that we are at this point not interested in the chronological order in which the single hopping processes occur, thus path a and c are actually the same, as path c is just the same as path a shifted one site to the left. The same applies for paths b and d of course.

So in summary, there is only one topologically unique diagram that has to be considered for the second order energy correction. This diagram has a multiplicity of 2 (figure 3.3(a)), as all open paths do not contribute to the energy (figure 3.3(b)).

As there is also just one sequence of Kato indices  $\{k_n\}$ , namely (1), the appropriation of which sequence applies for which diagram couldn't be simpler.

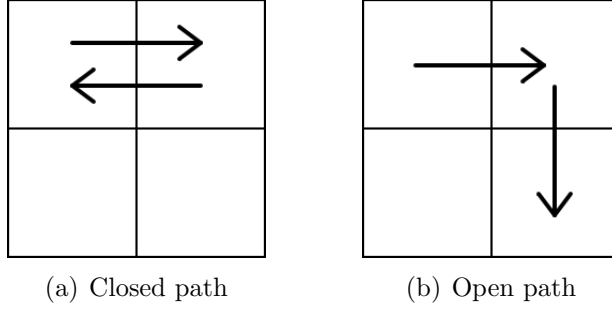


Figure 3.3: All topologically unique paths for two hopping processes.

The only thing left to do in order to calculate the energy correction is to generate all possible permutations of the single hopping processes for this one path and compute the energy. Luckily, the number of possible permutations is also very limited in case of the second order, as can be seen in figure 3.4.

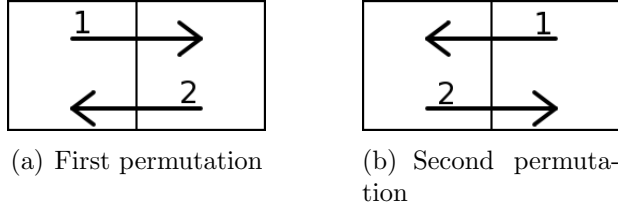


Figure 3.4: All possible permutations for the second order closed path.

Thus we can finally write for our two dimensional square lattice:  
 (As there are only changes in two of the sites we can set our ground state vector  $|\mathbf{g}\rangle = |g, g\rangle$  without loss of generality)

$$\begin{aligned}
 \Delta E_g^{(2)} &= 2 \left( \frac{t}{U} \right)^2 \frac{\langle g, g | \hat{a}_1^\dagger \hat{a}_2 | g-1, g+1 \rangle \langle g-1, g+1 | \hat{a}_2^\dagger \hat{a}_1 | g, g \rangle}{2 \left( \frac{n(n-1)}{2} - \frac{\mu}{U} n \right) - (n^2 - n + 1 - 2 \frac{\mu}{U} n)} \\
 &+ 2 \left( \frac{t}{U} \right)^2 \frac{\langle g, g | \hat{a}_2^\dagger \hat{a}_1 | g+1, g-1 \rangle \langle g+1, g-1 | \hat{a}_1^\dagger \hat{a}_2 | g, g \rangle}{2 \left( \frac{n(n-1)}{2} - \frac{\mu}{U} n \right) - (n^2 - n + 1 - 2 \frac{\mu}{U} n)} \\
 \Delta E_g^{(2)} &= -4n(n+1) \left( \frac{t}{U} \right)^2 \tag{3.11}
 \end{aligned}$$

### 3.3.2 Energy Corrections in Fourth Order

Let's take a look at the fourth order correction of the energy now. The cumulative sequences, i.e.  $\{k_1, k_1 + k_2, k_1 + k_2 + k_3\}$ , that meet the constraints (3.2) and (3.3) are now:

$$\{k_1, k_1 + k_2, k_1 + k_2 + k_3\} = \{(1, 2, 3), (1, 3, 3), (2, 2, 3), (2, 3, 3), (3, 3, 3)\} \quad (3.12)$$

Expressed in explicit sequences  $\{k_1, k_2, k_3\}$ , they correspond to:

$$\{k_1, k_2, k_3\} = \{(1, 1, 1), (1, 2, 0), (2, 0, 1), (2, 1, 0), (3, 0, 0)\} \quad (3.13)$$

Section 4.4 contains a detailed description on how to calculate these two types of Kato sequences. This results in an energy correction term that looks like:

$$\Delta E_g^{(4)} = \langle \mathbf{g} | V S_1 V S_1 V S_1 V | \mathbf{g} \rangle \quad (3.14a)$$

$$+ \langle \mathbf{g} | V S_1 V S_2 V S_0 V | \mathbf{g} \rangle \quad (3.14b)$$

$$+ \langle \mathbf{g} | V S_2 V S_0 V S_1 V | \mathbf{g} \rangle \quad (3.14c)$$

$$+ \langle \mathbf{g} | V S_2 V S_1 V S_0 V | \mathbf{g} \rangle \quad (3.14d)$$

$$+ \langle \mathbf{g} | V S_3 V S_0 V S_0 V | \mathbf{g} \rangle \quad (3.14e)$$

But not all of these terms actually yield non-vanishing contribution to the energy. If we evaluate just the effect of  $V$  on  $S_0$  and our ground state  $|\mathbf{g}\rangle$ , we find out that

$$S_0 V |\mathbf{g}\rangle = -|\mathbf{g}\rangle \langle \mathbf{g} | V | \mathbf{g} \rangle \quad (3.15)$$

$$= t |\mathbf{g}\rangle \langle \mathbf{g} | \hat{a}_i^\dagger \hat{a}_j | \mathbf{g} \rangle. \quad (3.16)$$

This means that the state  $|\mathbf{g}\rangle$  has to be present before and after one hopping process, as already discussed. This cannot be achieved by the terms with  $S_0 V |\mathbf{g}\rangle$  of course, thus all the terms (3.14b), (3.14d) and (3.14e) vanish, leaving us only with:

$$\Delta E_g^{(4)} = \langle \mathbf{g} | V S_1 V S_1 V S_1 V | \mathbf{g} \rangle \quad (3.17a)$$

$$+ \langle \mathbf{g} | V S_2 V S_0 V S_1 V | \mathbf{g} \rangle \quad (3.17b)$$

The next step now is to create all topologically unique closed paths with four hopping terms as well as their multiplicities. For the fourth order this is still quite a simple task as there are only three diagrams possible, which are depicted in figure 3.5.

The question we face now is to find out which Kato sequence corresponds to which path. Therefor we take a look at equation (3.17b). The term  $S_0$  in the middle of the sequence means that our system is in the ground state  $|\mathbf{g}\rangle$

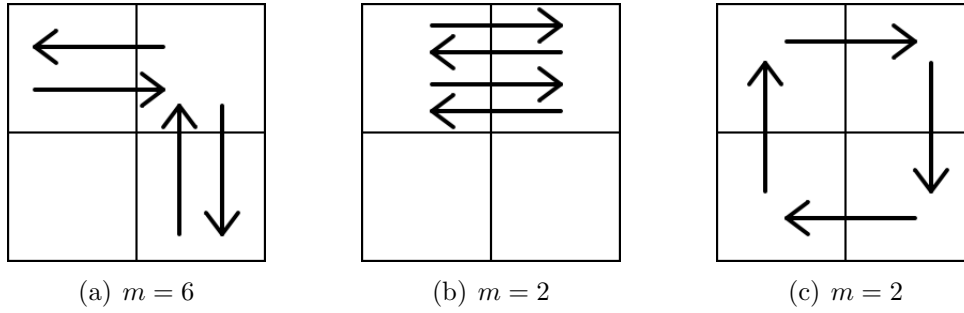


Figure 3.5: All possible topologically unique closed paths in fourth order with their multiplicities  $m$ .

again after two hopping processes. As the ground state is never reached but at the very end of the process in path 3.5(c), the Kato sequence (3.17a) has to be taken to calculate the energy for this path.

For the paths 3.5(a) and 3.5(b) the situation is not that simple as it depends on the chronological order of the single hopping processes whether the ground state will be recovered after the second hopping or not.

Figure 3.6 shows the same topological path but with two different successions of hopping processes. In figure 3.6(a) the ground state is only reached after all hoppings took place, meaning that equation (3.17a) has to be used to calculate the energy correction.

The order in which the hoppings occur in figure 3.6(b) however results in the ground state being present at the end but also after two hopping processes, thus one has to choose equation (3.17b) to calculate the energy correctly.

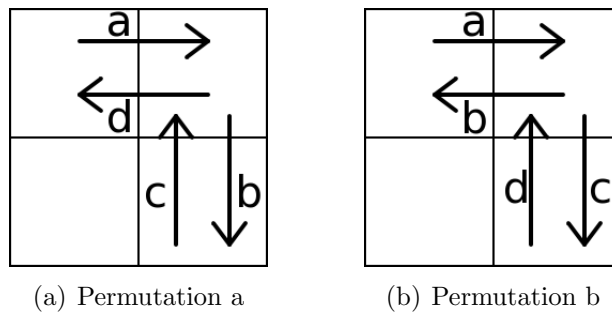


Figure 3.6: Two possible permutations of path 3.5(a).

We will now calculate the energy contributions of these two specific permutations to show once again how the Kato approach has to be treated. To make the equations more readable we reduce our ground state vector to the concerned sites only, i.e.  $|\mathbf{g}\rangle = |g, g, g\rangle$ , and also spare writing the full energy

denominators as they always yield  $E_g^{(0)} - E_i^{(0)} = -1$ , due to the fact that maximally one particle-hole pair is present in this diagram.

Path 3.6(a):

$$\begin{aligned}
 \Delta E_a^{(4)} &= \left(\frac{t}{U}\right)^4 (-1)^3 \langle g, g, g | \hat{a}_1^\dagger \hat{a}_2 | g-1, g+1, g \rangle \\
 &\quad \cdot \langle g-1, g+1, g | \hat{a}_2^\dagger \hat{a}_3 | g-1, g, g+1 \rangle \\
 &\quad \cdot \langle g-1, g, g+1 | \hat{a}_3^\dagger \hat{a}_2 | g-1, g+1, g \rangle \\
 &\quad \cdot \langle g-1, g+1, g | \hat{a}_2^\dagger \hat{a}_1 | g, g, g \rangle \\
 \Delta E_a^{(4)} &= -g(g+1)^3 \left(\frac{t}{U}\right)^4 \tag{3.18}
 \end{aligned}$$

Path 3.6(b):

$$\begin{aligned}
 \Delta E_b^{(4)} &= \left(\frac{t}{U}\right)^4 (-1)^4 \langle g, g, g | \hat{a}_2^\dagger \hat{a}_3 | g, g-1, g+1 \rangle \\
 &\quad \cdot \langle g, g-1, g+1 | \hat{a}_3^\dagger \hat{a}_2 | g, g, g \rangle \\
 &\quad \cdot \langle g, g, g | \hat{a}_1^\dagger \hat{a}_2 | g-1, g+1, g \rangle \\
 &\quad \cdot \langle g-1, g+1, g | \hat{a}_2^\dagger \hat{a}_1 | g, g, g \rangle \\
 \Delta E_b^{(4)} &= g^2(g+1)^2 \left(\frac{t}{U}\right)^4 \tag{3.19}
 \end{aligned}$$

As one can see, those two permutations of the same diagram yield quite different results, thus there is no avoiding the fact that for every diagram we have to compute all possible permutations and evaluate their contribution to the energy.

To squeeze these results in a more compact form one can write for the fourth energy correction

$$\Delta E_g^{(4)} = \alpha^{(4)}(g) \left(\frac{t}{U}\right)^4, \tag{3.20}$$

where the coefficient  $\alpha^{(4)}(g)$  is the sum of all paths' factors stemming from the scalar products and the energy denominators.

If one extends this thought to the case where the energy corrections have been calculated up to order infinity, one could write for the energy correction

$$\Delta E_g = \sum_n \alpha^{(2n)}(g) \left(\frac{t}{U}\right)^n, \tag{3.21}$$

which is a power series in respect to the hopping strength  $t/U$ .

# Chapter 4

## Numerical Implementation

In the last chapter we introduced the Kato formalism to calculate the energy of the Bose-Hubbard model with a perturbative approach, but without the need to use the iterative Schrödinger-Rayleigh theory. Instead we can make use of a formalism that allows us to derive closed expressions for every order of correction without having to compute the preceding orders. It was also shown how these calculations would look like for the second and the fourth order, but it also became obvious that for every order larger than four doing these by hand is not feasible at all. Therefore we have to think about a numerical transcription. Such a program has to perform the following steps:

1. The first stage of the program has to construct all possible paths for a given order.
2. The second stage has to get rid of the translational redundancies.
3. Now the different paths have to be reduced until just topologically unique diagrams are left. Additionally, the multiplicity for each diagram has to be computed as well.
4. According to the given order all possible Kato sequences have to be created.
5. For all diagrams every permutation of the single hopping processes has to be computed and assigned to the appropriate Kato sequence. (One specific diagram can also belong to more than one Kato sequence.)
6. Evaluating the energy of every single permutation. The overall energy is then a result of summing over all permutations of a diagram, multiplying this energy with the multiplicity of the diagram and finally summing over all diagrams.

We will now discuss each of these steps in depth to make the process more transparent and easier to understand. First of all we have to think about

---

what the 'stage' of our Bose-Hubbard model is. In our case, everything takes place on an infinitely large lattice that has either one, two or three dimensions. In our further discussion we will focus on the two-dimensional case, as the situation can be described easier and most of the considerations can be upscaled to three dimensions as well as downscaled to one dimension without spending any additional thoughts. Each time the one or three dimensional implementation has to be treated differently from the two-dimensional case it will be pointed out and further elaborated on.

## 4.1 Constructing the Paths

Of course there are many possibilities to construct closed paths on a lattice. One for example would be to simply place single hopping processes on the lattice one after another until the required number of processes has been reached. After that one would check if a contiguous path has been created and whether it is closed or not.

There are however two issues with this approach. First of all it would consume much computational power. The second problem is that one would end up with a huge number of paths all over the lattice which would then need to be shifted to a common origin in order to get rid of translational redundancies.

A much more sophisticated and computational power friendly approach is to choose one site as the origin for all paths to come. As the paths have to be closed in the end, each one has to have as many hopping processes to the right as to the left and as many hoppings upwards as downwards, i.e.  $N_{+x} = N_{-x}$ ,  $N_{+y} = N_{-y}$ . (The left-right direction will from now on be referred to as x-direction and the up-down direction as y-direction.) This means that the actual number of hoppings that have to be decided on is only half the expansion order.

The next detail to decide on is how many steps in each of the two directions one takes. As the number of hoppings in x-direction is linked to the number of hoppings in y-direction it suffices to specify the number of hoppings to the right one wants to take.

$$\begin{aligned} N_0 &= N_{+x} + N_{-x} + N_{+y} + N_{-y} \\ &= 2(N_{+x} + N_{+y}) \end{aligned} \quad (4.1)$$

$$N_{+y} = \frac{N_0}{2} - N_{+x} \quad (4.2)$$

Thus for fixed  $N_0$  and  $N_{+x}$  the number of closed paths that return to the origin after  $N_0$  steps is

$$\begin{aligned} N(N_0, N_{+x}) &= \frac{N_0!}{N_{+x}!N_{-x}!N_{+y}!N_{-y}!} \quad (4.3) \\ &= \frac{N_0!}{(N_{+x}!(\frac{N_0}{2} - N_{+x})!)^2} \\ &= \frac{N_0!}{(N_{+x}!(\frac{N_0}{2} - N_{+x})!)^2} \\ &= \binom{N_0}{\frac{N_0}{2}} \left( \frac{(\frac{N_0}{2})!}{N_{+x}!(\frac{N_0}{2} - N_{+x})!} \right)^2. \end{aligned} \quad (4.4)$$

Hence, the total number of closed paths in two dimensions is

$$N(N_0) = \sum_{N_{+x}=0}^{\frac{N_0}{2}} \binom{N_0}{\frac{N_0}{2}} \left( \frac{(\frac{N_0}{2})!}{N_{+x}!(\frac{N_0}{2} - N_{+x})!} \right)^2 \quad (4.5)$$

$$\begin{aligned} &= \binom{N_0}{\frac{N_0}{2}} \sum_{N_{+x}=0}^{\frac{N_0}{2}} \left( \frac{(\frac{N_0}{2})!}{N_{+x}!(\frac{N_0}{2} - N_{+x})!} \right)^2 \\ &= \binom{N_0}{\frac{N_0}{2}}^2. \end{aligned} \quad (4.6)$$

While the argument that  $N_{+i} = N_{-i}$  for  $i \in (x, y, z)$  still applies for three dimensions as well, the fact that a fixed number of steps in x-direction does no longer conclusively determine the number of steps in y- and z-direction means that (4.6) is no longer true for three dimensions. For one dimension the number of closed path is simply  $N(N_0) = \binom{N_0}{\frac{N_0}{2}}$ .

If we assign numbers to the directions to take ( $+x \hat{=} 1, +y \hat{=} 2, -x \hat{=} 3$  and  $-y \hat{=} 4$ ) we can compute very conveniently every possible path from a common origin by just computing every unique permutation of these numbers. For  $N_0 = 2$  this would lead to the four rows of table 4.1, each of them representing a path that is drawn in figure 4.1.

Table 4.1: Representation of all two-dimensional closed path in second order.

1.	1	3
2.	2	4
3.	3	1
4.	4	2

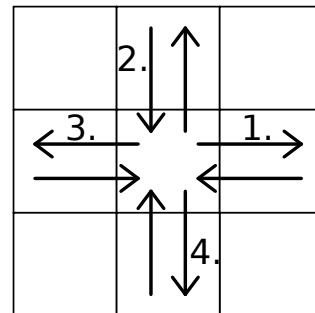


Figure 4.1: All paths in second order according to table 4.1.

To bring this section to a conclusion, table 4.2 shows the total number of closed paths for a given order in one, two or three dimensions.

Table 4.2: Number of paths for given order and dimension.

order	1-dim	2-dim	3-dim
2	2	4	6
4	6	36	90
6	20	400	1140
8	70	4900	14490
10	252	63504	189756

## 4.2 Translational Redundancies

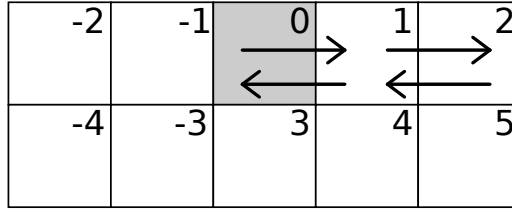
According to our list at the very beginning of this chapter the next step is to get rid of the translational redundancies. A very important point to consider is that path 1 and path 3 in figure 4.1 are not only topologically identical, but are actually the same. Thus only one of these duplicate paths has to be counted, otherwise this would lead to a wrong multiplicity.

To make this situation clearer let us take a look at figure 4.2. Besides we will change from the previous representation of a path, where we defined the directions in which the hoppings take place to a representation of sites connected with bonds. In figure 4.2 the sites have also been numbered in order to have a reference point for the origin. (The discontinuity at the edge of sites 3 and -3 has no influence in our discussion as the sites could always be renumbered in another way.) The transition from direction to bond representation for these three paths works as follows:

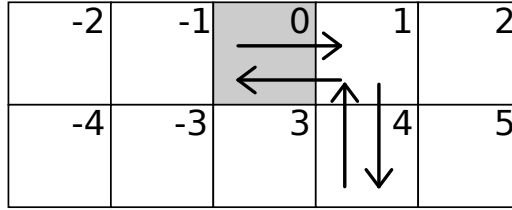
$$\text{Path 1, figure 4.2(a): } (1, 1, 3, 3) \implies \begin{array}{c} 0 \ 1 \\ 1 \ 2 \\ 2 \ 1 \\ 1 \ 0 \end{array} \quad (4.7)$$

$$\text{Path 2, figure 4.2(b): } (1, 2, 4, 3) \implies \begin{array}{c} 0 \ 1 \\ 1 \ 4 \\ 4 \ 1 \\ 1 \ 0 \end{array} \quad (4.8)$$

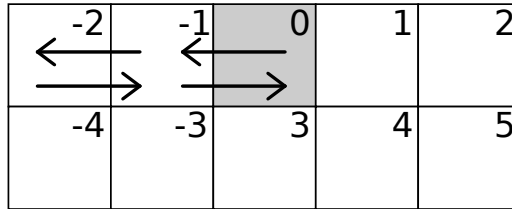
$$\text{Path 3, figure 4.2(c): } (3, 3, 1, 1) \implies \begin{array}{c} 0 \ -1 \\ -1 \ -2 \\ -2 \ -1 \\ -1 \ 0 \end{array} \quad (4.9)$$



(a) Path 1



(b) Path 2



(c) Path 3

Figure 4.2: Three possible paths with four hopping processes.

The next thing we do is shift each path along the x-direction so that the leftmost visited site of this path is the site with number 0, i.e. that there are no sites with negative indices integrated into the path. In analogy, one would shift a path in y and z direction so that no negative site-indices occur.

$$\text{Path 1 : } \begin{matrix} 0 & 1 \\ 1 & 2 \\ 2 & 1 \\ 1 & 0 \end{matrix}, \quad \text{Path 2 : } \begin{matrix} 0 & 1 \\ 1 & 4 \\ 4 & 1 \\ 1 & 0 \end{matrix}, \quad \text{Path 3 : } \begin{matrix} 2 & 1 \\ 1 & 0 \\ 0 & 1 \\ 1 & 2 \end{matrix}$$

As we are at this point not at all interested in which order which site is visited, we can rearrange the order of the bonds. We do that in a way that the sum over the two columns should be ascending. Whenever there are two rows with the same sum the row with the lower first element should be placed first. Our three paths ordered accordingly to these rules look as follows:

$$\text{Path 1 : } \begin{matrix} 0 & 1 \\ 1 & 0 \\ 1 & 2 \\ 2 & 1 \end{matrix}, \quad \text{Path 2 : } \begin{matrix} 0 & 1 \\ 1 & 0 \\ 1 & 4 \\ 4 & 1 \end{matrix}, \quad \text{Path 3 : } \begin{matrix} 0 & 1 \\ 1 & 0 \\ 1 & 2 \\ 2 & 1 \end{matrix}$$

It becomes obvious now that path 1 and path 3 are the same. Therefore one of them has to be dropped without changing the multiplicity of the other.

Table 4.3 shows the number of paths after they have been examined accordingly to the algorithm presented in this chapter. We no longer keep track of a one-dimensional lattice as it would provide no additional information that couldn't be derived with a two- or three-dimensional lattice.

Table 4.3: Number of paths for given order and dimension after eliminating the translational redundancies.

order	2-dim	3-dim
2	2	3
4	10	24
6	64	177
8	474	1383

The remaining paths we do have now do not contain any translational redundancies anymore, therefore whenever we drop a path, because we found a topologically identical path, we have to adjust the multiplicity of that diagram accordingly so that the total number of paths stays the same.

### 4.3 Reducing the Paths to Topologically Unique Diagrams

After eliminating all multiple paths that differ from each other just by a simple shift, we now want to reduce these paths to just a few topologically unique diagrams that are representative for the whole set of paths. In order to do so we have to remind ourselves what the starting situation is. We have a regular lattice on which hopping processes take place. As the chemical potential and the hopping parameter are both independent of the site, i.e. are constant for any site, the only distinguishing parameters are the occupation numbers of each site at a given moment or after a certain hopping.

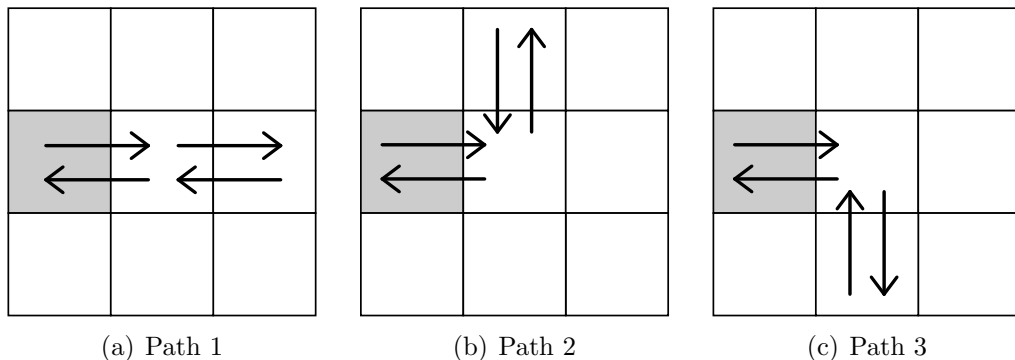


Figure 4.3: Three topologically identical paths

Therefore, all three paths of figure 4.3 have the same topology and it is sufficient to keep just one path of them, say the first one and remember how many other paths of the same topology there are.

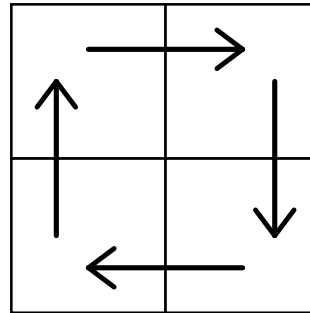
As we have to compute every permutation of hopping processes, reducing the paths to just a few unique diagrams allows for huge savings of both processing power and time. Just take the three paths of figure 4.3: To compute the energy contribution of these one would need to evaluate  $3 \cdot 4! = 72$  paths due to the permutations, whereas computing the energy contribution of path 1 and multiplying the outcome with three would deliver the same value for the energy, but in a third of the calculating time.

A very elegant way to find the topologically unique diagrams makes use of adjacency matrices, which are often used in graph theory. These matrices tell you which vertices of a network are connected with which. As our algorithms make heavy use of adjacency matrices the concept shall be explained more extensively here.

Let's consider the following path of figure 4.4, whose bond representation is shown in table 4.4

Table 4.4: Bond representation of path figure 4.4.

	i	j
1.	1	2
2.	2	3
3.	3	4
4.	4	1


 Figure 4.4:  $1 \rightarrow 2 \rightarrow 3 \rightarrow 4 \rightarrow 1$ 

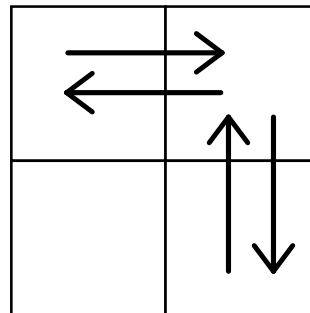
We start out with a zero matrix that has as many rows and columns as there are unique sites in the path, in our case four. For every bond from site  $i$  to site  $j$  we add 1 to the matrix element  $m_{ij}$ . For our specific case of path figure 4.4 this means that we have to increase the values of  $m_{1,2}$ ,  $m_{2,3}$ ,  $m_{3,4}$  and  $m_{4,1}$  by one, resulting in an adjacency matrix that looks as follows:

$$M_1 = \begin{pmatrix} 0 & 1 & 0 & 0 \\ 0 & 0 & 1 & 0 \\ 0 & 0 & 0 & 1 \\ 1 & 0 & 0 & 0 \end{pmatrix} \quad (4.10)$$

Let's now apply the same procedure to another path, as shown in figure 4.5:

Table 4.5: Bond representation of path figure 4.5

	i	j
1.	1	2
2.	2	3
3.	3	2
4.	2	1


 Figure 4.5:  $1 \rightarrow 2 \rightarrow 3 \rightarrow 2 \rightarrow 1$ 

For this path the adjacency matrix has the form:

$$M_2 = \begin{pmatrix} 0 & 1 & 0 \\ 1 & 0 & 1 \\ 0 & 1 & 0 \end{pmatrix} \quad (4.11)$$

As a last example let us calculate the adjacency matrix of the last topologically unique diagram in fourth order (figure 3.5(b)).

Table 4.6: Bond representation of path figure 4.6

	i	j
1.	1	2
2.	2	1
3.	1	2
4.	2	1

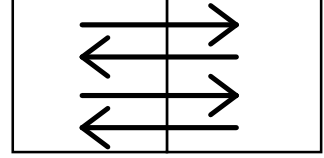


Figure 4.6:  $1 \rightarrow 2 \rightarrow 1 \rightarrow 2 \rightarrow 1$

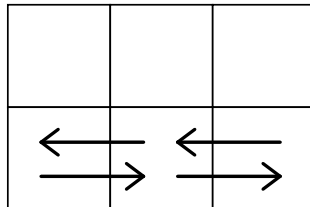
Here the adjacency matrix looks like:

$$M_3 = \begin{pmatrix} 0 & 2 \\ 2 & 0 \end{pmatrix} \quad (4.12)$$

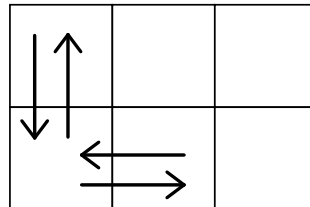
As one can see, these three matrices differ clearly from each other, but every closed path that can be generated out of four hopping processes will have one of these three adjacency matrices, i.e. all paths in fourth order can be reduced to these three diagrams.

The use of adjacency matrices can help us tremendously to reduce the number of paths, in fact most of the paths can be identified by the straightforward implementation of the adjacency matrix.

For a small amount of paths however this basic approach does not suffice to tell whether a path is topologically unique or not, as there are a few paths whose differences are more subtle. Thus our approach has to be adapted. We therefore take a look at the following two paths of figure 4.7 consisting of four single hopping processes:



(a) Path 1:  $1 \rightarrow 2 \rightarrow 3 \rightarrow 2 \rightarrow 1$



(b) Path 2:  $1 \rightarrow 2 \rightarrow 1 \rightarrow 3 \rightarrow 1$

Figure 4.7: Two topologically identical paths.

Their adjacency matrices look like:

$$M_1 = \begin{pmatrix} 0 & 1 & 0 \\ 1 & 0 & 1 \\ 0 & 1 & 0 \end{pmatrix} \quad (4.13)$$

$$M_2 = \begin{pmatrix} 0 & 1 & 1 \\ 1 & 0 & 0 \\ 1 & 0 & 0 \end{pmatrix} \quad (4.14)$$

As one can see, these two matrices are different but the topologies of the paths are not. Both are made of two double bonds and the hopping occurs between three sites. The only difference is that in path 1 (figure 4.7(a)) the origin for numbering the sites is at the edge of the two double bonds whereas the origin of path 2 (figure 4.7(b)) lies right in between the double bonds. But as we already agreed, the chronological order in which the hopping process occurs is of no interest at this point, so these paths have to be topologically identical. In order to make our algorithm sensitive for these kind of issues we have to permute the path in question circularly  $(N - 1)$  times ( $N$  shall be the number of hopping processes), i.e. shift the origin of the path at the beginning of each single hopping term, and compute the adjacency matrix of each permutation. Each of these matrices is then compared with the adjacency matrices of the already identified unique diagrams. If no matrices match each other the path is topologically different, otherwise it will be discarded and the multiplicity of the previous diagram increased by one. In our example of figure 4.7(b) the first permutation already has the same adjacency matrix as path figure 4.7(a), thus it can not be topologically unique. Another more complex example is shown in figure 4.8. There you can see two paths with eight hopping processes that look quite similar, but their course is different. The first four hopping processes have been depicted with red arrows to illustrate this fact better.

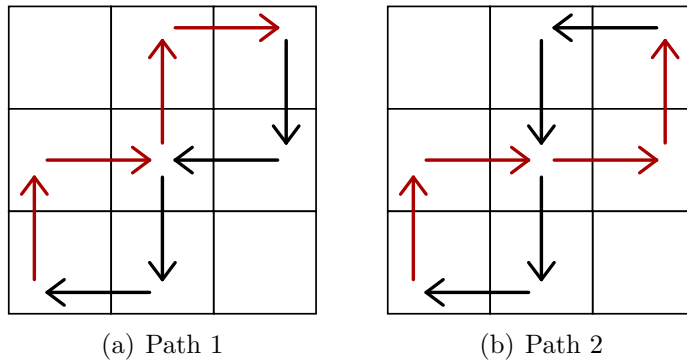


Figure 4.8: Two topologically identical paths.

Their adjacency matrices also look different, but by computing the adjacency

matrices of all permutations of the second path it is possible to find a matrix identical to matrix (4.15)

$$M_1 = \begin{pmatrix} 0 & 1 & 0 & 0 & 0 & 0 & 0 \\ 0 & 0 & 1 & 0 & 0 & 0 & 0 \\ 0 & 0 & 0 & 1 & 0 & 0 & 1 \\ 0 & 0 & 0 & 0 & 1 & 0 & 0 \\ 0 & 0 & 0 & 0 & 0 & 1 & 0 \\ 0 & 0 & 1 & 0 & 0 & 0 & 0 \\ 1 & 0 & 0 & 0 & 0 & 0 & 0 \end{pmatrix} \quad (4.15)$$

$$M_2 = \begin{pmatrix} 0 & 1 & 0 & 0 & 0 & 0 & 0 \\ 0 & 0 & 1 & 0 & 0 & 0 & 0 \\ 0 & 0 & 0 & 1 & 0 & 0 & 0 \\ 0 & 0 & 0 & 0 & 1 & 0 & 0 \\ 0 & 0 & 0 & 0 & 0 & 1 & 1 \\ 0 & 0 & 1 & 0 & 0 & 0 & 0 \\ 1 & 0 & 0 & 0 & 0 & 0 & 0 \end{pmatrix} \quad (4.16)$$

## 4.4 Computing the Kato Sequences

Creating all possible Kato sequences for a given order is a straightforward approach. We start with computing all cumulative sequences that meet constraint (3.3) which says that the highest index of our sequence must be  $N - 1$  ( $N$  being the considered order).

As the value of the last index is fixed with  $N - 1$ , we only have to care about the previous  $N - 2$  indices. Each of these indices  $n_i$  can take any number that is higher or equal that of the previous index but lower or equal than the value of the next index (constraint (3.2)), i.e.

$$n_{i-1} \leq n_i \leq n_{i+1} \quad (4.17)$$

For the fourth order energy correction the cumulative sequences are listed in table 4.7.

Table 4.7: All cumulative Kato sequences for the fourth order.

	$n_1$	$n_2$	$n_3$
1.	1	2	3
2.	1	3	3
3.	2	2	3
4.	2	3	3
5.	3	3	3

The next thing we have to do is to make the transition from the cumulative indices  $n_i$  to sequential indices  $k_i$ . This again is a very simple task when we consider that

$$n_i = \sum_{j=1}^i k_j \quad (4.18)$$

$$= n_{i-1} + k_i$$

$$k_i = n_i - n_{i-1} . \quad (4.19)$$

Therefore, the corresponding sequential sequences to table 4.7, which are shown in table 4.8, can be calculated very easily. We already mentioned in chapter 3.3.2 that not all of these sequences describe a valid path. In general, the sequence  $(k_1, k_2, k_3)$  is just the short form of writing  $\langle \mathbf{g} | V S_{k_1} V S_{k_2} V S_{k_3} V | \mathbf{g} \rangle$ . This means, that if either the first or the last index  $k$  is equal to zero we would have a configuration where a hopping term  $V$  is between two ground states, i.e.  $\langle \mathbf{g} | V | \mathbf{g} \rangle$ . This cannot be fulfilled as there can't be the ground state present after any hopping from the ground state. Likewise, any sequence where two or more indices, which are succeeding each other, are equal to zero, cannot be a valid Kato sequence and thus has to be eliminated. This

#### 4.4. COMPUTING THE KATO SEQUENCES

---

Table 4.8: All sequential Kato sequences for the fourth order.

	$k_1$	$k_2$	$k_3$
1.	1	1	1
2.	1	2	0
3.	2	0	1
4.	2	1	0
5.	3	0	0

leaves us with just two possible sequences for the fourth order energy correction, as shown in table 4.9.

Table 4.9: All valid Kato sequences for the fourth order.

	$k_1$	$k_2$	$k_3$
1.	1	1	1
2.	2	0	1

To conclude this section, table 4.10 shows all valid sequential Kato sequences for the sixth order of the energy correction.

Table 4.10: All valid Kato sequences for the sixth order.

	$k_1$	$k_2$	$k_3$	$k_4$	$k_5$
1.	1	1	1	1	1
2.	2	0	1	1	1
3.	1	2	0	1	1
4.	2	1	0	1	1
5.	1	1	2	0	1
6.	1	2	1	0	1
7.	2	1	1	0	1
8.	2	0	2	0	1
9.	3	0	1	0	1

## 4.5 Assigning the Appropriate Kato Sequences to a Certain Path

In order to calculate the energy contribution of a specific path correctly one has to know which Kato sequences belong to that path. To understand how one can identify the right sequence let us again look at the sequences of table 4.10 from the previous chapter. The first sequence (1,1,1,1,1) corresponds to a Kato term

$$(1, 1, 1, 1, 1) \implies \langle \mathbf{g} | V S_1 V S_1 V S_1 V S_1 V S_1 V | \mathbf{g} \rangle. \quad (4.20)$$

This term describes a path that never returns to the ground state until the very end, i.e. the situation where every site is occupied with exactly  $g$  bosons is only present before the first and after last hopping process.

The second sequence of table 4.10, which is (2,0,1,1,1) belongs to the Kato term

$$(2, 0, 1, 1, 1) \implies \langle \mathbf{g} | V S_2 V S_0 V S_1 V S_1 V S_1 V | \mathbf{g} \rangle. \quad (4.21)$$

As  $S_0 = -|\mathbf{g}\rangle\langle\mathbf{g}|$  (equation (3.5)) the sequence can be rewritten to

$$(2, 0, 1, 1, 1) \implies -\langle \mathbf{g} | V S_2 V | \mathbf{g} \rangle \langle \mathbf{g} | V S_1 V S_1 V S_1 V | \mathbf{g} \rangle. \quad (4.22)$$

The last equation tells us that the ground state is present not only before the first and after the last hopping process, but also after four hopping processes. Thus only paths that return to the ground state after four hoppings are being described by this Kato sequence.

What one has to do now is to compute if and after how many hopping processes a path returns to the ground state. Once this is known it is easy to pick the appropriate Kato sequence. It has to be noted however that one path could be described by several Kato sequences. The sequences 5 to 7 in table 4.10 for example describe paths that return to the ground state once after the first two hopping processes. So all three sequences have to be assigned to a path that recovers the ground state after two hoppings.

## 4.6 Evaluating the Energy

We now have everything needed to calculate the energy correction for every desired order assuming that we have enough computational power on our hands. We reduced all the paths that can occur on our lattice to topologically unique closed diagrams and we also computed all possible Kato sequences for a given order. Thus all we have to do now is put the information we gained together correctly to evaluate the energy correction.

### 1. Order of the hopping processes

Up until now we didn't concern ourselves with the chronological order in which the hopping processes occur. To finally calculate the energy contribution of each diagram we have to abandon this restriction. Therefore we have to take each diagram explicitly and permute the single hopping processes the diagram consists of in every possible way. In doing so we get a set of paths for every diagram.

### 2. Checking for intermediate ground states

In the second step we have to search each path for intermediate ground states and assign the appropriate Kato sequences to the paths. We cannot do this assignment for the whole set of a diagram at once, because the intermediate states of the paths do differ in general. To illustrate this let us take a look at figure 3.6 again.

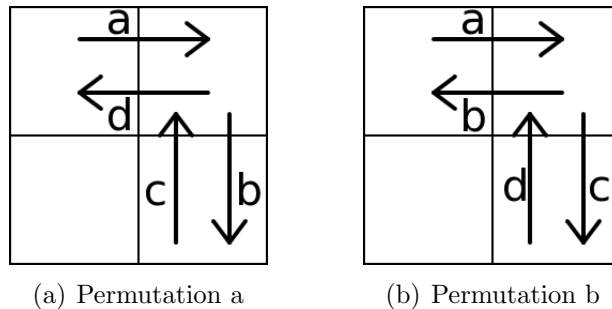


Figure 4.9: Two possible permutations of path 3.5(a).

As you can see, the first path (figure 4.9(a)) does not have the ground state as an intermediate state, whereas the second path (figure 4.9(b)) does recover the ground state after the first two hopping processes, although both do have the same topology.

Another fact that needs to be paid attention to is that a path can be described by several Kato sequences as has been explained in chapter 4.5, in which case all of these sequences have to be assigned to the path.

### 3. Evaluating the energy contribution of a path

Now we calculate the energy contribution of each path using the formula

$$\Delta E_{path}^{(n)} = \langle \mathbf{g} | V S_{k_1} V S_{k_2} V \dots V S_{k_{n-1}} V | \mathbf{g} \rangle \quad (4.23)$$

If several Kato sequences have been assigned to a specific path we evaluate equation (4.23) for each of these sequences and then take the sum of these energies:

$$\Delta E_{path}^{(n)} = \sum_{\{k_i\}} \langle \mathbf{g} | V S_{k_1} V S_{k_2} V \dots V S_{k_{n-1}} V | \mathbf{g} \rangle . \quad (4.24)$$

### 4. Energy of a diagram

At this point we have the energy contribution of every path of our set of paths belonging to a single diagram, so we have to sum up all these energy contributions. As one diagram represents several paths of the same topology on our lattice we also have to multiply this energy value with the multiplicity of the diagram. This leaves us with the energy contribution of all paths with the same topology.

### 5. Energy correction for the system

All of the above steps have to be executed for every diagram. Once we know the energy contributions of all the diagrams we can sum up all these contributions and thus get the energy correction of the  $n^{th}$  order for our system.

## 4.7 Results

In this section, a few results shall be presented that were achieved by using the Kato formalism. It is quite interesting to note, that the expansion coefficients  $\alpha^{(\nu)}$  we used in equation (3.21) to describe the energy do in fact grow almost exponentially, which can be seen in figure 4.10.

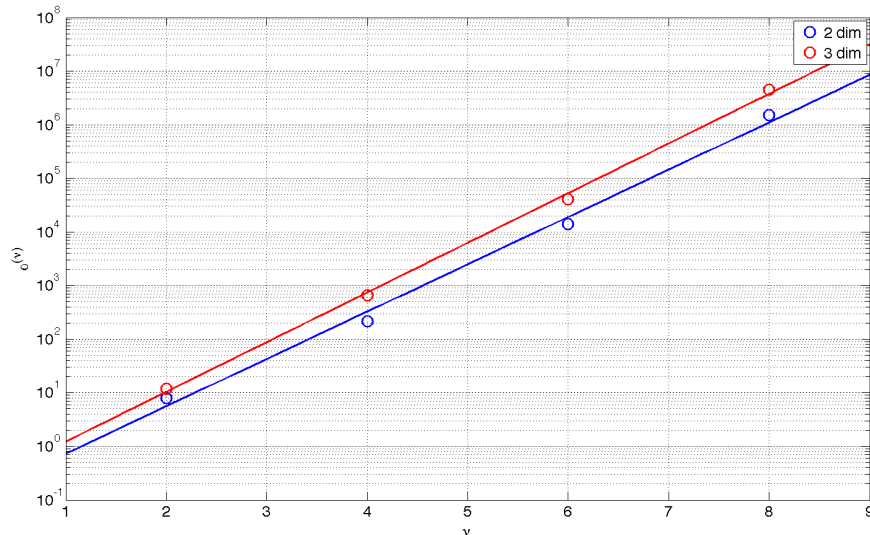


Figure 4.10: Exponential growth of the coefficients  $\alpha^{(\nu)}$ .

The dots represent the actual values of the coefficients, while the solid lines show a linear fit of those points. In this figure, blue stands for a system with 2 dimensions and red for a system with 3 dimensions. The case with a system of just 1 dimension is not shown here as the expansion coefficients for such a system do not show this strict exponential behavior.

Figure 4.11 shows the energy corrections  $\Delta E$  for systems with 1, 2 and 3 dimensions and unity filling factors as functions of the tunneling parameter  $t$ . As expected, at  $t = 0$  the energy correction is zero, as no tunneling of particles occurs and the system is therefor described by the unperturbed hamiltonian  $\hat{H}_0$ , whose energy  $E^{(0)}$  can be calculated exactly.

The bigger the hopping strength  $t$  gets, the bigger  $|\Delta E|$  becomes. One can also see, that while  $|\Delta E|$  for 1 dimension grows quite moderately, the curvature increases significantly for higher and higher dimensions.

In figure 4.12 one can see the energy correction for 2 and 3 dimensions and filling factors  $g = 1$  and  $g = 2$ . Note that when the abscissa is scaled with  $2d \cdot \sqrt{g(g+1)}$ , where  $d$  denotes the number of dimensions, the curves for the same number of dimensions, but with different filling factors, coincide, as is shown in figure 4.12

Another method to determine the correct energy of such a system is the Vari-

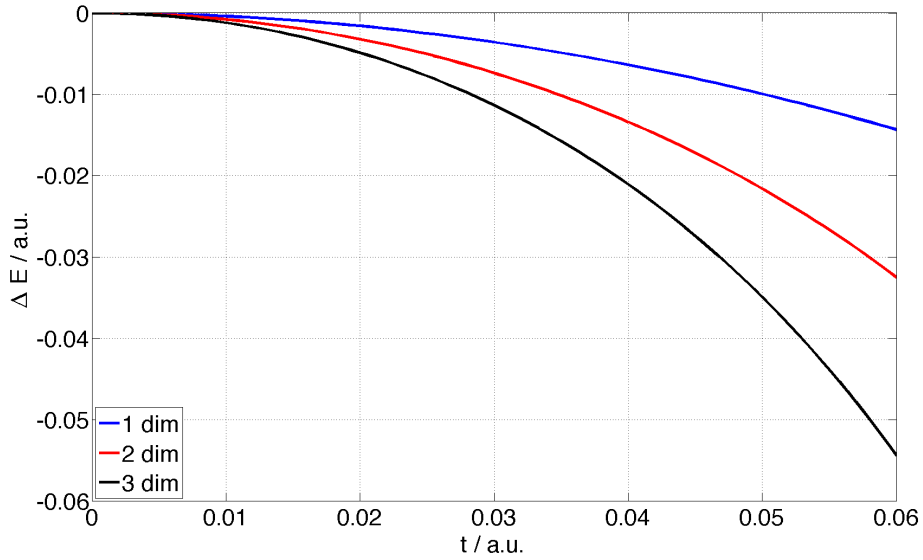


Figure 4.11: Energy corrections (up to 8<sup>th</sup> order) for 1, 2 and 3 dimensions and filling factor  $g = 1$ .

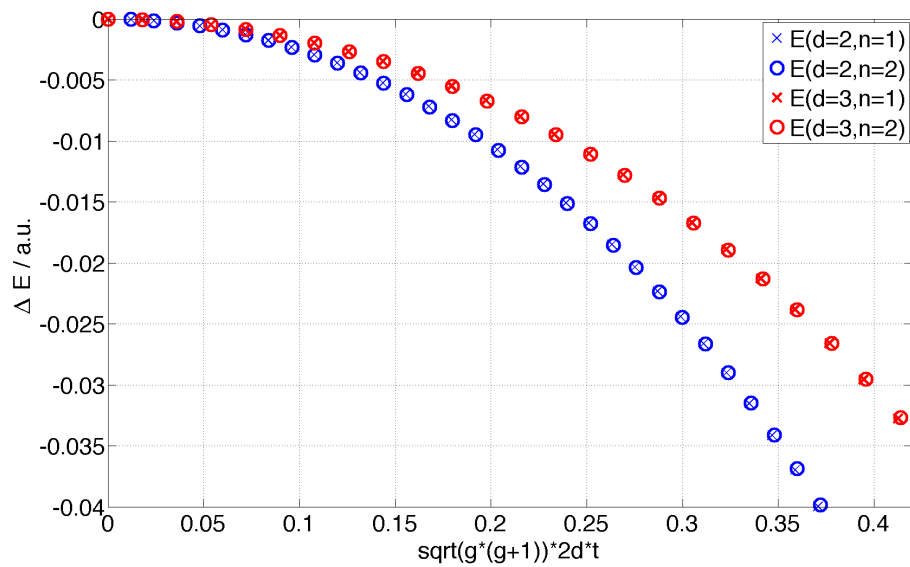


Figure 4.12: Energy correction up to 8<sup>th</sup> order for 2 and 3 dimensions with filling factors  $g = 1$  and  $g = 2$ .

ational Cluster Approach (VCA). As the name suggests, the bosonic lattice is divided in smaller clusters with this method. The determining equations for these small clusters can then be solved, in contrast to the equations of the whole systems, which are far too big for our recent computers. After solving the situation in the small clusters one then puts them back together to recover the complete system. The problem however is, that while hopping is allowed in the clusters, the particles can not tunnel between two different clusters, thus introducing an error to the computation. To keep this error as low as possible, the hopping between clusters is considered perturbatively after the cluster systems have been solved.

Figure 4.13 shows a comparison of results obtained with our Kato formalism and of results from a VCA computation. As one can see, the results with these two methods are in very good agreement with each other.

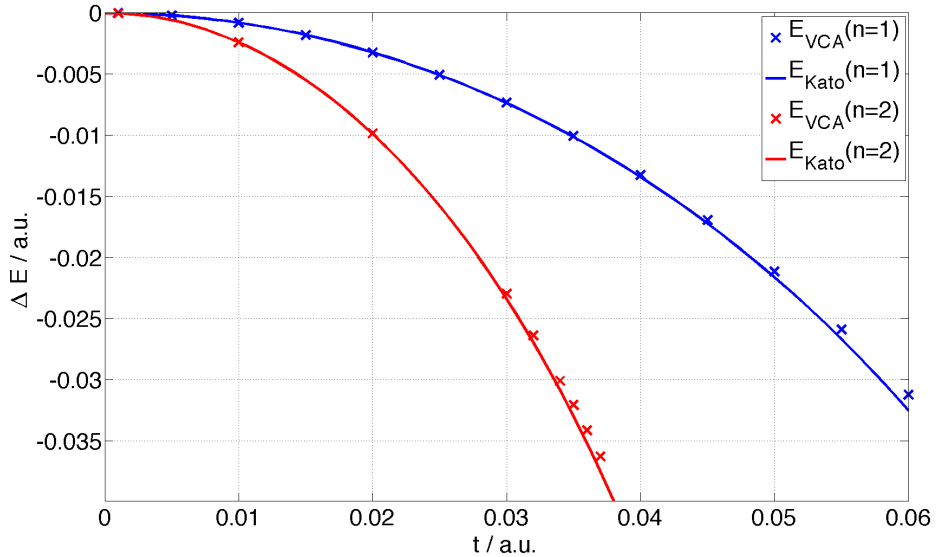


Figure 4.13: Computed energy corrections with the Kato approach (up to 8<sup>th</sup> order) for 1 dimension and filling factors  $g = 1$  and  $g = 2$  compared with results obtained with VCA.

# Chapter 5

## The Mott Insulator-Superfluid Phase Transition

### 5.1 Introduction

The behavior of a Bose-Hubbard system at zero temperature depends extremely on the ratio between hopping strength  $t$  and potential energy  $U$ . If  $U$  is very large in comparison to  $t$ , no hopping will occur at all in our sites, which is therefor in a Mott insulator state (MI). In such a state, all the particles are localized at the sites and there will be no particle "current".

On the other hand, when  $t$  is very large compared to  $U$ , the site potential will not notably affect the particles, which are then able to move freely in the volume of the material. This state, where the particles' wave function is spread across the whole volume is called a superfluid state (SF) [32]. Figure 5.1 shows a sketch of these two phases in dependency of the hopping parameter  $t$  and the chemical potential  $\mu$  in relation to the on-site potential  $U$ .

It is now of great interest to study the properties of these very different phases, in particular one is interested in the moment when a Mott insulator becomes a superfluid or vice versa. Simply speaking, when we start with  $t = 0$  and increase  $t$  continuously, there will be a specific value  $t_c$  for  $t$  where our system undergoes a transition from the Mott insulator phase to the superfluid one and it is this critical value we are interested in.

While many computational methods struggle a lot with the simultaneous description of both phases, the Kato formalism is very well suited for this task, as you will see in the subsequent pages. But before we can get to the actual implementation, we first have to develop the theoretical frame to deal with this problem, called the method of Effective Potential in the formulation of [33, 34].

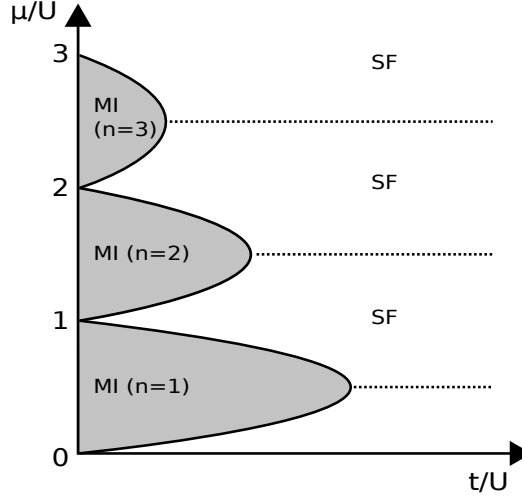


Figure 5.1: Schematic drawing of the Mott insulator and superfluid phases of a Bose-Hubbard at zero temperature as function of the hopping strength and the chemical potential.

## 5.2 Method of Effective Potential

Let us consider a hamiltonian that depends on a parameter  $\lambda$  and can be written as follows:

$$\hat{H}(\lambda) = \hat{H}_0 + \lambda \hat{H}_1 \quad (5.1)$$

The derivative of the partition function with respect to  $\lambda$  reads

$$\frac{\partial}{\partial \lambda} Z(\lambda) = \frac{\partial}{\partial \lambda} \text{Tr} \left( e^{-\beta(\hat{H}_0 + \lambda \hat{H}_1)} \right) \quad (5.2)$$

and, written as a total derivative of  $\lambda$ ,

$$\frac{\partial}{\partial \lambda} Z(\lambda) = \frac{1}{d\lambda} \left[ \text{Tr} \left( e^{-\beta(\hat{H}_0 + \lambda \hat{H}_1 + d\lambda)} \right) - \underbrace{\text{Tr} \left( e^{-\beta(\hat{H}_0 + \lambda \hat{H}_1)} \right)}_{Z(\lambda)} \right]. \quad (5.3)$$

To deal with this expression further, we use the Trotter decomposition first, since  $\hat{H}_0$  and  $\hat{H}_1$  do not commute, i.e.  $[\hat{H}_0, \hat{H}_1] \neq 0$ . Then we are going to factorize the terms for  $(\lambda + d\lambda)$  into  $e^{-\Delta\tau \hat{H}} e^{-\Delta\tau d\lambda \hat{H}_1}$ , i.e.:

$$\text{Tr} \left( e^{-\beta(\hat{H}_0 + \lambda \hat{H}_1 + d\lambda)} \right) = \text{Tr} \left( \prod_{\tau=1}^m e^{-\Delta\tau \hat{H}} e^{-\Delta\tau d\lambda \hat{H}_1} \right) \quad (5.4)$$

Next we rewrite our formula as a Taylor expansion in  $d\lambda$  up to first order. The leading order term is

$$\text{Tr} \left( \prod_{\tau=1}^m e^{-\Delta\tau \hat{H}} \cdot 1 \right) = Z(\lambda). \quad (5.5)$$

For the first order contribution we merely need a single one of the  $d\lambda$  terms, so only one out of the  $m$  factors contributes, while the others are equal to one, as the  $d\lambda$  term can originate from one of the  $m$  factors. Due to the cyclic invariance of the trace, all  $m$  terms yield the same result. This means, that in total we have a first order contribution of

$$-m\Delta\tau d\lambda \text{Tr} \left( \prod_{\tau=1}^m e^{-\Delta\tau \hat{H}} \hat{H}_1 \right) = -\beta d\lambda Z(\lambda) \langle \hat{H}_1 \rangle . \quad (5.6)$$

Higher order contributions vanish in the limit  $d\lambda \rightarrow 0$  and the final result reads

$$\frac{\partial}{\partial\lambda} Z(\lambda) = \frac{Z(\lambda) - \beta d\lambda Z(\lambda) \langle \hat{H}_1 \rangle - Z(\lambda)}{d\lambda} \quad (5.7)$$

$$= -\beta Z \langle \hat{H}_1 \rangle . \quad (5.8)$$

We can therefore write for the expectation value of  $\hat{H}_1$

$$\langle \hat{H}_1 \rangle = -\frac{1}{\beta} \frac{\partial}{\partial\lambda} Z(\lambda) \quad (5.9)$$

$$= \frac{\partial}{\partial\lambda} F(\lambda) . \quad (5.10)$$

The same reasoning also applies to a general parameter dependence, with the linearization  $\hat{H}(\lambda + d\lambda) = \hat{H}(\lambda) + d\lambda \frac{\partial}{\partial\lambda} \hat{H}(\lambda)$ .

This means that  $\hat{H}_1 = \frac{\partial}{\partial\lambda} \hat{H}(\lambda)$  and we obtain the thermodynamic version of the Hellmann-Feynman theorem

$$\frac{\partial}{\partial\lambda} F(\lambda) = \left\langle \frac{\partial}{\partial\lambda} H(\lambda) \right\rangle . \quad (5.11)$$

For our further calculations we stick to the linear case and consider the response of the expectation value  $\langle \hat{H}_1 \rangle$  to changes of  $\lambda$ , which is a susceptibility

$$\chi := \frac{\partial}{\partial\lambda} \langle \hat{H}_1 \rangle \quad (5.12)$$

$$= \frac{\partial}{\partial\lambda} \langle \hat{H}_1 \rangle . \quad (5.13)$$

We also want to introduce the hamiltonian that governs our system in the superfluid phase:

$$\tilde{H}(\eta, \eta^*) = \hat{H}_0 + \hat{H}_{hop} + \sum_i \left( \eta^* \hat{a}_i + \eta \hat{a}_i^\dagger \right) , \quad (5.14)$$

where  $\hat{H}_0$  and  $\hat{H}_{hop}$  are the already well known operators we introduced in equation (2.3). The third term is the effective potential which takes into account that our system may have sources and drains, i.e.  $\hat{a}_i$  annihilates a

particle at site  $i$  with probability  $\eta^*$  and  $\hat{a}_i^\dagger$  creates a particle at site  $i$  with strength  $\eta$ .

Each system tries to minimize its energy, thus before anything else we have to know, how the free energy of this new system described by equation (5.14) looks like.

### 5.2.1 Power Series Representation of the Partition Function $Z$ and the Free Energy $F$

As the hamiltonian of equation (5.14) depends strongly on the drain and source strength  $\eta^*$  and  $\eta$  we will write the partition function  $Z$  as a power series in  $\eta$  about  $\eta = 0$ , as  $\eta = 0$  represents the case of the unperturbed hamiltonian.

$$\tilde{H} = \underbrace{\hat{H}_0 + \hat{H}_{hop}}_{\tilde{H}_0} + \underbrace{\sum_i (\eta^* \hat{a}_i + \eta \hat{a}_i^\dagger)}_{\tilde{H}_1}$$

We also want to combine the sum of operators into a single operator to make the coming formulae easier to read

$$\begin{aligned} \tilde{H}_1 &= \eta \underbrace{\sum_i \hat{a}_i^\dagger}_{=: \hat{A}^\dagger} + \eta^* \underbrace{\sum_i \hat{a}_i}_{=: \hat{A}} \\ &= \eta \hat{A}^\dagger + \eta^* \hat{A} . \end{aligned} \quad (5.15)$$

$$(5.16)$$

The expectation value of an operator  $\hat{O}$  for the unperturbed system can be written as

$$\langle \hat{O} \rangle_0 = \frac{1}{Z_0} \text{Tr} \left( \hat{O} e^{-\beta \tilde{H}_0} \right) \quad (5.17)$$

with

$$Z_0 = \text{Tr} \left( e^{-\beta \tilde{H}_0} \right) . \quad (5.18)$$

Obviously, due particle number conservation in  $\tilde{H}_0$ , following equation has to hold

$$\langle \hat{A} \rangle_0 = \langle \hat{A}^\dagger \rangle_0 = 0 . \quad (5.19)$$

A term  $\eta^n (\eta^*)^m$  in the power series implies  $n$  factors of  $\hat{A}$  and  $m$  factors of  $\hat{A}^\dagger$  in a trace which otherwise contains Boltzmann factors  $e^{-\tau \tilde{H}_0}$ . Since  $\tilde{H}_0$  is the bare Bose Hubbard hamiltonian, the particle number has to be conserved.

This means, that  $m = n$ , as otherwise the number of particles in our system would change. Hence, the power series is of the form

$$Z = Z_0 + \sum_{i=1}^{\infty} Z_{2i} |\eta|^{2i} . \quad (5.20)$$

Since  $[\tilde{H}_0, \tilde{H}_1] \neq 0$  we need the Trotter decomposition first before we can go on with our calculations:

$$Z(\eta, \eta^*) = \text{Tr} \left( \prod_{l=1}^m e^{-\Delta\tau \tilde{H}_0} e^{-\Delta\tau (\eta \hat{A}^\dagger + \eta^* \hat{A})} \right) . \quad (5.21)$$

We are merely interested in terms up to order  $|\eta|^4$ , i.e. second order in  $\eta$  as well as in  $\eta^*$ .

Let's go through this order by order:

- The leading order  $|\eta|^0$  is given by  $Z_0 = Z(\eta = 0, \eta^* = 0)$ .
- The first order vanishes.
- There are  $m$  factors which can contribute parts or all of the  $\hat{A}^\dagger$  and  $\hat{A}$  operators. So in second order we need to gather one factor  $\hat{A}$  and one factor  $\hat{A}^\dagger$ . There are  $m$  sites for each one of them. Hence, there are  $m^2$  terms contributing and each term is of the order  $O(\Delta\tau)^2 = O((1/m)^2)$  and therefore the result is of the order  $O(1)$ .

The term where both operators stem from the same Trotter time is of the order  $O(1/m)$ , as there are  $m$  time slots and each term is of the order  $O((1/m)^2)$ . We can therefore ignore this case in the limit  $m \rightarrow \infty$ . That is, we consider the case, that the two operators belong to different Trotter times, say  $l_1$  and  $l_2$  ( $l_1 < l_2$ ), and we merely need the first order term of the power series for the times under consideration.

All other time slots contribute a factor of 1 from the powers series of  $e^{-\Delta\tau \tilde{H}_1}$ . The first Trotter time  $l_1$  can contribute  $\hat{A}$  or  $\hat{A}^\dagger$ , likewise the second Trotter time  $l_2$ . So we have the cases:

$$\begin{aligned} & \hat{A} \text{ at } l_1 \quad \text{and} \quad \hat{A}^\dagger \text{ at } l_2 \\ \text{or} \quad & \hat{A}^\dagger \text{ at } l_1 \quad \text{and} \quad \hat{A} \text{ at } l_2 . \end{aligned}$$

Hence  $\hat{A}$  can occur at  $l_1$  or at  $l_2$  with  $\hat{A}^\dagger$  at the opposite position. So, along with the definition  $\hat{U} = e^{-(l_1-1)\Delta\tau \tilde{H}_0}$  we have

$$Z_2 = (\Delta\tau)^2 \sum_{\substack{l_1, l_2 \\ l_1 \neq l_2}} \text{Tr} \left( \hat{U} \cdot \hat{U} \overbrace{\hat{A}^\dagger}^{\text{position } l_1} \hat{U} \cdot \hat{U} \overbrace{\hat{A}}^{\text{position } l_2} \hat{U} \cdot \hat{U} \right) . \quad (5.22)$$

By virtue of the cyclic invariance, we can get  $\hat{A}$  to the very right position, making the summation independent of  $l_2$ , while  $l_1$  runs from 1 to  $m - 1$

$$Z_2 = m \left( \frac{\beta}{m} \right)^2 \cdot \sum_{l=1}^{m-1} \text{Tr} \left( \hat{U} \cdot \hat{U} \overbrace{\hat{A}^\dagger}^{\text{position } l} \hat{U} \cdot \hat{U} \hat{A} \right). \quad (5.23)$$

We do not include the case where  $l = m$ , as it has a vanishing contribution, leaving us with

$$Z_2 = \beta \Delta \tau \sum_{l=1}^m \text{Tr} \left( \hat{U}^{l-1} \hat{A}^\dagger \hat{U}^{m-l+1} \hat{A} \right).$$

Substituting  $m - l + 1$  with  $n$  gives us

$$Z_2 = \beta \Delta \tau \sum_{n=1}^m \text{Tr} \left( \hat{U}^{m-n} \hat{A}^\dagger \hat{U}^n \hat{A} \right)$$

and after sliding in  $\mathbb{1} = \hat{U}^n \hat{U}^{-n}$

$$Z_2 = \beta \Delta \tau \sum_{n=1}^m \text{Tr} \left( \hat{U}^{m-n} \hat{U}^n \hat{U}^{-n} \hat{A}^\dagger \hat{U}^n \hat{A} \right).$$

Finally we use the cyclic invariance of the trace and in that way get to the expression

$$\begin{aligned} Z_2 &= \beta \sum_{n=1}^m \text{Tr} \left( \hat{U}^m \hat{U}^{-n} \hat{A}^\dagger \hat{U}^n \hat{A} \right) \Delta \tau \\ &= \beta Z_0 \int_0^\beta \langle \hat{A}^\dagger(\tau) \hat{A} \rangle d\tau \end{aligned} \quad (5.24)$$

with

$$\hat{A}^\dagger(\tau) := e^{\tau \tilde{H}_0} \hat{A}^\dagger e^{-\tau \tilde{H}_0}. \quad (5.25)$$

If we incorporate any non-vanishing contribution up to second order we now have

$$Z = Z_0 \left( 1 + \beta |\eta|^2 \int_0^\beta \langle \hat{A}^\dagger(\tau) \hat{A} \rangle d\tau \right). \quad (5.26)$$

In the limit  $|t|/U \rightarrow 0$  the integral is easy to evaluate. With  $\hat{A}^\dagger = \sum_i \hat{a}_i^\dagger$  and  $\hat{A} = \sum_j \hat{a}_j$  it reads

$$\begin{aligned} \int_0^\beta \langle \hat{A}^\dagger(\tau) \hat{A} \rangle d\tau &= \sum_{ij} \int_0^\beta \underbrace{\langle \hat{a}_i^\dagger(\tau) \hat{a}_j \rangle}_{\propto \delta_{ij}} d\tau \\ &= \sum_i \int_0^\beta \langle \hat{a}_i^\dagger(\tau) \hat{a}_i \rangle d\tau . \end{aligned} \quad (5.27)$$

From basic quantum mechanics we know that the time derivative of an operator, in our case  $\hat{a}_i^\dagger$  can be written as

$$\frac{d}{d\tau} \hat{a}_i^\dagger = e^{\tau \tilde{H}_0} [\tilde{H}_0, \hat{a}_i^\dagger] e^{-\tau \tilde{H}_0} , \quad (5.28)$$

and to evaluate the above expression we first have to compute the commutator of  $\tilde{H}_0$  and  $\hat{a}_i^\dagger$

$$\begin{aligned} [\tilde{H}_0, \hat{a}_i^\dagger] &= U[\hat{n}_i(\hat{n}_i - 1), \hat{a}_i^\dagger] \\ &= U(\hat{n}_i[(\hat{n}_i - 1), \hat{a}_i^\dagger] + [\hat{n}_i, \hat{a}_i^\dagger](\hat{n}_i - 1)) \\ &= U(\hat{n}_i \hat{a}_i^\dagger + \hat{a}_i^\dagger(\hat{n}_i - 1)) \\ &= 2U \hat{a}_i^\dagger \hat{n}_i . \end{aligned} \quad (5.29)$$

Going back to equation (5.27) we now have

$$\langle \hat{a}_i^\dagger(\tau) \hat{a}_i \rangle = \frac{1}{Z} \sum_{\{n_i\}} e^{-\beta \sum_l E(n_l)} \prod_{l \neq i} \langle n_l | | n_l \rangle \langle n_i | \hat{a}_i^\dagger(\tau) \hat{a}_i | n_i \rangle \quad (5.30)$$

and with the definition of  $Z$

$$\begin{aligned} \langle \hat{a}_i^\dagger(\tau) \hat{a}_i \rangle &= \frac{\prod_{l \neq i} \left( \sum_{n_l} e^{-\beta E(n_l)} \right) \sum_{n_i} e^{-\beta E(n_i)} \langle n_i | \hat{a}_i^\dagger(\tau) \hat{a}_i | n_i \rangle}{\prod_l \left( \sum_{n_l} e^{-\beta E(n_l)} \right)} \\ &= \frac{\sum_{n=0}^{\infty} e^{-\beta E(n)} \langle n | \hat{a}_i^\dagger(\tau) \hat{a}_i | n \rangle}{\sum_n e^{-\beta E(n)}} . \end{aligned} \quad (5.31)$$

To get equation (5.31) in a more compact form we take a closer look at the scalar product  $\langle n | \hat{a}_i^\dagger(\tau) \hat{a}_i | n \rangle$  to simplify the expression

$$\begin{aligned} \langle n | \hat{a}_i^\dagger(\tau) \hat{a}_i | n \rangle &= \langle n | e^{\tau \tilde{H}_0} \hat{a}_i^\dagger e^{-\tau \tilde{H}_0} \hat{a}_i | n \rangle \\ &= e^{\tau E(n)} e^{-\tau E(n-1)} \langle n | \hat{a}_i^\dagger \hat{a}_i | n \rangle \\ &= n e^{\tau(E(n) - E(n-1))} . \end{aligned} \quad (5.32)$$

The energy difference  $E(n) - E(n-1)$ , that appears in the exponent can be cooked down to a more comprehensible form too, as these energies are the already known eigenvalues of the unperturbed hamiltonian, i.e.

$$\begin{aligned} E(n) - E(n-1) &= \frac{U}{2}n(n-1) - \mu n - \frac{U}{2}(n-1)(n-2) + \mu(n-1) \\ &= \frac{U}{2}(n^2 - n - n^2 + 3n - 2) - \mu \\ &= U(n-1) - \mu . \end{aligned} \quad (5.33)$$

So if we plug equation (5.33) into equation (5.32) for the scalar product  $\langle n|\hat{a}^\dagger(\tau)\hat{a}|n\rangle$ , we end up with

$$\langle n|\hat{a}^\dagger(\tau)\hat{a}|n\rangle = ne^{\tau(U(n-1)-\mu)} , \quad (5.34)$$

which means, that the initial equation (5.31) for the expectation value  $\langle \hat{a}_i^\dagger(\tau)\hat{a}_i \rangle$  can finally be written as

$$\langle \hat{a}_i^\dagger(\tau)\hat{a}_i \rangle = \frac{\sum_{n=0}^{\infty} ne^{\tau(U(n-1)-\mu)} \cdot e^{-\beta E(n)}}{\sum_n e^{-\beta E(n)}} \quad (5.35)$$

- The fourth order term has 4 operators (twice  $\hat{A}$  and twice  $\hat{A}^\dagger$ ) at Trotter times  $l_1, \dots, l_4$ .  
If 2 Trotter times are identical, then there are  $\binom{m}{3} < m^3$  possibilities, while the prefactor is  $m^{-4}$ . As in the second order case, there is only a non vanishing contribution if the operators stem from different Trotter times.

We have now finally arrived at a point where we can write down an expression for our free energy  $F$

$$F = -\frac{1}{\beta} \ln Z \quad (5.36)$$

$$= -\frac{1}{\beta} \ln \left[ Z_0(1 + C_2 |\eta|^2 + C_4 |\eta|^4 + O(|\eta|^6)) \right] . \quad (5.37)$$

To simplify the notation we set  $\epsilon := |\eta|^2$ :

$$\begin{aligned} F &= \underbrace{-\frac{1}{\beta} \ln Z_0}_{=F_0} - \frac{1}{\beta} \ln \left[ 1 + C_2 \epsilon + C_4 \epsilon^2 + O(\epsilon^3) \right] \\ &= F_0 - \frac{1}{\beta} \left[ (C_2 \epsilon + C_4 \epsilon^2 + O(\epsilon^3)) - \frac{1}{2} (C_2 \epsilon + C_4 \epsilon^2 + O(\epsilon^3))^2 + O(\epsilon^3) \right] \\ &= F_0 - \frac{1}{\beta} \left[ C_2 \epsilon + C_4 \epsilon^2 - \frac{1}{2} C_2^2 \epsilon^2 + O(\epsilon^3) \right] \\ &= F_0 - \frac{1}{\beta} \left[ C_2 \epsilon + \left( C_4 - \frac{C_2^2}{2} \right) \epsilon^2 + O(\epsilon^3) \right] \end{aligned} \quad (5.38)$$

### 5.2.2 Developing a Phase Boundary Criterion

The considerations of the last section lead us to an expression for the free energy per site of the form:

$$f(\eta, \eta^*) = f_0 + \sum_{n=1}^{\infty} c_{2n} |\eta|^{2n} \quad (5.39)$$

and as we are only interested in terms up to fourth order we have

$$f(\eta, \eta^*) = f_0 + c_2 |\eta|^2 + c_4 |\eta|^4 . \quad (5.40)$$

The coefficients  $c_{2n}$  that appear in equation (5.39) are defined by following power series as functions of the hopping parameter  $t/U$ , similarly to the power series expansion of the energy in chapter 3:

$$c_{2n} = \sum_{\nu=0}^{\infty} \alpha_{2n}^{(\nu)} \left( \frac{t}{U} \right)^{\nu} \quad (5.41)$$

Hence the order parameter  $\psi$  and  $\psi^*$  can be defined as follows:

$$\begin{aligned} \psi &:= \langle \hat{a}_i \rangle_{\eta} = \frac{\partial}{\partial \eta^*} f(\eta) \\ &= c_2 \eta + 2c_4 |\eta|^2 \eta \\ &= (c_2 + 2c_4 |\eta|^2) \eta . \end{aligned} \quad (5.42)$$

Next we perform a legendre transform

$$\begin{aligned} \Gamma(\psi, \psi^*) &:= f(\eta, \eta^*) - \psi \eta^* - \psi^* \eta \\ &= f_0 + c_2 |\eta|^2 + c_4 |\eta|^4 - 2(c_2 + 2c_4 |\eta|^2) |\eta|^2 \\ &= f_0 - c_2 |\eta|^2 - 3c_4 |\eta|^4 . \end{aligned} \quad (5.43)$$

No we use (5.42) in order to determine  $x := |\eta|^2$  in terms of  $y := |\psi|^2$

$$\begin{aligned} y &= (c_2 + 2c_4 x)^2 x \\ x &= \frac{1}{(c_2 + 2c_4 x)^2} y \\ &= \frac{y}{c_2^2} \frac{1}{\left(1 + \frac{2c_4}{c_2} x\right)^2} \\ &= \frac{y}{c_2^2} \left(1 - \frac{4c_4}{c_2} x + 3x^2\right) . \end{aligned} \quad (5.44)$$

We use the last equation as iteration scheme to generate  $x(y)$  up to order  $y^2$

$$x^{(n+1)} = \frac{y}{c_2^2} \left(1 - \frac{4c_4}{c_2} x^{(n)} + 3(x^{(n)})^2\right) . \quad (5.45)$$

Obviously,  $x = O(y)$ . Therefore, the third term in the iteration scheme can be dropped as it would produce in total a correction of order  $O(y^3)$ . In summary the iteration reduces to

$$\begin{aligned} x^{(n+1)} &= \frac{y}{c_2^2} \left( 1 - \frac{4c_4}{c_2} x^{(n)} \right) \\ &= \frac{y}{c_2^2} - \frac{4c_4}{c_2} \frac{y}{c_2^2} x^{(n)}. \end{aligned} \quad (5.46)$$

$x^{(n)}$  on the right hand side has only to be correct up to order  $O(y)$ . Starting with  $x^{(0)} = 0$ , the first iteration yields  $x^{(1)} = \frac{y}{c_2^2}$ . The next iteration leaves us with

$$x^{(2)} = \frac{y}{c_2^2} - \frac{4c_4}{c_2} \left( \frac{y}{c_2^2} \right)^2. \quad (5.47)$$

Further iterations are not necessary, since  $x^{(1)}$  was already correct in order  $O(y)$ . So we have

$$\begin{aligned} |\eta|^2 &= x \\ &= \frac{|\psi|^2}{c_2^2} - \frac{4c_4}{c_2^5} |\psi|^4 + O(|\psi|^6), \end{aligned} \quad (5.48)$$

and furthermore

$$|\eta|^4 = \frac{|\psi|^4}{c_2^4} + O(|\psi|^6). \quad (5.49)$$

If we now insert these expression in the Legendre transform (5.43), we get

$$\begin{aligned} \Gamma(\psi, \psi^*) &= \underbrace{f_0}_{:=\Gamma_0} - c_2 \left( \frac{|\psi|^2}{c_2^2} - \frac{4c_4}{c_2^5} |\psi|^4 \right) - 3c_4 \frac{|\psi|^4}{c_2^4} + O(|\psi|^6) \\ &= f_0 - \frac{|\psi|^2}{c_2} + \frac{4c_4}{c_2^4} |\psi|^4 - 3\frac{c_4}{c_2^4} |\psi|^4 + O(|\psi|^6) \\ &= f_0 - \frac{|\psi|^2}{c_2} + \frac{c_4}{c_2^4} |\psi|^4 + O(|\psi|^6). \end{aligned} \quad (5.50)$$

For sufficiently small  $|\psi|$ , which is the case near the quantum phase transition, we can ignore the terms  $O(|\psi|^6)$ , leaving us with

$$\Gamma(\psi, \psi^*) = \Gamma_0 - \frac{|\psi|^2}{c_2} + \frac{c_4}{c_2^4} |\psi|^4. \quad (5.51)$$

Figure 5.2 shows the Legendre transform  $\Gamma$  for two specific cases. The blue line represents a case with  $c_2 > 0$ , i.e. the superfluid regime and the red line depicts the Mott insulator regime where  $c_2 < 0$ .

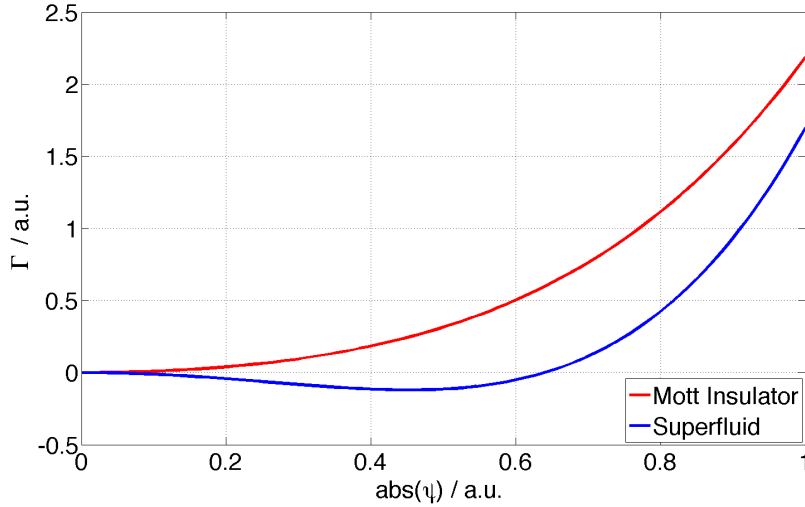


Figure 5.2: The Legendre transform  $\Gamma$  for positive  $c_2$  (blue line) and negative  $c_2$  (red line).

Because  $\eta$  and  $\psi^*$ , as well as  $\eta^*$  and  $\psi$  are Legendre pairs, one also has the identities

$$\begin{aligned}\frac{\partial \Gamma}{\partial \psi^*} &= -\eta \\ \frac{\partial \Gamma}{\partial \psi} &= -\eta^*.\end{aligned}$$

The original system is recovered for  $\eta = \eta^* = 0$ . Hence  $\frac{\partial \Gamma}{\partial \psi} = 0$  as well as  $\frac{\partial \Gamma}{\partial \psi^*} = 0$  has to hold true, i.e.  $\Gamma$  has to be stationary with respect to  $\psi$ . In other words the original system adopts that value of  $\psi$  that leads to a constant  $\Gamma$ .  $\Gamma$  has the meaning of an energy, hence the name 'effective potential'. As long as  $\mu/U$  in the Bose-Hubbard model is not an integer, one finds  $c_2 < 0$  for very small hopping strengths  $t$ , while  $c_4 > 0$  (see [18]).

So the potential is of the form

$$\Gamma = \Gamma_0 + a |\psi|^2 + b |\psi|^4 \quad (5.52)$$

with the coefficients  $a$  and  $b$ . The derivative  $d\Gamma/d|\psi| = 2a|\psi| + 4b|\psi|^3$  becomes zero for  $|\psi| = 0$  and for the negative value  $|\psi|^2 = -a/(2b)$ , which is therefore not allowed. Hence in this case the order parameter vanishes and there is no superfluid solution, i.e. no long range phase coherence. The parameter  $c_4$  is always positive and so is  $b$ .

But for increasing hopping strength,  $c_2$  and likewise  $a$  become negative. In that case, there exists a finite order parameter solution, which reduces the effective potential and in turn free energy, so it is the physical solution.

The order parameter then reads

$$|\psi|^2 = -\frac{a}{2b}. \quad (5.53)$$

So obviously the phase transition occurs when  $a$  changes sign, or rather when  $a$  vanishes which is the case when  $c_2 = 1/a$  diverges.

### 5.3 Consequences for the Kato Formalism

Now that we have developed all the theory needed, we can start thinking about how to alter our current Kato formalism in order to calculate the Mott insulator-superfluid phase boundary.

By taking a closer look at equation (5.39) which shall be rewritten here for ease of reading,

$$f(\eta, \eta^*) = f_0 + \sum_{n=1}^{\infty} c_{2n} |\eta|^{2n}$$

one realizes, that  $\eta$  and  $\eta^*$  only occur as powers of the square of the absolute value. As  $\eta$  is the probability with which a particle is created and  $\eta^*$  the probability of annihilating a particle, this means that the system we have to consider has the same amount of drains and sources. Therefore, after all hopping, creation and annihilation processes have occurred, our system has the same amount of particles as before.

But as we still have sequences that start with the ground state  $\langle \mathbf{g} |$  and end with the ground state  $|\mathbf{g}\rangle$ , i.e.  $\langle \mathbf{g} | V S_{k_1} V S_{k_2} \dots V S_{k_{n-1}} V | \mathbf{g} \rangle$ , the constraint, that the ground state has to be present before and after all perturbation processes has to be present, still has to hold. We are only interested in the point, where  $c_2$  of equation (5.40) changes sign, thus we have a system where only one source and one drain are present, according to equation (5.41).

Equation (5.41) can be seen as a power series in the form:

$$f(z) = \sum_{\nu=0}^{\infty} b_{\nu} z^{\nu}, \quad (5.54)$$

whose convergence radius is given by d'Alembert's law (see for example [35]):

$$R(f(z)) = \lim_{\nu \rightarrow \infty} \left| \frac{b_{\nu-1}}{b_{\nu}} \right| \quad (5.55)$$

The expansion coefficients  $b_{\nu}$  here correspond to the  $\alpha_2^{(\nu)}$  in the case of  $c_2$ . These  $\alpha_2^{(\nu)}$  can be obtained by computing the energy of all paths with one drain and one source and  $\nu$  hopping processes that start and end with the ground state (see figure 5.3).

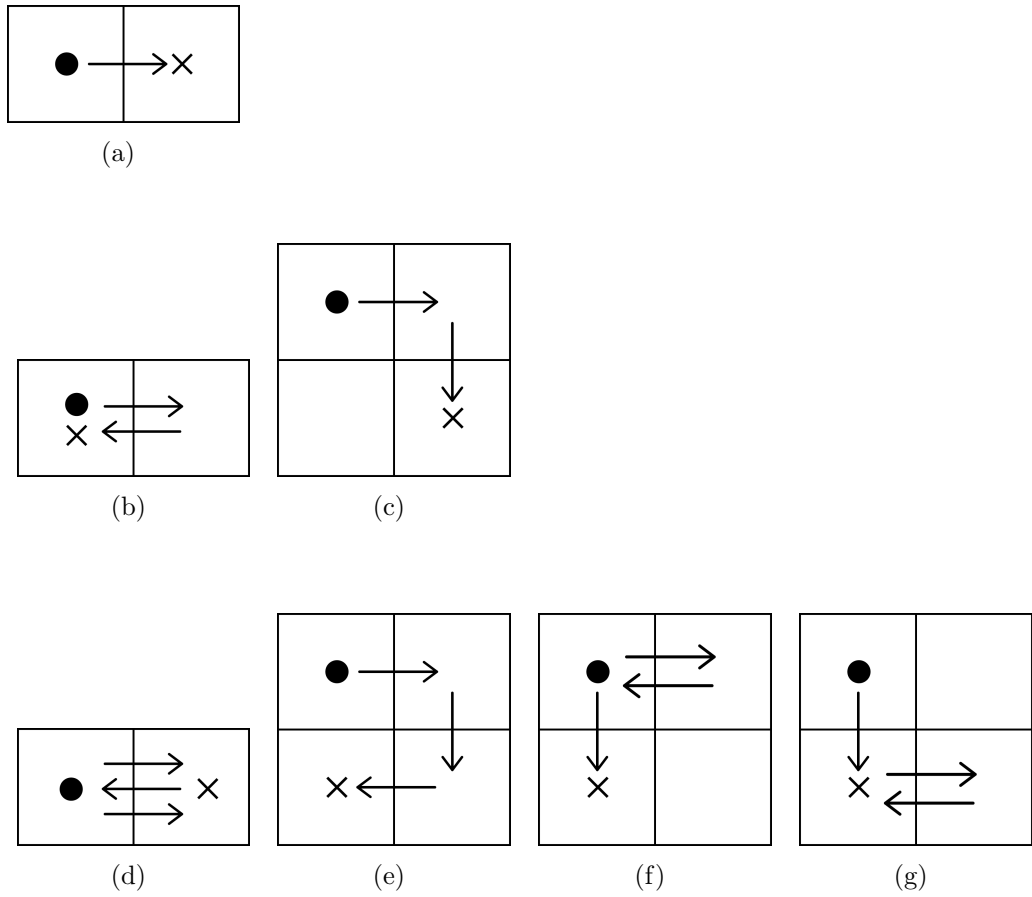


Figure 5.3: All paths up to third order with one source, depicted by a solid circle, and one drain, marked with  $\times$ , that have a non-vanishing contribution.

### 5.3.1 Changes in the Path Creation and Identification

The energy evaluation of our computation algorithm therefor stays the same, we only have to adjust the path creation in a way that all paths with one source and one drain are created that start with the ground state and end with it too. Additionally the way of identifying topologically identical paths has to be altered too.

For the creation of the paths we used a straight forward approach: First one assigns numbers to the directions one can take in our  $n$ -dimensional lattice. In case of a 2 dimensional lattice one could for example assign a hopping to the right to the number 1, a hopping to the left to 2, hopping up to 3 and down to 4, as we already did in chapter 4.1.

Now one just calculates every possible permutation of  $N_0$  sites that can all take the values from 1 to 4. This results in  $N = (2d)^{N_0}$  paths, where  $d$  denotes the number of dimensions. So in case of  $N_0 = 2$  and two dimensions, one gets the 16 permutations shown in table 5.1

Table 5.1: All possible paths consisting of 2 hoppings on a 2 dimensional lattice.

1.	1	1	9.	3	1
2.	1	2	10.	3	2
3.	1	3	11.	3	3
4.	1	4	12.	3	4
5.	2	1	13.	4	1
6.	2	2	14.	4	2
7.	2	3	15.	4	3
8.	2	4	16.	4	4

Now one has to deduce where the source and where the drain are. A very easy way to do this is calculate the adjacency matrices of each path, as these matrices tell us how many hoppings go to site  $i$  and how many off site  $i$ . If more particles hop away from site  $i$  then to it, there has to be a source at site  $i$ . On the other hand it is clear that if more particles hop to site  $i$  then away from it there has to be a drain at  $i$ , otherwise the ground state cannot be present at the end of the perturbation process (see figure 5.3(c)).

If there is a path, where at each site as many particles hop away as hop to it, the drain and source have to be at the same site of course, but they can be at each visited site. This is shown for example in figure 5.3(b). Here the source and drain have to be at the same site, but they could either be on the left or on the right site.

Without the information about the source and the drain, the graphs shown in figures 5.3(f) and 5.3(g) would be topologically identical. But with the

source and the drain added to the paths, they are in fact topologically unique as there are configurations that can only be produced by path 5.3(f) and vice versa. This means, that the algorithm we devised in chapter 4.3 would eliminate paths we need to calculate the coefficients correctly.

Luckily there is a very easy solution. What one does is add 1 to the  $i, i$  entry of adjacency matrix for a source at site  $i$  and 2 to the position  $j, j$  for a drain at size  $j$ . Let us go through this with some simple examples.

The bond representation we already used to deal with the diagrams for calculating the energy in chapter 4.1 of the path depicted in figure 5.4 can be written as follows:

Table 5.2: Bond representation of path figure 5.4

	i	j
1.	1	2
2.	2	1
3.	1	3

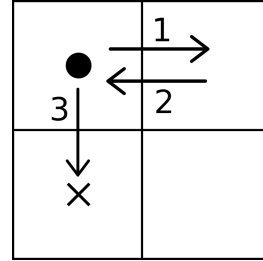


Figure 5.4: One possible permutation of path 5.3(f)

The adjacency matrix of this particular path  $M_{old}$  now looks as follows

$$M_{old} = \begin{pmatrix} 0 & 1 & 1 \\ 1 & 0 & 0 \\ 0 & 0 & 0 \end{pmatrix} .$$

As we have said above, we have to add 1 to the entry of the source site and 2 for the drain. Hence, our new adjacency matrix  $M_{new}$  is of the form

$$M_{new} = \begin{pmatrix} 1 & 1 & 1 \\ 1 & 0 & 0 \\ 0 & 0 & 2 \end{pmatrix} .$$

By adding information about the position of the drain and source it is now impossible to alter this new adjacency matrix by pure renumbering of the sites to look the same as the adjacency of the path depicted in figure 5.3(g). This way we are again in a position where we have a very simple, yet powerful method to distinguish between topologically unique paths.

As before with the energy computation we calculate every possible site-permutation and compare the adjacency matrices of these paths with the matrices of the diagrams we already identified as unique. If no permutation can be found that has the same adjacency matrix as the previously obtained

paths it is topologically unique and has to be added to our list of diagrams. Let us apply the same procedure to two more paths to make this procedure perfectly clear:

Table 5.3: Bond representation of path figure 5.5.

	i	j
1.	1	2
2.	2	3
3.	3	4

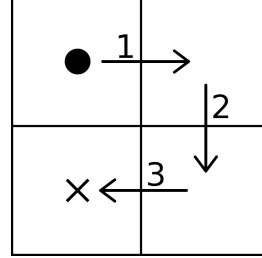


Figure 5.5: One possible permutation of path 5.3(e).

$$M_{old} = \begin{pmatrix} 0 & 1 & 0 & 0 \\ 0 & 0 & 1 & 0 \\ 0 & 0 & 0 & 1 \\ 0 & 0 & 0 & 0 \end{pmatrix} \implies M_{new} = \begin{pmatrix} 1 & 1 & 0 & 0 \\ 0 & 0 & 1 & 0 \\ 0 & 0 & 0 & 1 \\ 0 & 0 & 0 & 2 \end{pmatrix} \quad (5.56)$$

But what if the source and the drain are actually at the same site? In that case we can still apply the same rules as above, and thus end up with adding 3 to the position of the source and drain in the adjacency matrix.

Table 5.4: Bond representation of path figure 5.6.

	i	j
1.	1	2
2.	2	3
3.	3	4

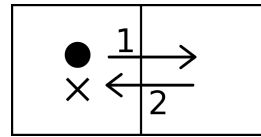
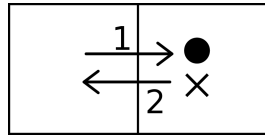


Figure 5.6: One possible permutation of path 5.3(c).

$$M_{old} = \begin{pmatrix} 0 & 1 \\ 1 & 0 \end{pmatrix} \implies M_{new} = \begin{pmatrix} 3 & 1 \\ 1 & 0 \end{pmatrix} \quad (5.57)$$

If we now have a path that has the same hopping processes in the same order as that of path in figure 5.6, but with source and drain on the right site, as seen in figure 5.7, the adjacency matrix of that path would be that



$$\implies M_{new} = \begin{pmatrix} 0 & 1 \\ 1 & 3 \end{pmatrix} \quad (5.58)$$

Figure 5.7: Path with the same hopping processes but with source and drain at the other site than in path 5.6

of equation (5.58)

By simply renumbering the sites in a way that the left site is now number 2 and the right site 1 we get an adjacency matrix that looks the same as the one in equation (5.57). This means, that the translational redundancy of these two paths has been detected successfully and our algorithm works as we intended it to do.

To conclude this section, table 5.5 shows the number of topologically unique diagrams as a function of the order  $\nu$  for systems with 1, 2 and 3 dimensions. The 7<sup>th</sup> and 8<sup>th</sup> order for a 3-dimensional system could not be computed because the memory of the computers used was too low and writing to the hard drives would have taken too much time.

Table 5.5: Number of topologically unique diagrams for given order and dimension

order	1-dim	2-dim	3-dim
1	1	1	1
2	2	2	2
3	4	4	4
4	8	10	10
5	14	22	22
6	25	58	58
7	45	140	-
8	79	390	-

### 5.3.2 Determining $t_c/U$

We have now adopted our algorithms for computing the new open paths with one drain and one source and for identifying the topologically unique diagrams. The next thing to do is to actually calculate the expansion coefficients  $\alpha_2^{(\nu)}$  we used in equation (5.41) to get an expression for the free energy coefficient  $c_2$ . Luckily, the only thing that differentiates this calculation from the actual energy calculation is the fact that we have two more perturbation processes. As with the energy computation,  $\nu$  stands for the number of hopping processes for a specific path. But now we do have to add one particle and also remove one particle during the whole permutation process.

Therefore, the Kato sequences we computed in chapter 4.4 are no longer valid for the Mott insulator-superfluid calculations. But as adding a particle and removing a particle are also permutation processes, we simply add two processes to the Kato sequence, i.e.  $\nu \rightarrow \nu + 2$ .

With this little adjustment we can use the same algorithms to calculate the  $c_2$ -coefficients  $\alpha_2^{(\nu)}$  as we used when computing the energy-coefficients  $\alpha^{(\nu)}$ . There is however one little detail one has to pay attention to: During the energy calculations we always had to deal with hopping processes that are actually a product of a creation and an annihilation operator that lead to a factor

$$\hat{a}_1^\dagger \hat{a}_2 |n_1, n_2\rangle = \sqrt{n_2(n_1 + 1)} |n_1 + 1, n_2 - 1\rangle .$$

With the addition of a source and a drain we no longer have only pairs of creation and annihilation operators but also just a creation operator and annihilation operator respectively. These do lead to factors

$$\begin{aligned} \hat{a}^\dagger |n\rangle &= \sqrt{n+1} |n+1\rangle \\ \hat{a} |n\rangle &= \sqrt{n} |n-1\rangle . \end{aligned}$$

This means we have to make sure to remember, which perturbations are hopping processes and which belong to the drain and source to correctly evaluate the scalar products of the Kato formula.

With these little changes implemented we can reuse the energy-algorithm to get the expansion coefficients of  $c_2$ .

In order to get the critical value  $t_c/U$  at which our system, that is at first in a Mott insulator phase, becomes superfluid, we need to calculate all expansion coefficients  $\alpha_2^{(0)}, \alpha_2^{(1)}, \alpha_2^{(2)}, \dots$  and evaluate the ratio  $|\alpha_2^{(\nu-1)}/\alpha_2^{(\nu)}|$  in the limit  $\nu \rightarrow \infty$  according to equation (5.55).

Reaching the limit  $\nu = \infty$  is of course impossible to do, so we have to help ourselves with a little trick. By calculating the ratios  $|\alpha_2^{(\nu-1)}/\alpha_2^{(\nu)}|$  as a function of  $1/\nu$  the limit becomes

$$\nu \rightarrow \infty \implies \frac{1}{\nu} \rightarrow 0 .$$

Therefore, we are plotting the ratios of the coefficients as a function of  $1/\nu$  and extrapolate to  $1/\nu = 0$ . At this point, where the fit intersects the ordinate, one can read off the critical value  $t_c/U$ , as shown in figure 5.8

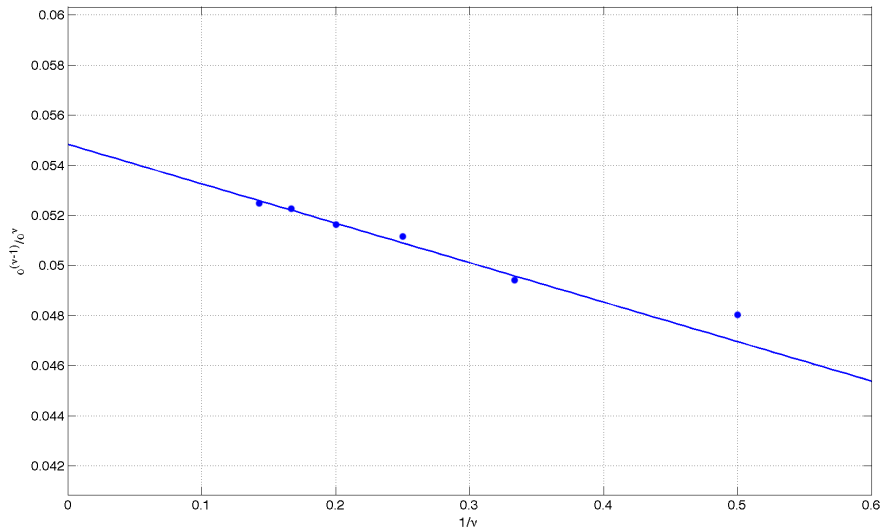


Figure 5.8: The ratios  $|\alpha_2^{(\nu-1)}/\alpha_2^{(\nu)}|$  as a function of  $1/\nu$  and extrapolated to  $\nu \rightarrow \infty$  using a linear fit for a system with 2 dimensions and parameters  $g = 1$ ,  $\mu/U = 0.3$ .

This value now represents a single point of the Mott insulator-superfluid phase boundary. In order to get a grasp of how the whole Mott lobe from  $\mu/U = 0$  to  $\mu/U = 1$  looks like, one would have to do the complete computation of  $c_2$  and extrapolation again with different values of  $\mu$ .

## Results

We have carried out several calculations with different sets of parameters, whose results we are going to discuss. In figure 5.9 one can see the Mott insulator-superfluid phase boundary for systems with filling factor  $g = 1$  and dimensions  $d = 2$  and  $d = 3$ . The 2-dimensional system is depicted in blue and the 3-dimensional one in red. For the calculations in 2-dimensional case we considered all contributions up to 7<sup>th</sup> order, while in the 3-dimensional case we stopped at the 6<sup>th</sup>. (This however does not result in more inexact data, as the convergence of the  $|\alpha_2^{(\nu-1)}/\alpha_2^{(\nu)}|$ -series improves rapidly with increasing dimensionality.)

Comparisons of our results with calculations from other groups [18, 36] confirm the excellent agreement of our data.

An extension of figure 5.9 can be seen in figure 5.10. Here we computed the phase boundary for the same two systems with 2 and 3 dimensions, but with

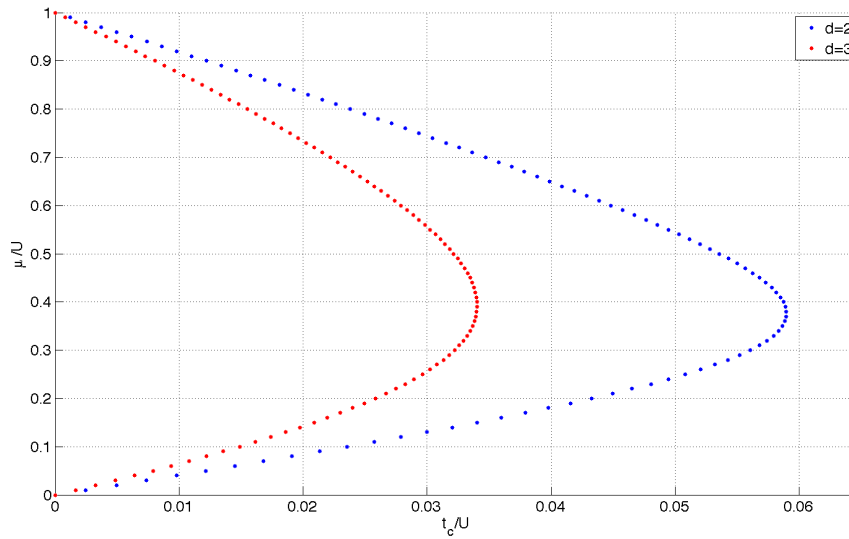


Figure 5.9: The Mott insulator-superfluid phase boundary for systems with two and three dimensions and unity filling factors  $g = 1$ .

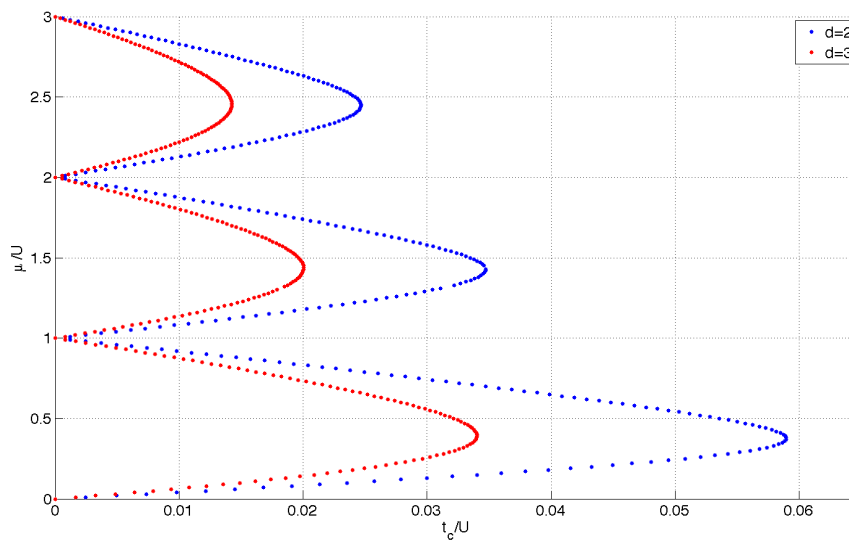


Figure 5.10: The Mott insulator-superfluid phase boundary for systems with two and three dimensions and with filling factors  $g = 1, g = 2$  and  $g = 3$ .

different filling factors. The first Mott lobes that stretch from  $\mu/U = 0$  to  $\mu/U = 1$  belong to the case with unity filling factor as in figure 5.9, but the Mott lobes with  $\mu/U \in (1, 2)$  do belong to a filling factor of  $g = 2$  and  $\mu/U \in (2, 3)$  corresponds to a filling factor of  $g = 3$ . The blue dotted line stands again for the 2-dimensional case and the red line to the 3-dimensional system. One can clearly see the shrinking of the Mott insulating regions

with growing filling factors, which is exactly what was expected. (See also figure 5.1 at the beginning of this chapter.)

To show this  $g$ -dependent behavior better, figure 5.11 depicts only the two-dimensional case, but again with the three different filling factors  $g = 1$  in blue,  $g = 2$  in red and  $g = 3$  in black. Additionally, the ordinate has a different scaling than before. Instead of just plotting  $\mu/U$  the y-coordinate is scaled like  $(\mu - g + 1)/U$ , which results in all three phase boundaries being projected in the y-interval  $(0, 1)$ .

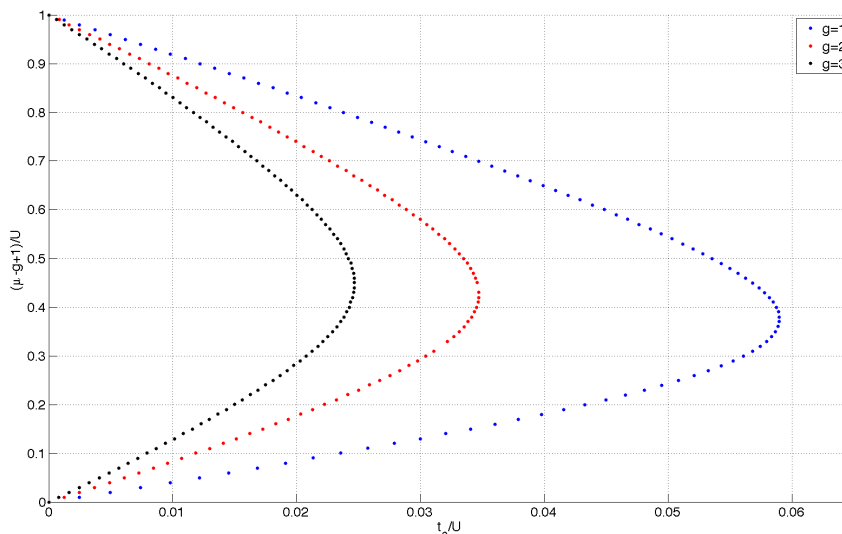


Figure 5.11: The Mott insulator-superfluid phase boundary for a two-dimensional system with filling factors  $g = 1$ ,  $g = 2$  and  $g = 3$ .

With a scaling like this it is easy to notice that the bigger  $g$  gets, the more symmetric the Mott lobe gets. While the peak of the ' $g=1$ '-lobe is about  $(\mu - g + 1)/U \approx 0.38$  it moves up to  $(\mu - g + 1)/U \approx 0.43$  for  $g = 2$  and to  $(\mu - g + 1)/U \approx 0.46$  for  $g = 3$ . In the limit  $g \rightarrow \infty$  the Mott lobe would be perfectly symmetric with the maximum at  $(\mu - g + 1)/U = 0.5$ .

The same reasoning also applies to systems with other dimensions, of course, which is shown for the three-dimensional case in figure 5.12. It is also worthwhile to note, that the higher the number of the dimensions of a system is, the more symmetric and parabola-shaped the Mott lobes are.

There is however one big limitation of this approach, which shall not be swept under the table: The Mott insulator-superfluid phase transition of a 1-dimensional system can not be computed correctly with our current algorithms due to two problems:

- First of all, the extrapolation depicted in figure 5.8 relies on the fact, that there is a bijective relation between  $\mu$  and  $t_c$ . A Bose-Hubbard system in one dimension however exhibits a reentrance phenomenon [22]:

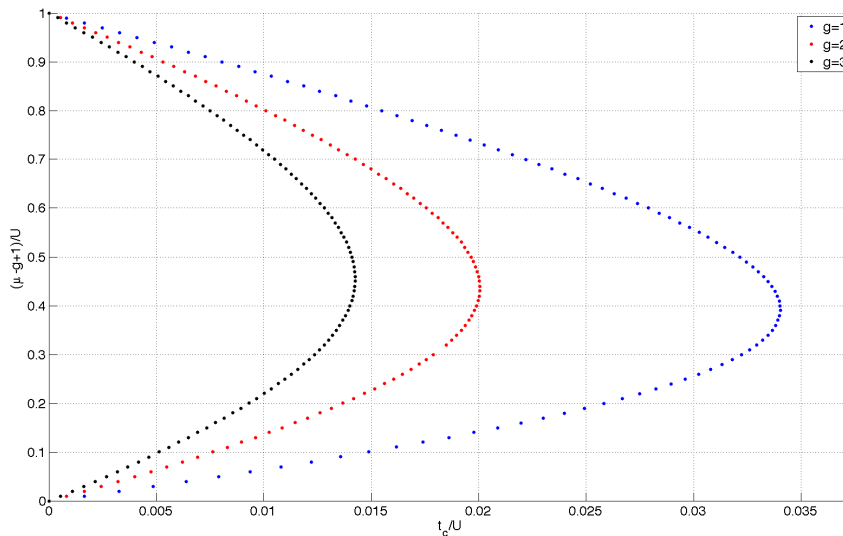


Figure 5.12: The Mott insulator-superfluid phase boundary for a three-dimensional system with filling factors  $g = 1$ ,  $g = 2$  and  $g = 3$ .

If one starts in the Mott insulating phase at  $t = 0$  and begins to increase  $t$ , there will be one point at which the undergoes a phase transition and becomes superfluid, as we already explained before. For a 1-dimensional system it is now possible for certain values of  $\mu$  to get back into the Mott insulator phase when the hopping strength is increased even further, as shown in figure 5.13.

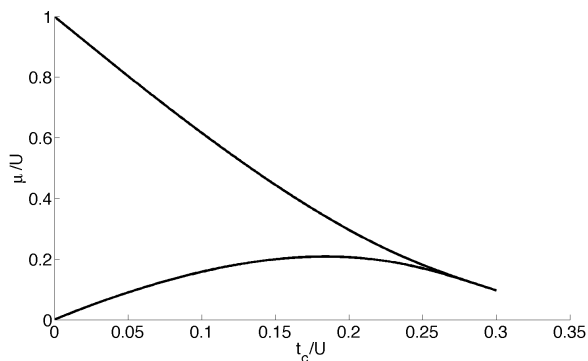


Figure 5.13: The Mott insulator-superfluid phase boundary for a one-dimensional system with filling factor  $g = 1$ .

This means, that in a specific interval of  $\mu$  there is no bijective mapping  $\mu \Leftrightarrow t_c$ . It is therefore not possible to determine all three  $t_c$  values for these specific values of  $\mu$ ; only the first one can be identified.

- Secondly, the determination of the phase boundary relies on the fact

that in the Mott insulator regime the atom-atom correlation function  $\xi(r)$  decays exponentially with the radius  $r$ , while in the superfluid phase it adopts a non-vanishing value for  $r \rightarrow \infty$ . On the other hand, the order parameter will vanish in the Mott insulator phase and take on a non-vanishing value in the superfluid phase analogously.

For a 1-dimensional system this is no longer the case. While it still holds true, that the correlation function in the superfluid phase has a constant, non-vanishing value for large  $r$ , it does not follow an exponential decay in the Mott insulator phase, but a power-law behavior according to the Kosterlitz-Thouless phase transition [37, 22]

$$\xi_{SF} = r^{-\frac{K}{2}}, \quad (5.59)$$

with a coefficient  $K$ . For small tunneling strengths this is not a big problem, as the particles can not hop far away, which results in small values for  $r$  in the correlation function. But the bigger the tunneling strength gets, the more severe the difference between the power-law dependence and the exponential decay becomes, resulting in a complete break down of the algorithm at large hopping strengths. This can be seen in figure 5.14.

A way out of this dilemma while still using the Kato formalism could be the calculation of the correlation function  $\xi(r)$  itself, as explained in [18]. By knowing the value of the correlation function one could determine the coefficients  $K$  in dependence of the hopping strength. For a Kosterlitz-Thouless transition at  $g = 1$  the coefficient  $K$  is known to be  $K_c = 0.5$ . This means if one can fit the different values of  $K$  as a function of  $t$  one can determine the point where  $K(t)$  equals  $1/2$ . At this point one could then read off the critical value  $t_c$  at which the phase transition takes place (see also [22]).

Figure 5.14 shows these two limitations very well. It considers a one-dimensional system with unity filling factor and compares our results depicted by the blue dots with results obtained with DMRG [38], which is the most trusted method to deal with 1-dimensional quantum systems. When we take a look at the section with low values of  $\mu$ , we see that our results are in good agreement with the DMRG-data. When the lower phase boundary goes beyond its maximum however, our algorithms break down and we can no longer determine the phase boundary correctly due to the non-bijective relation between  $\mu$  and  $t_c$ .

At very high values of  $\mu$ , i.e.  $\mu \in [0.5, 1]$ , our data again match the ones from DMRG, because the critical hopping parameters in this area are small enough to ensure convergence of the  $|\alpha_2^{(\nu-1)}/\alpha_2^{(\nu)}|$ -series. Once the hopping parameter becomes bigger than 0.14 the series of ratios diverges, thus no longer allowing the correct determination of the phase boundary.

As said in the previous section, there might be a workaround to this problem

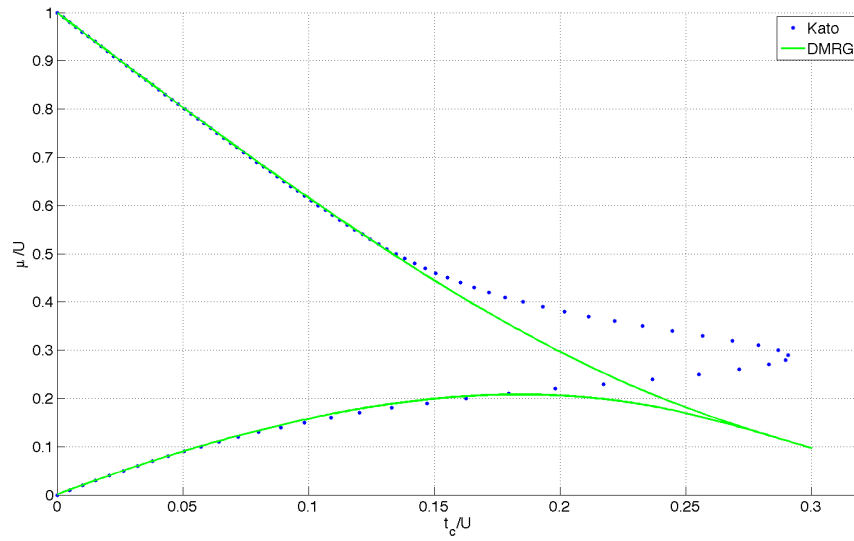


Figure 5.14: Comparison of the results obtained with our Kato approach and DMRG from [38] for a 1-dimensional system with filling factor  $g = 1$ .

by calculating the correlation function  $\xi(r)$  directly, which is a main point of interest in our current work.

### 5.3.3 Introducing Disorder to the System

Before we are going to discuss the results obtained with the Kato formalism, we will go through another very interesting topic, namely introducing a disorder to the system. Up until now the system considered has the same chemical potential at every site, which is a very rough assumption. A system, where the sites do have different chemical potentials is a far better model for what is going on in a real lattice.

Therefore, we want to assign a different chemical potential to every site according to the following scheme:

$$\mu_i = \mu_0 + \epsilon_i \cdot \Delta\mu \quad (5.60)$$

$\mu_0$  is the mean value of the chemical potential of our whole system and  $\Delta\mu$  is the maximum difference that an onsite chemical potential can vary from the mean value  $\mu$ .  $\epsilon_i$  is a parameter in the interval  $[-1, 1]$  and determines how much of  $\Delta\mu$  is added or subtracted at a specific site. This  $\epsilon_i$  has to be set for every single site and therefore stands for the disorder that is introduced to the system. Choosing  $\epsilon_i$  can be done completely random, where a random number generator determines unbiased values for  $\epsilon_i$ . Another possibility of choosing  $\epsilon_i$  is according to a Beta-distribution, as shown in figure 5.15. Here,

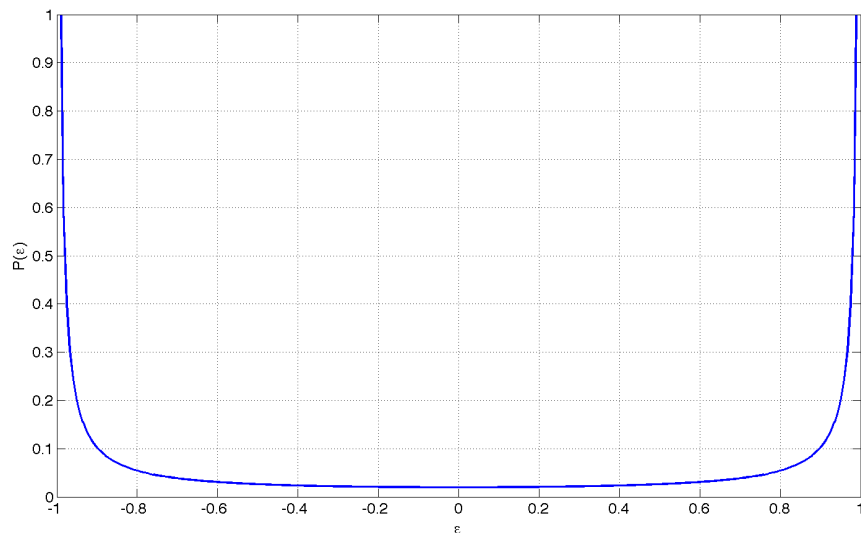


Figure 5.15: The probability density function  $P(\epsilon)$  as a function of  $\epsilon$ .

the extreme values of  $\epsilon_i$  have a big weight, while the intermediate values will be chosen very seldom. For our purpose however it is sufficient to consider a binary distribution for  $\epsilon_i$  and  $\Delta\mu = 1$ , i.e.

$$\mu_i = \mu_0 \pm \epsilon, \quad (5.61)$$

where the sign is chosen randomly. Such a distribution is extremely easy to create and resembles the Beta-distribution of figure 5.15 well enough for our needs.

In order to use the Kato formalism there is however one big drawback. The big strength and beauty of this formalism relies on the fact that we have a system with translational and rotational invariance. Only in the cases, where our system is invariant under translation- and rotation-operations we can reduce all the possible paths on our lattice to only topologically unique ones. With a constant chemical potential  $\mu$  for the whole lattice these requirements are well fulfilled, but if we start to assign a different chemical potential to every site, our system will no longer be invariant under translations and rotations.

The solution to this problem is to create many systems with different configurations of the chemical potential. Additionally, the generation of the chemical potential must be the same for every site, i.e. the  $\epsilon_i$  have to be chosen by the same scheme for every site. If these requirements are met, no site is special by any means, and by averaging over many different configurations one gains the translational and rotational invariances again, on which our Kato algorithm relies on.

So what do we have to do to deal with a disordered system? The path creation can stay the same as can the identification of the topologically unique diagrams and the generation of Kato sequences. Before the energy is calculated for a specific path however, the chemical potentials  $\mu_i$  for every site  $i$  involved in the current hopping process has to be chosen. One then calculates the energy of this special configuration. Then another configuration is chosen for the same path and the energy of this new configuration is calculated. This is done until enough configurations have been computed. One then averages over the energies of all these configurations and then moves on to the next diagram where this whole procedure of generating and evaluating different configurations starts again.

The question, how many different configurations are sufficient to assure that the average values behave the same as values from a system with translational and rotational invariances would, is hard to answer. It is clear that the more sites are involved in a hopping process the more configurations one has to generate. But even when sampling 500, 1000 or more different configurations the time savings are huge compared to an approach where one takes no advantage of translational and rotational invariances.

## Results

Before we are going to discuss the results concerning the Mott insulator-superfluid phase transition of a disordered system, some results for the energy of a disordered Bose-Hubbard model shall be subsequently added. It is easy to understand that a system, where the chemical potentials of the sin-

gle sites are not the same, will have energy corrections, whose absolute value will be bigger than those from a system with a constant chemical potential throughout the whole lattice.

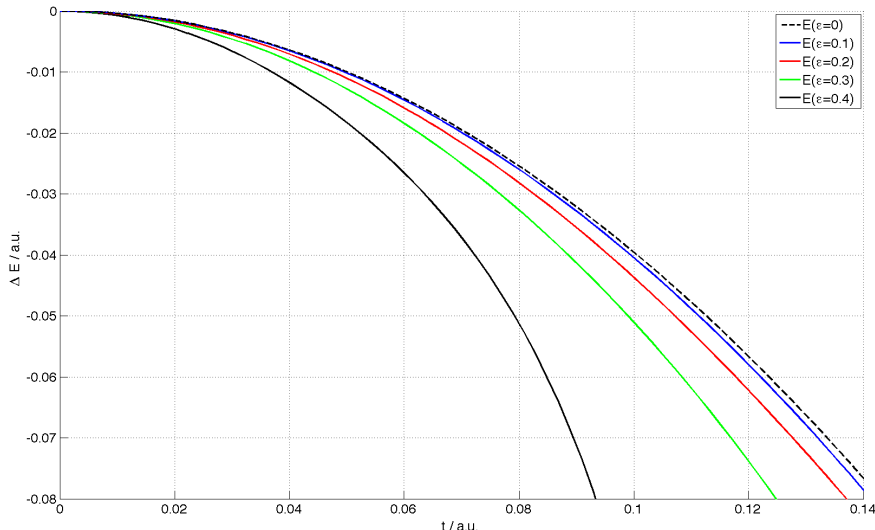


Figure 5.16: Energies of a 1-dimensional system with disorder parameters  $\epsilon = 0$  (black dashed line),  $\epsilon = 0.1$  (blue solid line),  $\epsilon = 0.2$  (red solid line),  $\epsilon = 0.3$  (green solid line) and  $\epsilon = 0.4$  (black solid line).

This can be seen in figure 5.16, which shows the situation for a 1-dimensional lattice. Energy corrections were included up to 7<sup>th</sup> order (8<sup>th</sup> order for the ordered system). The black dotted line stands for a perfectly ordered system, i.e. the disorder parameter  $\epsilon = 0$ . The subsequent solid lines represent systems with different disorder 'strength'; the blue line depicts the case for *epsilon* = 0.1, the red line shows the energy correction for a system with  $\epsilon = 0.2$ , and the green and black line for a system with  $\epsilon = 0.3$  and  $\epsilon = 0.4$  respectively.

As one can see, the bigger the disorder parameter  $\epsilon$  gets, the bigger the absolute value of the energy correction gets, which was expected at the beginning. We also took the opportunity and compared our results to those obtained with the Variational Cluster approach, as is shown in figure 5.17. Again a 1-dimensional system was used with the same disorder parameters as used in figure 5.16. The solid lines are our results calculated with the Kato algorithm and the  $\times$  mark the results from VCA.

As before, our results are in excellent agreement with those computed with VCA, which can be seen especially well for the  $\epsilon = 0.1$  and  $\epsilon = 0.2$  cases. Unfortunately we don't have data from VCA for  $\epsilon = 0.3$  and  $\epsilon = 0.4$  at higher hopping parameters, so the possibilities to compare these two methods for these parameters are rather little, but the data at low hopping strength and

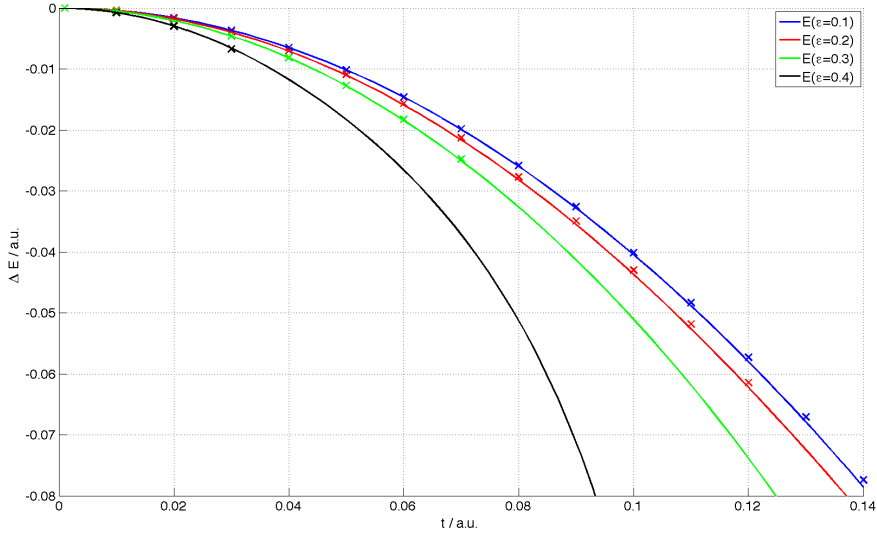


Figure 5.17: Energies of a 1-dimensional system with disorder parameters  $\epsilon = 0.1$  (blue solid line),  $\epsilon = 0.2$  (red solid line),  $\epsilon = 0.3$  (green solid line) and  $\epsilon = 0.4$  (black solid line) compared to results obtained with VCA, which are marked with  $\times$ .

the general information gathered up to this point suggest a good agreement of Kato and VCA never the less.

Let's move on now to see how different the Mott insulator-superfluid phase transition behaves for a disordered system compared to an ordered one. We therefor take a look at three different 2-dimensional systems, as shown in figure 5.18.

The blue graph stands for an ordered system, i.e.  $\epsilon = 0$ , the red one for a system with disorder parameter  $\epsilon = 0.1$  and the black one depicts the case with  $\epsilon = 0.2$ . We went up to 7<sup>th</sup> order and while the circles stand for the actual data received from our computations, the dashed lines come from a polynomial fit of these data points. It is easy to see, that the bigger  $\epsilon$  gets, the smaller the Mott insulating region becomes.

This is due to the fact that the most extreme situations that can happen are that either all of the sites have the chemical potential  $\mu_i = \mu_0 + \epsilon$  or all of them have the chemical potential  $\mu_i = \mu_0 - \epsilon$ . Both of these cases actually represent ordered system as the chemical potential is the same for all sites; but the actual value is shifted by  $+\epsilon$  and  $-\epsilon$ .

Therefor one would expect the phase boundary of the disordered system to be parallel to the phase boundary of the ordered system. This is fulfilled quite nice for low critical hopping strengths  $t_c$ , as can be seen in figure 5.18, but with increasing  $t_c$  the situation gets worse. The reason for this is, that the higher the hopping strength is, the more important the higher orders of

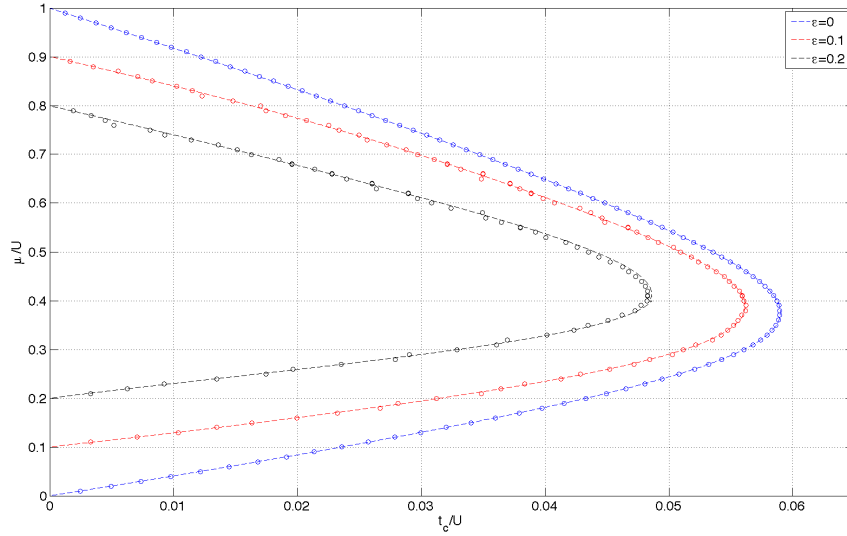


Figure 5.18: The Mott insulator - superfluid phase boundary for a two dimensional system with disorder parameters  $\epsilon = 0$ ,  $\epsilon = 0.1$  and  $\epsilon = 0.2$ . The circles represent the actual data and the dashed lines are the polynomial fits generated from these data.

the Kato approach are. As we were limited to 7<sup>th</sup> by the computational resources we had at hand, we unfortunately couldn't investigate the situation with higher order corrections to see if the phase boundaries of the disordered systems would get aligned better along the one of the ordered system.

In figure 5.19 we plotted the width of the Mott insulator regions for the systems depicted in figure 5.18 as a function of the critical hopping strengths  $t_c$ . Again the blue solid line stands for the ordered system, the red one for the system with  $\epsilon = 0.1$  and the black one for  $\epsilon = 0.2$ . At  $t_c = 0$  the Mott insulator phase stretches from  $\mu_1 = 0$  to  $\mu_2 = 1$  for the ordered system, resulting in a  $\mu_{gap} = \mu_2 - \mu_1 = 1$ . Because in the extreme situations the chemical potentials would just get shifted as was explained above, the insulating regions for the  $\epsilon = 0.1$  starts at  $\mu = 0.1$  and ends at  $\mu = 0.9$ , leading to  $\mu_{gap} = 0.8$  and  $\mu_{gap} = 0.6$  for the system with  $\epsilon = 0.2$ .

The bigger  $t_c$  now becomes, the smaller  $\mu_{gap}$ , i.e. the Mott insulating phase gets; additionally the slope of the curves for the two disordered system deviates more and more the bigger  $t_c$  is.

With these results we want to conclude the discussion about the Bose-Hubbard model and apply our attention to the Jaynes-Cummings model, another class of bosonic systems that can be treated with our Kato approach.

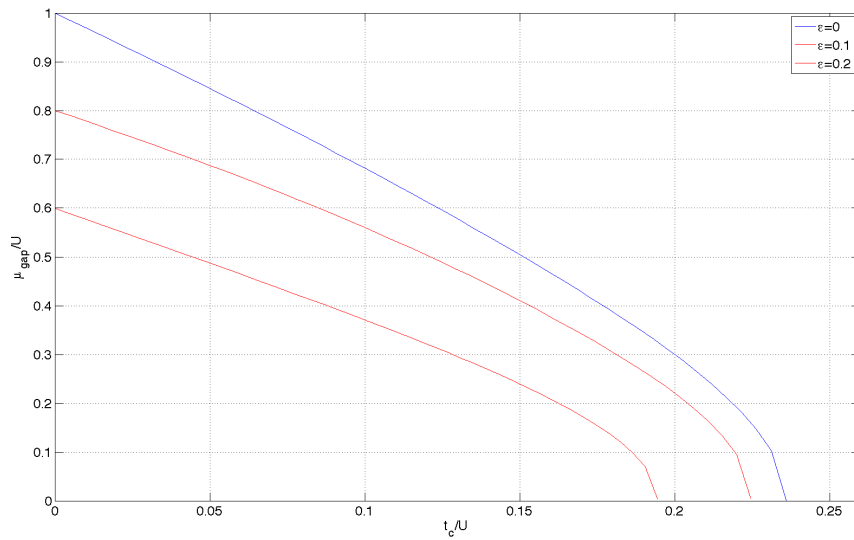


Figure 5.19: The Mott insulator gap as a function of the critical hopping strength for a 2-dimensional system with zero disorder, a system with  $\epsilon = 0.1$  and for a system with  $\epsilon = 0.2$ .

### 5.3. CONSEQUENCES FOR THE KATO FORMALISM

---

## **Part III**

# **The Jaynes-Cummings Model**



# Chapter 6

## Introduction

The Jaynes-Cummings model is an enhancement of the Rabi model [39]. While the semi-classical Rabi model considers a two-level atomic system that is disturbed by an electromagnetic field, the Jaynes-Cummings model takes this thoughts further and describes a two-level atomic system that interacts with quantized modes of light. In other words, the classical electromagnetic field of the Rabi model is translated into a quantized field.

The Jaynes-Cummings model is very important for quantum physics, as it describes atoms coupled to cavity modes, therefor being a way to realize quantum bits and computing (figure 6.1).

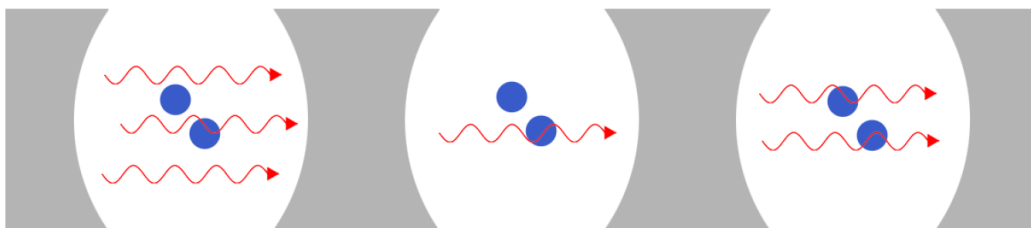
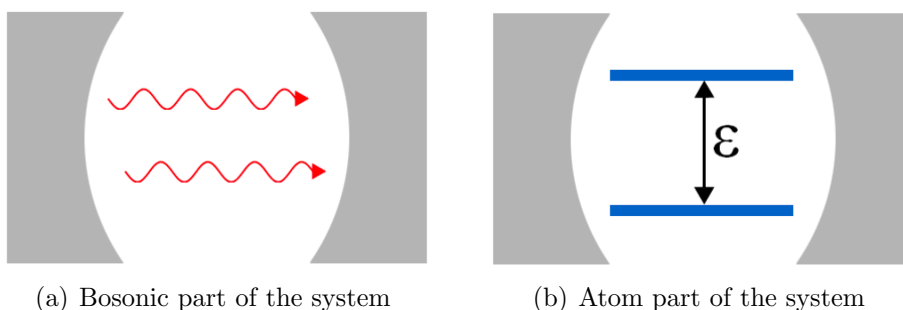


Figure 6.1: Sketch of a 1 dimensional Jaynes-Cummings lattice (from [13]).



(a) Bosonic part of the system

(b) Atom part of the system

Figure 6.2: The two different parts of the Jaynes-Cummings model (from [13]).

---

The following short explanation follows strongly the approach of [40, chapter 3] and all quantities are expressed in units of  $\hbar$ .

The hamiltonian of a Jaynes-Cummings system consists of three parts, an atom part  $\hat{H}_a = \epsilon|\uparrow\rangle\langle\uparrow|$  which assigns the energy  $\epsilon$  to the excited atom states (figure 6.2(b)), a cavity part  $\hat{H}_c = \omega_c \hat{a}_i^\dagger \hat{a}_i$  counting the bosons in the cavity and appointing them the energy  $\omega_c$  (figure 6.2(a)) and a part that describes the coupling between atom and cavity  $\hat{H}_{ac}$ , which can be written like

$$\hat{H}_{ac} = -\frac{1}{\hbar} \hat{\mathbf{d}} \cdot \hat{\mathbf{E}}_c . \quad (6.1)$$

With the expression for the quantum mechanical dipole operator  $\hat{\mathbf{d}} = \mathbf{d}(\mathbf{e}_a \sigma_- + \mathbf{e}_a^* \sigma_+)$  and the cavity field operator  $\hat{\mathbf{E}}_c = \mathcal{E}_0(\mathbf{e}_c \hat{a} + \mathbf{e}_c^* \hat{a}^\dagger)$  this becomes

$$\hat{H}_{ac} = -\frac{d}{\hbar} (\mathbf{e}_a \sigma_- + \mathbf{e}_a^* \sigma_+) \cdot \mathcal{E}_0 (\mathbf{e}_c \hat{a} + \mathbf{e}_c^* \hat{a}^\dagger) . \quad (6.2)$$

Here,  $\hat{a}$  and  $\hat{a}^\dagger$  are again the bosonic annihilation and creation operators for the cavity modes,  $\sigma_+$  and  $\sigma_-$  are the atomic raising and lowering operators that raise a ground state atom to its excited state and vice versa.  $\mathbf{e}_a$  and  $\mathbf{e}_c$  are vectors describing the field polarization in the atom or the cavity system and  $\mathcal{E}_0$  is a normalization factor. Usually there is also a factor  $f(r)$  present, which describes the spatial configuration of the field mode, but for sake of simplicity it is set to unity here.

If we get rid of the braces in equation (6.2), we are left with four terms. The term with  $\sigma_- \hat{a}$  stands for the process where the excited atom relaxes to its ground state while a photon is annihilated. The  $\sigma_+ \hat{a}^\dagger$  describes the opposite effect, i.e. the atom is shifted to the higher state and a photon is created. In our case, where the resonance frequencies of the atom and the cave are very close together, these two effects do play a very minor role and are therefor omitted from this point on.

The two much more important terms are those with  $\sigma_- \hat{a}^\dagger$  and  $\sigma_+ \hat{a}$ . The first one explains the emission of a photon when the atom relaxes to its lower state and the second one translates to an excitation of the atom when absorbing a photon. Hence, our simplified hamiltonian  $\hat{H}_{ac}$  has the form

$$\hat{H}_{ac} = -\frac{\Omega}{2} (\sigma_+ \hat{a} + \sigma_- \hat{a}^\dagger) \quad (6.3)$$

with the Rabi frequency  $\Omega$

$$\Omega = 2 \frac{d \mathcal{E}_0 \mathbf{e}_a^* \mathbf{e}_c}{\hbar} . \quad (6.4)$$

This frequency is a measurement for the strength of the coupling of the two systems. The eigenstates of the atom hamiltonian  $\hat{H}_a$  are  $|\downarrow\rangle$ ,  $|\uparrow\rangle$ , the first denoting the ground state, the second the excited state. On the other hand,

the cavity hamiltonian  $\hat{H}_c$  has the eigenstates  $|g\rangle$ , the already known Fock-states from chapter 2. Therefor the eigenstates of the uncoupled system will be the tensor products  $|g, \downarrow\rangle$  and  $|g, \uparrow\rangle$ .

If the detuning of the system  $\Delta = \omega_c - \epsilon$  is zero or very small compared to  $\omega_c$ , the states with the same particle number, i.e.  $|g, \downarrow\rangle$  and  $|g - 1, \uparrow\rangle$  are degenerated or nearly degenerated respectively. The complete energy of a system with  $g$  particles is therefor saved in a state with  $g$  photons and no atom excitations  $|g, \downarrow\rangle$  or a state with  $g - 1$  photons and 1 atom excitation  $|g - 1, \uparrow\rangle$ . (The exception being a system with no particles, which of course can only be described by  $|0, \downarrow\rangle$ .) The coupling hamiltonian  $\hat{H}_{ac}$  only translates between those states with the same particle number.

We are therefor dealing with a two-level system, hence the operators  $\sigma_+$  and  $\sigma_-$  can be computed using the Pauli matrices

$$\begin{aligned}\sigma_+ &= \sigma_x + i\sigma_y \\ &\hat{=} \begin{pmatrix} 0 & 1 \\ 0 & 0 \end{pmatrix}\end{aligned}\quad (6.5)$$

and

$$\begin{aligned}\sigma_- &= \sigma_x - i\sigma_y \\ &\hat{=} \begin{pmatrix} 0 & 0 \\ 1 & 0 \end{pmatrix}.\end{aligned}\quad (6.6)$$

With this, we can write down a matrix equation for the dimensionless hamiltonian of the complete system with  $n$  particles [41]:

$$H_{JC} = \begin{pmatrix} (1 + \Delta)\hat{a}^\dagger\hat{a} + 1 + \frac{\Delta}{2} & \frac{\Omega}{2}\hat{a} \\ \frac{\Omega}{2}\hat{a}^\dagger & (1 + \Delta)\hat{a}^\dagger\hat{a} + \frac{\Delta}{2} \end{pmatrix}\quad (6.7)$$

As this equation resembles the governing equation for a spin in a magnetic field very closely, it is therefor easy to prove that the eigenvalues of equation (6.7) can be written as

$$E_{g,\pm} = g\omega_c - \frac{\Delta}{2} \pm q(g)\quad (6.8)$$

with

$$q(g) = \sqrt{\left(\frac{\Delta}{2}\right)^2 + g\left(\frac{\Omega}{2}\right)^2}.\quad (6.9)$$

The  $\pm$ -sign refers to the sign of  $|g, -\rangle$  and  $|g, +\rangle$ , introduced in equations (6.10) and (6.11).

It has been said previously, that if there are no particles in the system, we have to treat it differently as there is just one state possible, which is  $|0, \downarrow\rangle$ . Therefore, the energy eigenvalue for this case is  $E_{g=0} = 0$ . The eigenstates corresponding to the energies (6.8) are

$$|g, -\rangle = \cos \Theta_g |g-1, \uparrow\rangle - \sin \Theta_g |g, \downarrow\rangle \quad (6.10)$$

$$|g, +\rangle = \sin \Theta_g |g-1, \uparrow\rangle + \cos \Theta_g |g, \downarrow\rangle, \quad (6.11)$$

where we used the short notations

$$\sin \Theta_g = \sqrt{\frac{q(g) - \frac{\Delta}{2}}{2q(g)}} \quad \text{and} \quad \cos \Theta_g = \sqrt{\frac{q(g) + \frac{\Delta}{2}}{2q(g)}}. \quad (6.12)$$

The states (6.10) and (6.11) are linear combinations of the two possible states with the same total particle number. As  $|g, -\rangle$  corresponds to the lower energy, it is the 'ground state' of our system while  $|g, +\rangle$  is the excited state with the higher total energy. Be aware that we are talking here about the atom-cavity system as a whole, so the ground state  $|g, -\rangle$  should not be confused with the atom ground state  $|\downarrow\rangle$ .

Recapitalizing, the final Jaynes-Cummings hamiltonian for an atom-cavity system looks as follows:

$$\hat{H}_{JC} = \omega_c \hat{a}^\dagger \hat{a} + \epsilon |\uparrow\rangle\langle\uparrow| + g(\hat{a}|\uparrow\rangle\langle\downarrow| + \hat{a}^\dagger|\downarrow\rangle\langle\uparrow|) - \mu(\hat{a}^\dagger \hat{a} + |\uparrow\rangle\langle\uparrow|) \quad (6.13)$$

The first term counts all bosons in our cavity and allocates each of them the energy  $\omega_c$  and the second term checks whether the atom is in the excited state or not. If it is, the energy  $\epsilon$  is added to the system's energy. The third term takes into account, that an atom in the ground state can be lifted to its excited state by the absorption of a photon (figure 6.3(a)).

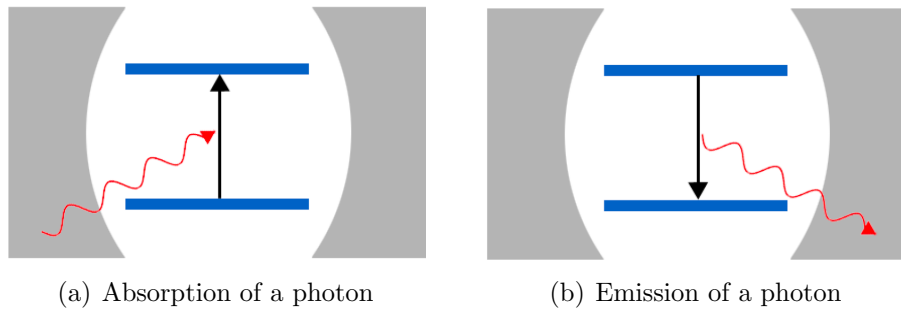


Figure 6.3: The two different interactions between atom and cavity part (from [13]).

The opposite effect, the emission of a photon when an atom relaxes from its excited state to the ground state (figure 6.3(b)) is taken care of by the fourth

term in equation (6.13). An atom-cavity site may also have an additional energy that is dependent on the total particle number, due to a chemical potential  $\mu$ , which is considered with the last term in our Jaynes-Cummings hamiltonian.

It has the eigenvalues given in equation (6.8) and the eigenstates stated by equations (6.10) and (6.11), with the exception for zero particles, in which case we have  $E = 0$  and just one possible eigenstate  $|0, \downarrow\rangle$ .



# Chapter 7

## Changes in the Algorithm

### 7.1 Energy Corrections

In chapter 6, we took a look at the hamiltonian of a single atom-cavity site. Now we are going to construct a regular lattice by arranging a large array of such sites and allow the bosons to tunnel to neighbouring sites with tunneling strength  $t$ . The Jaynes-Cummings hamiltonian of a single site  $\hat{H}_{JC,i}$  is given in equation (6.13) and the 'hopping' hamiltonian is the same as for the Bose-Hubbard model (see chapter 2), hence

$$\hat{H}_{JCL} = \sum_i \hat{H}_{JC,i} + \hat{H}_{hop} \quad (7.1)$$

$$= \sum_i \left( \omega_c \hat{a}_i^\dagger \hat{a}_i + \epsilon |\uparrow_i\rangle \langle \uparrow_i| + g(\hat{a}_i |\uparrow_i\rangle \langle \downarrow_i| + \hat{a}_i^\dagger |\downarrow_i\rangle \langle \uparrow_i|) - \mu(\hat{a}_i^\dagger \hat{a}_i + |\uparrow_i\rangle \langle \uparrow_i|) \right) - t \sum_{\langle i,j \rangle} \hat{a}_i^\dagger \hat{a}_j . \quad (7.2)$$

We now have to split the hamiltonian of the complete lattice  $\hat{H}_{JCL}$  in a perturbative and a non-perturbative part. The Jaynes-Cummings site hamiltonian  $\hat{H}_{JC}$  does not alter the particle number of the eigenstates, but the hopping hamiltonian  $\hat{H}_{hop}$  does.  $t \cdot \hat{a}_i^\dagger \hat{a}_j$  takes away a particle from site  $j$ , adds one at  $i$  and changes the weights of the components  $|g, -\rangle$  and  $|g, +\rangle$  of which they were initially composed of.

$$\begin{aligned} \hat{a}|g, -\rangle &= \sqrt{g-1} \cos \Theta_g |g-2, \uparrow\rangle - \sqrt{g} \sin \Theta_g |g-1, \downarrow\rangle \\ \hat{a}^\dagger|g, -\rangle &= \sqrt{g} \cos \Theta_g |g, \uparrow\rangle - \sqrt{g+1} \sin \Theta_g |g+1, \downarrow\rangle \end{aligned} \quad (7.3)$$

and analogous for  $|g, +\rangle$ . Because of the new factors, these states are no longer eigenstates of  $\hat{H}_{JC}$ . It is therefore clear, that the hopping term is again the perturbative part, as it was for the Bose Hubbard model.

The fact, that there are two eigenstates of the Jaynes-Cummings model now, belonging to the particle number  $g$ , involves another disadvantage. As we

know, the term  $S_k$  of our Kato formula projects the current state to the according eigenstate of  $\hat{H}_0$ . In case of the Bose-Hubbard model, this was

$$S_k = \begin{cases} -|\mathbf{g}\rangle\langle\mathbf{g}| & \text{for } k = 0 \\ \sum_{i \neq g} \frac{|\mathbf{i}\rangle\langle\mathbf{i}|}{\left(E_g^{(0)} - E_i^{(0)}\right)^k} & \text{otherwise} \end{cases} \quad (7.4)$$

with  $|\mathbf{i}\rangle$  being the eigenstates of the unperturbed lattice hamiltonian. In case of the Jaynes-Cummings model however, the current state will either be projected onto  $|g, -\rangle$  or  $|g, +\rangle$ . This means, that one has to add the information, in which eigenstate we are projecting, i.e.  $S_k \rightarrow S_{k,\sigma}$  with  $\sigma$  telling whether we should take the eigenstate with  $-$  or with  $+$ .

$$S_{k,\pm} = \begin{cases} -|g, -\rangle\langle g, -| & \text{for } k = 0 \\ \sum_{|i,\pm\rangle \neq |g,-\rangle} \frac{|i,\pm\rangle\langle i,\pm|}{\left(E_{g,-}^{(0)} - E_{i,\pm}^{(0)}\right)^k} & \text{otherwise} \end{cases} \quad (7.5)$$

In order to calculate the energy correctly, we now also have to consider not only every possible sequence  $\{k_{n-1}\}$  but also every possible permutation of the signs  $\{\sigma_{n-1}\}$ .

Our equation for the complete energy correction of  $n^{\text{th}}$  order therefor reads now

$$\Delta E_g^{(n)} = \sum_{\{\sigma_{n-1}\}} \Delta E_{g,\sigma}^{(n)} \quad (7.6)$$

$$= \sum_{\{\sigma_{n-1}\}} \sum_{\{k_{n-1}\}} \langle \mathbf{g}, - | V S_{k_1, \sigma_1} V S_{k_2, \sigma_2} \dots V S_{k_{n-1}, \sigma_{n-1}} V | \mathbf{g}, - \rangle, \quad (7.7)$$

with a sum over all allowed sequences  $\{k_{n-1}\}$  that have to meet the constraints

$$\sum_{l=1}^s k_l \geq s \quad \text{for } s = 1, 2, \dots, n-2 \quad (7.8)$$

$$\sum_{l=1}^{n-1} k_l = n-1 \quad (7.9)$$

and a sum over all sequences of signs  $\{\sigma_{n-1}\}$ . The answer to the question, which  $\sigma$ -sequences are valid and which are not is not a trivial one. In order to deduce the right sequences we will take a look at a few different paths. Let's consider the most simple path there is, depicted in figure 7.1 appearing at the second order energy correction:

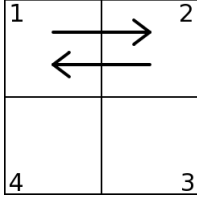


Figure 7.1: One possible path in second order.

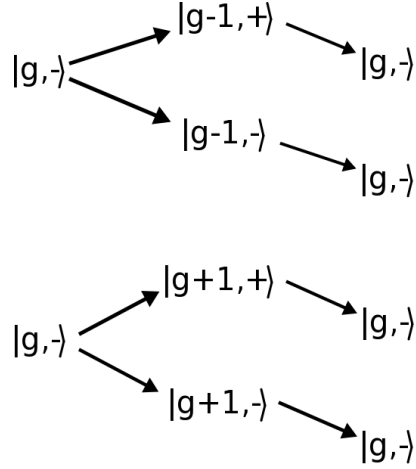


Figure 7.2: Spanning tree of the path in the left figure.

After the first hop from site 1 to site 2, we do have  $g - 1$  particles at site 1. But the state of this site could have either been projected to  $|g - 1, -\rangle$  or  $|g - 1, +\rangle$ . An exception would of course be, if there were  $g = 1$  particles at each site before the hopping, in which case only the  $|0, \downarrow\rangle$  state would be possible for site 1 after the first hopping. We will from now on omit mentioning this exception as it always results in the same state.

Site 2 contains  $g + 1$  particles after the first tunneling and it will be projected in either the  $|g + 1, -\rangle$  or the  $|g + 1, +\rangle$  state. After the second hopping takes place, both sites are again populated by  $g$  particles and in each site the ground-state  $|g, -\rangle$  has to be present in order to lead to a non-vanishing energy contribution. A graphical depiction of this can be seen in figure 7.2.

To calculate the energy contribution of this path correctly, we would now have to calculate the energy of each of the 4 possible sequences and sum them up.

We will now move on to the next simple path, shown in figure 7.3. It consists of four hopping processes and the starting situation is not restored before the last hopping: The first tunneling process from site 1 to site 2 leads to the same situation as in the previous case of figure 7.1. Sites 3 and 4 do not experience any perturbation, they therefor stay in the ground state. After the second hopping from site 2 to site 3 the state of site 3 will be projected to either  $|g + 1, -\rangle$  or  $|g + 1, +\rangle$ . Site 2 however returns to the ground state. This happens, because this site will not be involved in any hopping process. Its state can therefor not be changed anymore and since all sites have to be in the ground state at the end of the whole perturbation process it has to adopt the ground state. Site 1 and 4 are not involved at this point and stay in the state they were before the second hopping.

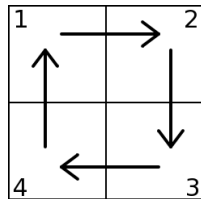


Figure 7.3: One possible path in fourth order.

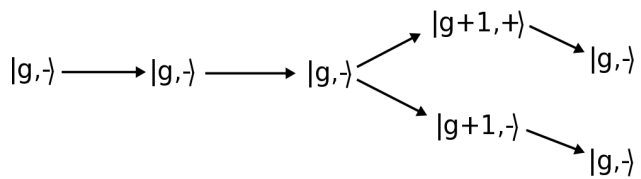
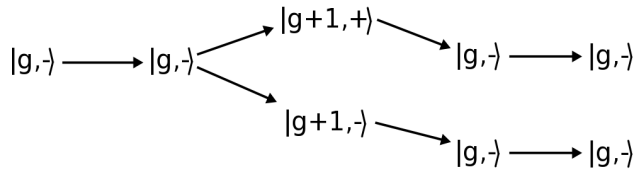
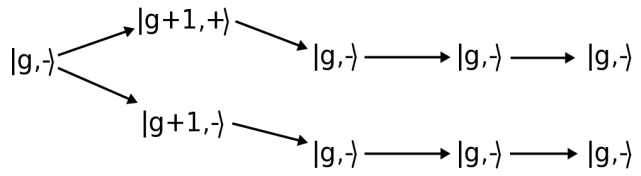
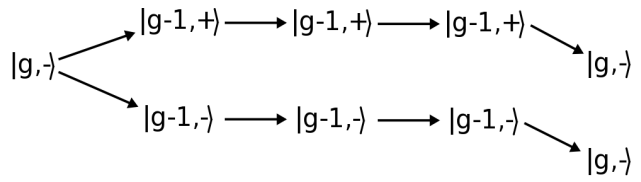


Figure 7.4: Spanning tree of the path in the left figure.

After the third hopping, site 3 is also already in the ground state, site 4 is either in the state  $|g + 1, -\rangle$  or  $|g + 1, +\rangle$  and site 1 is still in the states  $|g - 1, -\rangle$  or  $|g - 1, +\rangle$ .

Finally, at the end of the whole perturbation, i.e. after the fourth hopping, all sites have returned to the initial ground state (figure 7.8). The energy of this path is a sum of the energy of the  $2^4 = 16$  possible sequences.

Let's move on to the next path, sketched in figure 7.5:

Although it is a path belonging to the fourth order correction, only two sites are involved. The first two hoppings transport particles from site 1 to site 2, therefor site 1 is in one of the states  $|g - 1, \pm\rangle$  after the first tunneling and in  $|g - 2, \pm\rangle$  after the second tunneling. Site 2 is described by the states  $|g + 1, \pm\rangle$  and  $|g + 2, \pm\rangle$  respectively.

After the first two hopping processes the last two move the particles back from site 2 to site 1, resulting in the spanning tree shown in figure 7.6. There are therefor  $2^{2 \cdot 3} = 64$  different sequences to consider. One might therefor believe, that the number of sequences  $N_{seq}$  can be calculated like  $N_{seq} = 2^{2N_0 - N_S}$ , with  $N_0$  being the number of hopping processes and  $N_S$  the number of sites involved in the complete perturbation process.

But before drawing conclusions prematurely, we will take a look at the same diagram, but with a different chronological order as the previous one, shown in figure 7.7.

Here, a particle first hops from site 1 to site 2, but already jumps back in the next step, which is indicated in the Kato formula by  $S_0$ . This means, that after the second hopping process the ground state  $|g, -\rangle$  has to be restored in all sites. This results in a constriction of the spanning tree depicted in figure 7.8, as the projection to the '-' state is the only one allowed. Based on this configuration, the third hopping transports a particle again from site 1 to site 2 and the fourth hopping restores the ground state at every site again. We are therefor left with merely  $2^4 = 16$  possible sequences, which cannot be explained with the formula for  $N_{seq}$  given before. In order to get the right number of sequences, we have to include information about the number of nodal points, i.e. how many times the ground state is restored before the whole perturbation process is finished.

It should also be noted, that the number of different sequences has not to be the same for all sites. To show this, we will turn to the paths shown in figure 7.9 and figure 7.11. As you can see in the spanning tree of figure 7.10, the path of figure 7.9 does not restore the ground state until the very end of the complete perturbation process. But there are just two possible sequences for site 1 and site 3, the second site however has 8 possible sequences. This is because there is one tunneling from site 1 and one tunneling to site 1, while particles hop away from and to site 2 twice. The easiest thing to do is to count the arrows that point to a site and away from it. For site 1 we have one arrow pointing to it and one pointing away, the same applies for site 3.

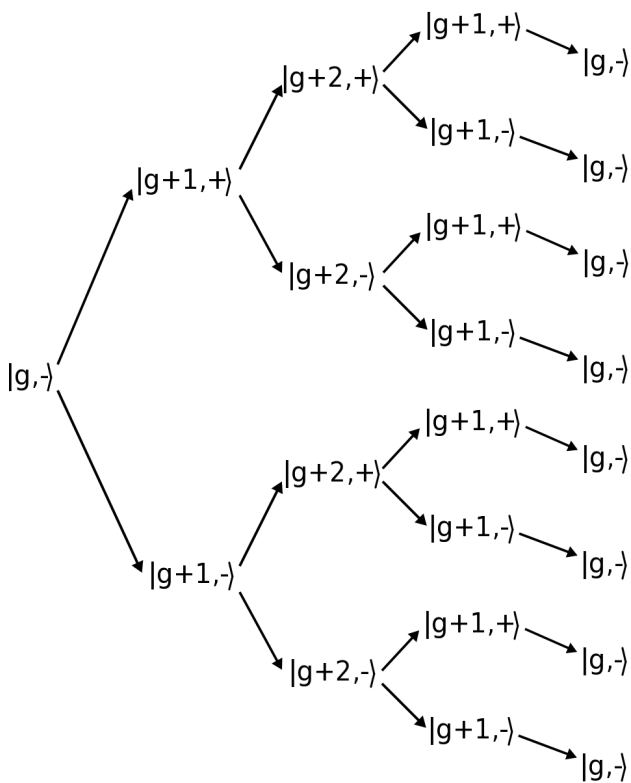
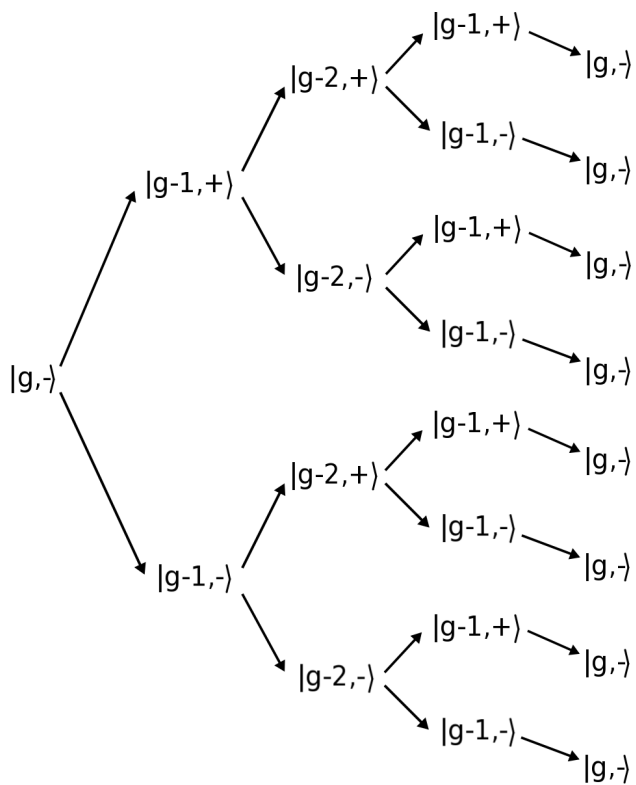
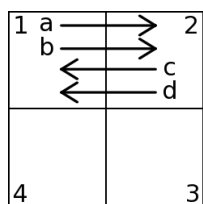


Figure 7.5: One possible path in fourth order.

Figure 7.6: Spanning tree of the path in the left figure.

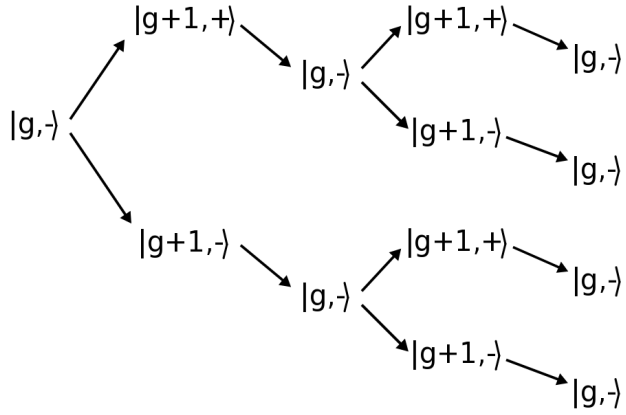
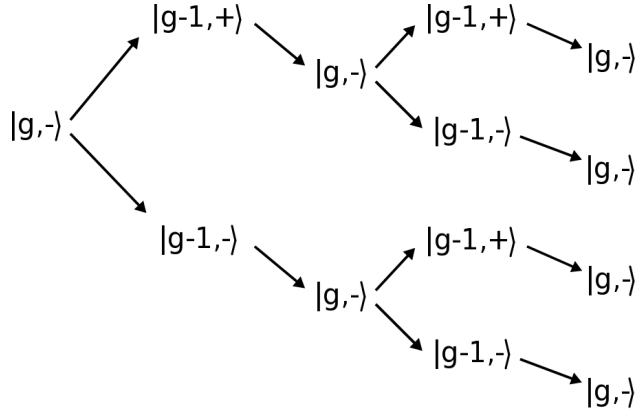
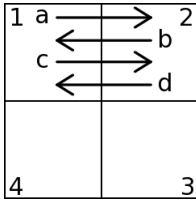


Figure 7.7: One possible path in fourth order.

Figure 7.8: Spanning tree of the path in the left figure.

But there are two arrows pointing to site 2 and 2 arrows pointing away. Figure 7.12 shows a similar situation. It is in fact the same diagram as the previous one, but the chronological order of the hopping processes has changed. In this case it results in the ground state being present after the second hopping process. The numbers of arrows pointing to and away from the sites hasn't changed of course, because these numbers only depend on the topology of the path and not the order of the tunneling processes.

Now we can finally compute the total numbers of sequences for a certain path. First of all we compute the number of sequences for a single site. To do that, we count the number of arrows pointing to a site  $N_{a,i}$ . For closed paths this number has to be of course the same as the number of arrows pointing away from a site, the numbers of bonds of site  $i$  is therefor  $N_{B,i} = 2N_{a,i}$ . Additionally we need to know the number of nodal points  $N_{n,i}$  for this site, i.e. how often the ground state is present at this site after the first and before the last hopping process took place. The number of sequences  $N_{seq,i}$  for site

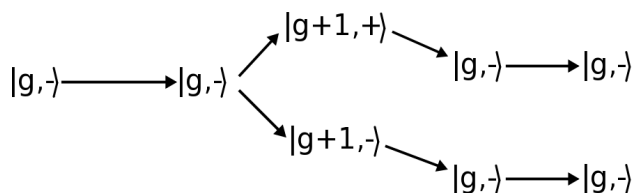
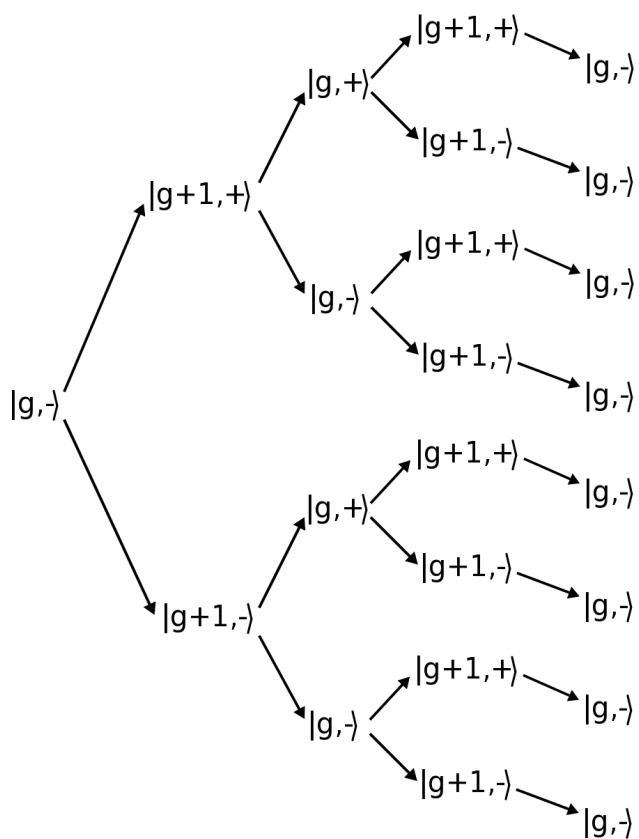
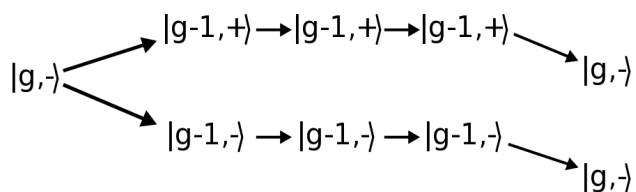
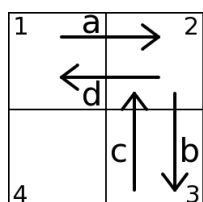


Figure 7.9: One possible path in fourth order.

Figure 7.10: Spanning tree of the path in the left figure.

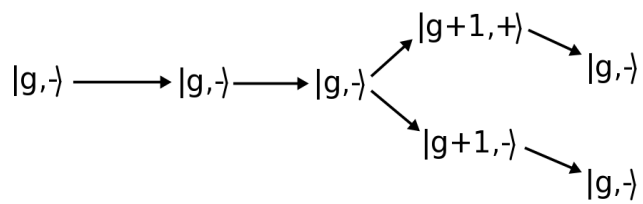
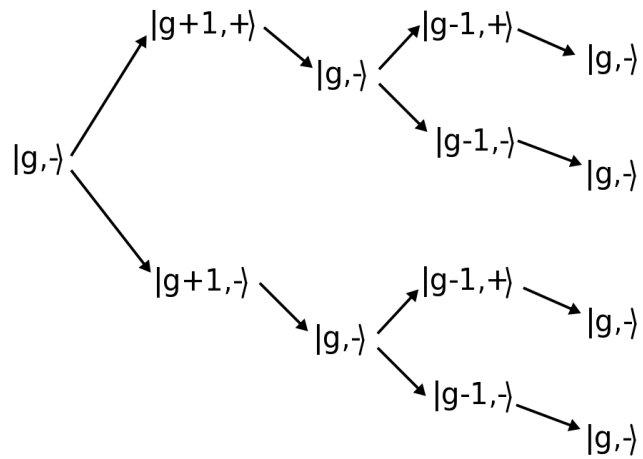
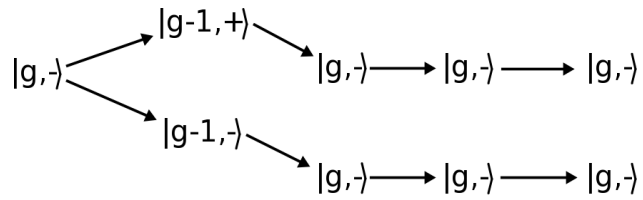
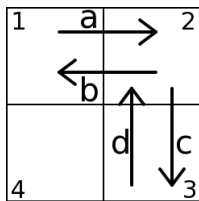


Figure 7.11: One possible path in fourth order.

Figure 7.12: Spanning tree of the path in the left figure.

$i$  is then

$$N_{seq,i} = 2^{N_{B,i} - (N_{n,i+1})} \quad (7.10)$$

and the total number of sequences  $N_S$  is therefor the product of these  $N_{S,i}$

$$N_{seq} = \prod_i N_{seq,i} . \quad (7.11)$$

The number of bonds for a specific site can be determined very easily with the aid of adjacency matrices. As we know, the  $i^{\text{th}}$  row tells us, to which sites particles hop originating from site  $i$ . The  $i^{\text{th}}$  column on the other hand contains the information from which sites arrows point to site  $i$ . The adjacency matrix for the path shown in figure 7.9 for example is

$$M = \begin{pmatrix} 0 & 1 & 0 \\ 1 & 0 & 1 \\ 0 & 1 & 0 \end{pmatrix} . \quad (7.12)$$

The rows tell us, that there is one hopping process from site 1 to site 2, one from site 2 to site 1, from site 2 to site 3 and from site 3 to site 2. Therefor, by summing over either the rows or the columns of the adjacency matrix of a specific path and multiplying this vector with 2, one gets the number of bonds of the sites involved. The vector  $v_B$  resulting when summing over all columns of the matrix stated by equation (7.12) reads  $v_B^T = (1, 2, 1)$ . Doubling it gives us  $(2, 4, 2)$  which means that there are two bonds at site 1, four bonds at site 2 and again two bonds at site 3.

With all that in mind we can reuse most of the algorithms we created for the energy calculations of the Bose-Hubbard model. The path creation and the reduction to topologically unique diagrams can be copied without any change. The algorithm for the energy calculation however has to be adopted at the point where all the permutations of a path are created. At this point we have to compute the adjacency matrix for every permutation and to determine the number of bonds for each site. With this information we can create the allowed  $\sigma$ -sequences for each permutation individually, calculate the energy for every sequence and sum them up. After all  $\sigma$ -sequences have been worked off we can proceed to the next permutation.

## Results

The additional summing over all  $\sigma$ -sequences of course slows down the complete energy computation compared to the calculations for the Bose-Hubbard model, but the computation times up to order 6 are still in the range of seconds, as table 7.1 shows. In figure 7.13 one can see the high quality of the data achieved. It shows the computed energy correction of a 2-dimensional system with filling factor  $g = 1$ , but for different orders of correction. The

Table 7.1: Computation times in seconds for the Jaynes-Cummings energy correction up to order  $\nu = 6$  for different filling factors  $g$  and dimensions  $d$ .

$\nu$	$g = 1$			$g = 2$		
	$d = 1$	$d = 2$	$d = 3$	$d = 1$	$d = 2$	$d = 3$
2	0, 25	0, 24	0, 35	0, 23	0, 22	0, 32
4	0, 37	0, 46	0, 53	0, 58	0, 72	0, 75
6	8, 30	27, 15	27, 71	58, 61	153, 06	156, 54

blue solid line contains only the second order energy correction  $\Delta E^{(2)}$ , the red line results by combining the second order and fourth order energy corrections, the green line shows the energy correction up to sixth order and the black dotted line up to the eighth order.

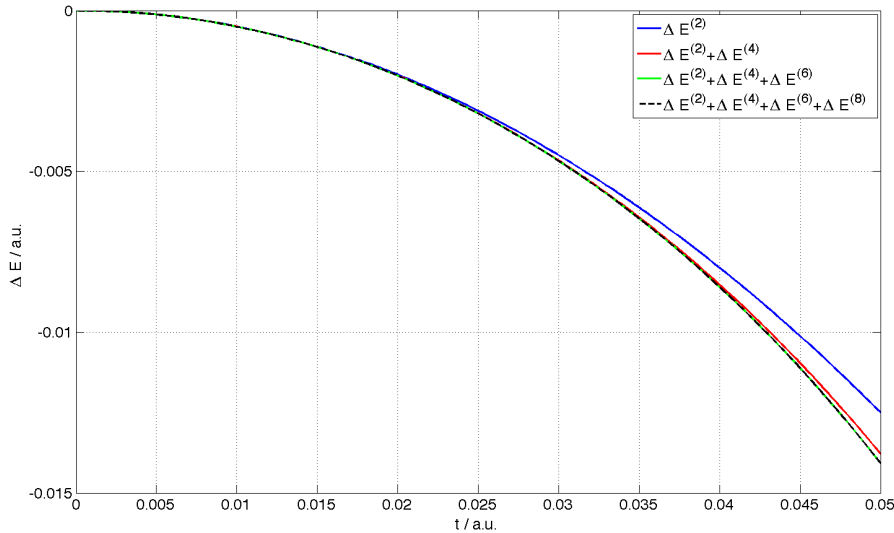


Figure 7.13: Comparing the fidelity of the computed energy corrections depending on the orders of correction included for a Jaynes-Cummings system with 2 dimensions and unity filling factor.

One can see, that while the blue line differs from the others quite significantly, the red, green and black dotted lines are very close to each other. In fact, the green and the black dotted line lie on top of each other perfectly at this scale, suggesting a very high fidelity already for the sixth order correction.

Additionally, figure 7.14 shows a comparison of data computed with the Variational Cluster Approach and with the Kato formalism. Two systems were simulated with the first having 2 dimensions and unity filling factor and the second also had 2 dimensions but filling factor  $g = 2$ .

The solid lines represent the results obtained with the Kato approach and

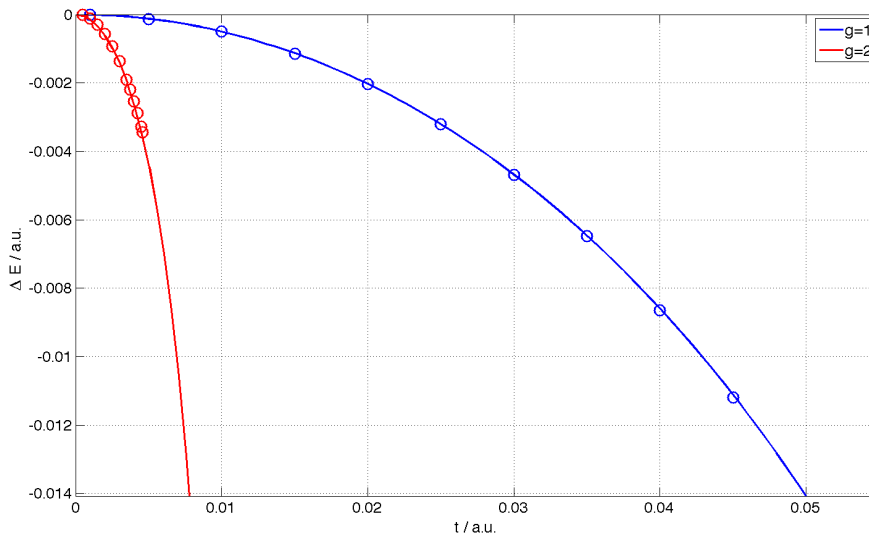


Figure 7.14: Comparison of calculations carried out with our Kato algorithm (solid line) and with VCA (circles) of two systems with dimension  $d = 2$  but different fillings factors  $g$ .

the circles those from VCA. As previously with the Bose-Hubbard system (see figure 4.13 in section 4.7) our results are in excellent agreement with VCA.

A comparison of the energy of different systems can be seen in figure 7.15. Simulated were systems with 1 (solid lines), 2 (dashed lines) and 3 (dotted lines) dimensions and with the filling factors  $g = 1$  (blue) and  $g = 2$  (blue). It is worthwhile to note, that the energies of systems with different  $g$  differs more than for systems with different dimensions  $d$ . With this we want to conclude this chapter and move on to the Mott insulator-superfluid phase transition calculations for the Jaynes-Cummings model.

## 7.2 The Mott Insulator-Superfluid Phase Transition

The same changes in the algorithm that have been discussed in the previous chapter have also to be taken into account if one wants to determine the Mott insulator-superfluid phase boundary for the Jaynes-Cummings model. But furthermore it is no longer necessarily true that the number of arrows pointing from a site is the same as the number of arrows pointing away from it. This little inconvenience is taken care of by just computing the sum along the rows and the sum along the columns of the adjacency matrix and adding these vectors point-wise, thereby getting the number of bonds per site.

With that in mind we can simply take the Mott insulator-superfluid algo-

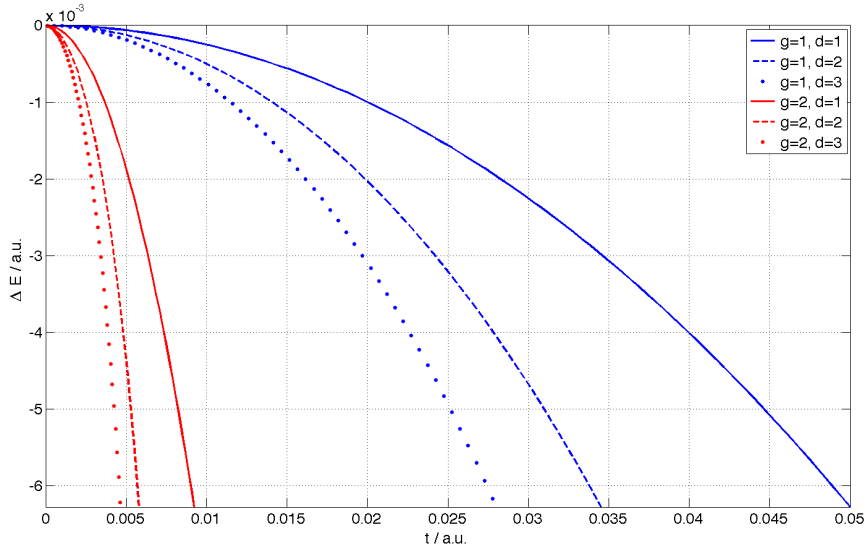


Figure 7.15: Comparison of the energies of systems with various filling factors  $g$  and dimensions  $d$  as a function of the hopping strength  $t$ .

rithm of the Bose-Hubbard model and apply the same changes to the  $c_2$  computation part as we applied to the energy correction algorithm in order to calculate the energy of the Jaynes-Cummings model instead of the Bose-Hubbard model.

## Results

All systems we are going to discuss have in common that we have chosen the parameter  $\Omega = 0$  and we have also set the detuning  $\Delta = 0$ . A more detailed look at different sets of parameters can be found in [42].

Figure 7.16 shows the Mott insulator-superfluid phase boundary for a 2-dimensional system with different filling factors  $g = 0$  (blue),  $g = 1$  (red) and  $g = 2$  (black).

The area that is confined by the blue line is the Mott insulator phase with a filling factor  $g = 0$ . Analogously, the red points limit the Mott insulator phase with  $g = 1$  and the black points the Mott insulator phase with  $g = 2$ . The same set of parameters we used in figure 7.16 have been used to determine the phase boundary for a 3-dimensional system (figure 7.17). In figure 7.18 one can see a comparison of these two systems with filling factors  $g = 0$  and  $g = 1$ . The system with 2 dimension is depicted by the blue graph and the 3-dimensional system by the red one.

As with the Bose-Hubbard system one can see that the lower the dimensionality of the system gets, the higher the values for the critical hopping parameter become. The 2-dimensional system has much higher  $t_c$  values for

## 7.2. MOTT INSULATOR-SUPERFLUID PHASE TRANSITION

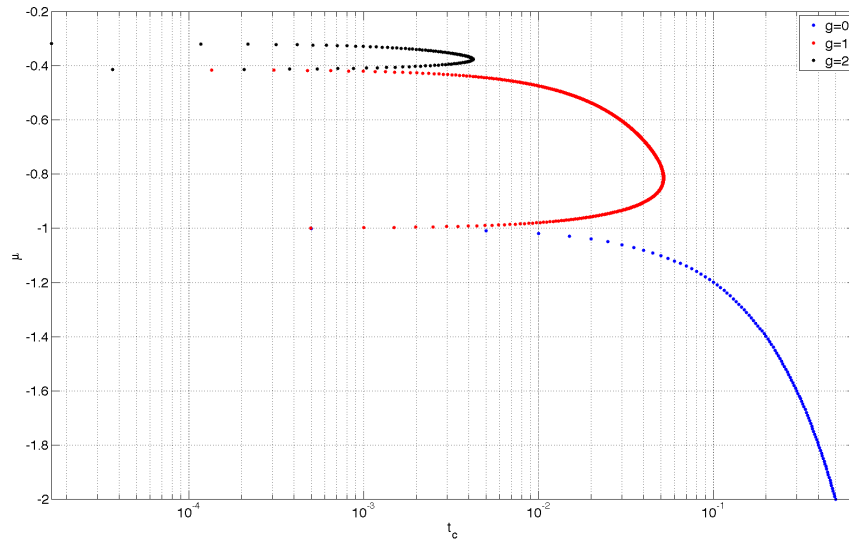


Figure 7.16: The Mott insulator-superfluid phase boundary for a system with 2 dimensions,  $\Delta = 0$ ,  $\Omega = 0$  and filling factors  $g = 0$  (blue), 1 (red) and 2 (black).

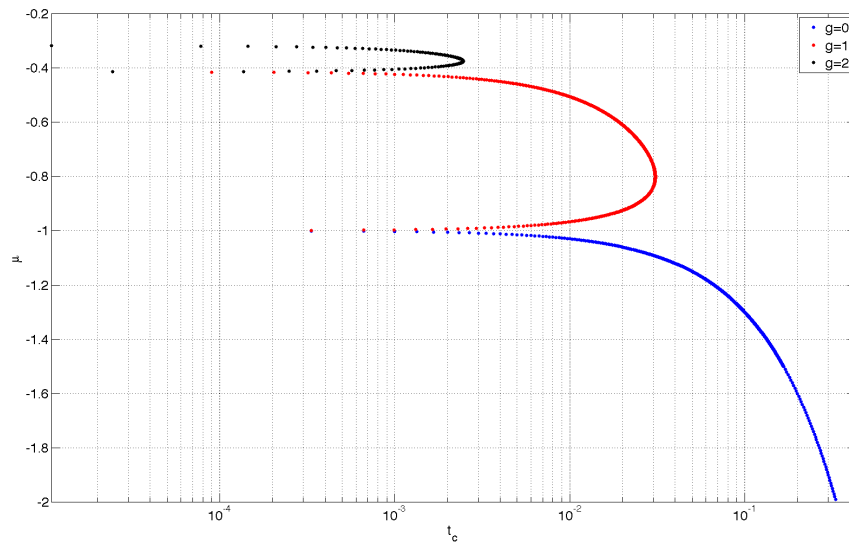


Figure 7.17: The Mott insulator-superfluid phase boundary for a system with 3 dimensions,  $\Delta = 0$ ,  $\Omega = 0$  and filling factors  $g = 0$  (blue), 1 (red) and 2 (black).

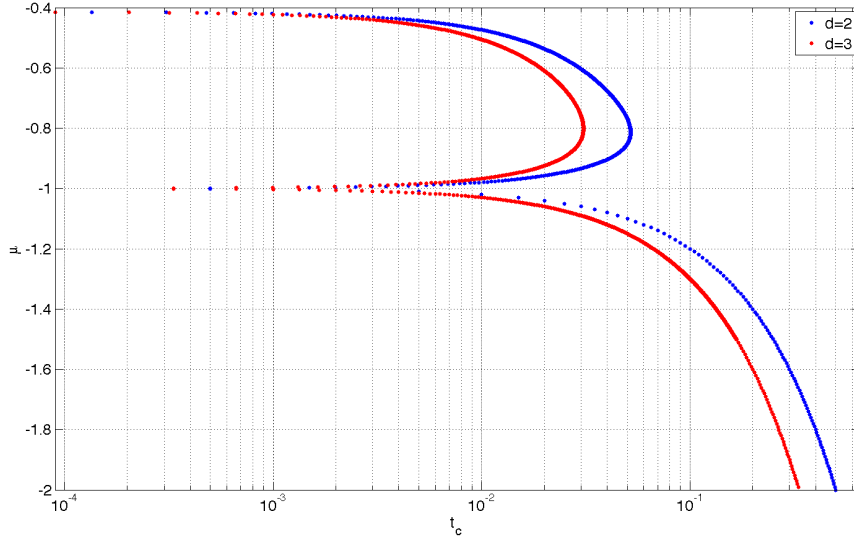


Figure 7.18: Comparison of the phase boundary for two systems with different number of dimensions ( $d = 2$  and  $d = 3$ ,  $\Delta = 0$ ,  $\Omega = 0$ ).

any chemical potential than the 3-dimensional one (mind the logarithmic scale).

It is also interesting to note that the point, where  $t_c = 0$  is independent of the dimension of the system and can be calculated easily with  $\sqrt{g} - \sqrt{g+1}$  (from [42]). If we want to know for example where the  $g = 1$  regime ends and where the  $g = 2$  regime begins, we simply compute  $\sqrt{1} - \sqrt{2}$ , which gives us  $\mu = -0,4142$ . As one can see, this coincides perfectly with our calculations. As was the case with the the Bose-Hubbard model, our current algorithms do not allow to determine the Mott insulator-superfluid phase boundary for larger critical hopping parameters  $t_c$  for a 1-dimensional system as the same reasoning applies as in section 5.3.2.

This is shown in figure 7.19, which contains a comparison of our data with results obtained with DMRG by [38].

Once again our results match those from DMRG quite good for low values of  $t_c$ , but as soon as the hopping parameter gets bigger than 0.12 our computations do no longer describe the system correctly. Additionally our results for low  $\mu$  do not follow the DMRG data as closely as they did for the Bose-Hubbard model, because we didn't include corrections of the order 7 or higher, as the computational time would have been too long.

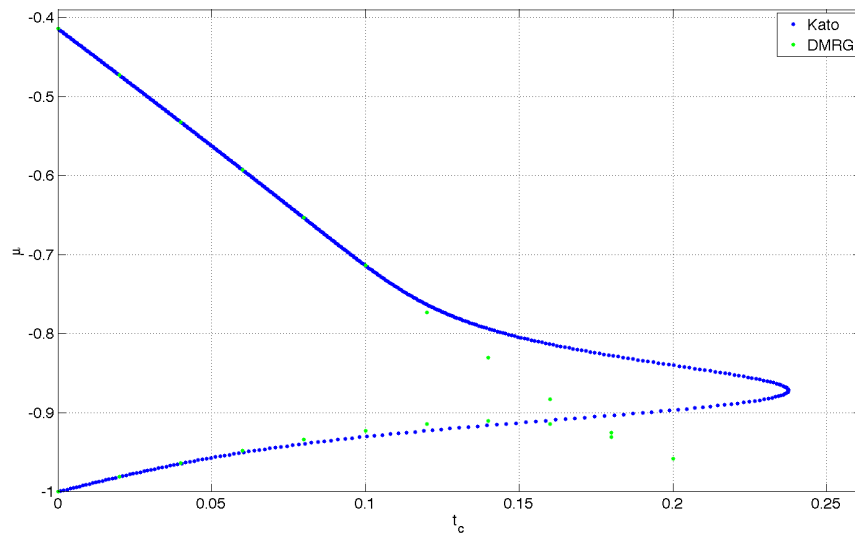


Figure 7.19: A comparison of our results with those obtained with DMRG [38]. A system was considered with 1 dimension,  $\Delta = 0$ ,  $\Omega = 0$  and filling factor  $g = 1$ .

# Chapter 8

## Conclusions and Outlook

In this work we have demonstrated how the Kato formalism, a very special approach to the perturbation theory in quantum mechanics, can be used to study two bosonic systems, described by the Bose-Hubbard and the Jaynes-Cummings model respectively. This formalism has the great advantage that any order of correction can be calculated explicitly without having to compute all the previous ones. We also introduced a diagrammatic representation of the tunneling processes that occur in such systems.

With that we were able to construct algorithms that are capable of computing the energy of these quantum systems very efficiently and in very short computational times compared to other numerical methods. Another advantage of this approach is that it also allows us to simulate other regular lattices, for example triangular or hexagonal ones, without much effort. One would only have to alter the path creation algorithms accordingly, the computation of the Kato sequences and the energy correction stays the same for every lattice.

We went on to explain how the Kato formalism can be implemented to determine the Mott insulator-superfluid phase boundary by introducing the method of effective potential. This allowed us to compute the phase boundary very accurately for systems with two or more dimensions with little computational effort.

Computing the phase boundary for a one-dimensional system is afflicted with some problems however, especially for high tunneling strengths  $t$ . We therefore suggested another approach, which still employs the Kato formalism, but works by calculating the correlation function  $\xi$  instead of the expansion coefficients  $c_2$  of the free energy. This is currently a main point of interest in our research.

Of course the Kato formalism can also be employed to calculate other properties of a quantum systems apart from the energy and the Mott insulator-superfluid phase boundary. A very interesting property would be for example the already mentioned atom-atom correlation function  $\xi$ , but the density-density correlation function or the occupation number fluctuations are also highly interesting parameters of a system worth to investigate (see for exam-

---

ple [18]).

In the course of this work we also introduced disorder to the Bose-Hubbard system and explained what one has to pay attention to in order to calculate the energy and the Mott insulator-superfluid phase transition correctly. It would now be also very interesting to investigate the differences between various disorder distributions.

Additionally it might also be worthwhile to consider a Bose-Hubbard system with nearest-neighbor interaction as suggested by [22] or other, different quantum systems.

# Acknowledgements

First of all, I want to thank my supervisor Prof. Wolfgang von der Linden, who gave me the opportunity to work on this very interesting subject. He was also very patient with me and all my questions and always found the time to discuss how to overcome the obstacles and problems I encountered during my work.

I also want to thank Michael Knap for the many fruitful discussions we had that helped me a lot to make progress with this topic and also for inducting me into the characteristics of scientific work. I also want to thank him for allowing me to use his nice schematic drawings explaining the Jaynes-Cummings model.

I'm also very grateful to Hannes Brandner, who agreed to proof-read this thesis.

On that note a big thanks also has to go to Andreas Hirczy and Prof. Winfried Kernbichler who helped me with the numerical implementation and the oddities of the soft- and hardware we used in order to obtain our results.

Last but not least I want to thank my family, especially my parents and my sister for their support, encouragement and understanding in this stressful time.



# Bibliography

- [1] Steven R. White. Density matrix formulation for quantum renormalization groups. *Physical Review Letters*, 69(19):2863, November 1992.
- [2] Adrian E. Feiguin and Steven R. White. Time-step targeting methods for real-time dynamics using the density matrix renormalization group. *Physical Review B*, 72(2):020404, July 2005.
- [3] Nicholas Metropolis and S. Ulam. The monte carlo method. *Journal of the American Statistical Association*, 44(247):335–341, September 1949. ArticleType: research-article / Full publication date: Sep., 1949 / Copyright ©1949 American Statistical Association.
- [4] Cyrus J. Umrigar. *Quantum Monte Carlo Methods in Physics and Chemistry (NATO Science Series C)*. Springer, 1 edition, December 1998.
- [5] D. Sénéchal, D. Perez, and M. Pioro-Ladrière. Spectral weight of the hubbard model through cluster perturbation theory. *Physical Review Letters*, 84(3):522, January 2000.
- [6] Claudius Gros and Roser Valentí. Cluster expansion for the self-energy: A simple many-body method for interpreting the photoemission spectra of correlated fermi systems. *Physical Review B*, 48(1):418, July 1993.
- [7] Zhaojun Bai, James Demmel, Jack Dongarra, Axel Ruhe, and Henk van der Vorst. *Templates for the Solution of Algebraic Eigenvalue Problems: A Practical Guide*. Society for Industrial Mathematics, 1 edition, January 1987.
- [8] Danny C. Sorensen. Numerical methods for large eigenvalue problems. *Acta Numerica*, 11, 2003.
- [9] Zhaojun Bai and Roland W. Freund. A symmetric band lanczos process based on coupled recurrences and some applications. *SIAM Journal on Scientific Computing*, 23(2):542, 2001.
- [10] M. Potthoff. Self-energy-functional approach to systems of correlated electrons. *The European Physical Journal B*, 32(4):8, 2003.

- [11] M. Potthoff, M. Aichhorn, and C. Dahnken. Variational cluster approach to correlated electron systems in low dimensions. *Physical Review Letters*, 91(20):206402, November 2003.
- [12] W Koller and N Dupuis. Variational cluster perturbation theory for Bose-Hubbard models. *Journal of Physics: Condensed Matter*, 18(41):9525–9540, 2006.
- [13] Michael Knap. Quantum many body properties of strongly correlated lattice bosons and polaritons. 2009.
- [14] Tosio Kato. On the convergence of the perturbation method. i. *Progress of Theoretical Physics*, 4(4):514–523, 1950.
- [15] Martin P. Gelfand, Rajiv R. P. Singh, and David A. Huse. Perturbation expansions for quantum many-body systems. *Journal of Statistical Physics*, 59(5-6):1093–1142, 1990.
- [16] Immanuel Bloch and Wilhelm Zwerger. Many-body physics with ultracold gases. *Reviews of Modern Physics*, 80(3):885–964, 2008.
- [17] Albert Messiah. *Quantum Mechanics*. Dover Publications, July 1999.
- [18] Niklas Teichmann, Dennis Hinrichs, Martin Holthaus, and André Eckardt. Process-chain approach to the Bose-Hubbard model: Ground-state properties and phase diagram. *Physical Review B*, 79(22):224515, June 2009.
- [19] André Eckardt. Process-chain approach to high-order perturbation calculus for quantum lattice models. *Physical Review B*, 79(19):195131, May 2009.
- [20] Matthew P. A. Fisher, Peter B. Weichman, G. Grinstein, and Daniel S. Fisher. Boson localization and the superfluid-insulator transition. *Physical Review B*, 40(1):546, July 1989.
- [21] Matthew P. A. Fisher, Peter B. Weichman, G. Grinstein, and Daniel S. Fisher. Boson localization and the superfluid-insulator transition. *Physical Review B*, 40(1):546, July 1989.
- [22] T. D. Kühner and H. Monien. Phases of the one-dimensional Bose-Hubbard model. *Physical Review B*, 58(22):R14741, December 1998.
- [23] S. Rapsch, U. Schollwöck, and W. Zwerger. Density matrix renormalization group for disordered bosons in one dimension. *Europhysics Letters*, 46(5):6, 1999.
- [24] C. Kollath, U. Schollwöck, J. von Delft, and W. Zwerger. Spatial correlations of trapped one-dimensional bosons in an optical lattice. *Physical Review A*, 69(3):031601, March 2004.

- [25] Corinna Kollath, Andreas M. Läuchli, and Ehud Altman. Quench dynamics and nonequilibrium phase diagram of the Bose-Hubbard model. *Physical Review Letters*, 98(18):180601, April 2007.
- [26] Ghassan George Batrouni and Richard T. Scalettar. World-line quantum monte carlo algorithm for a one-dimensional bose model. *Physical Review B*, 46(14):9051, October 1992.
- [27] Stefan Wessel, Fabien Alet, Matthias Troyer, and G. George Batrouni. Quantum monte carlo simulations of confined bosonic atoms in optical lattices. *Physical Review A*, 70(5):053615, November 2004.
- [28] B. Capogrosso-Sansone, N. V. Prokof'ev, and B. V. Svistunov. Phase diagram and thermodynamics of the three-dimensional Bose-Hubbard model. *Physical Review B*, 75(13):134302, April 2007.
- [29] Barbara Capogrosso-Sansone, Scedilebnem Günescedil Söyler, Nikolay Prokof'ev, and Boris Svistunov. Monte carlo study of the two-dimensional Bose-Hubbard model. *Physical Review A*, 77(1):015602, January 2008.
- [30] J. K. Freericks and H. Monien. Strong-coupling expansions for the pure and disordered Bose-Hubbard model. *Physical Review B*, 53(5):2691, February 1996.
- [31] N. Elstner and H. Monien. Dynamics and thermodynamics of the Bose-Hubbard model. *Physical Review B*, 59(19):12184, May 1999.
- [32] Subir Sachdev. *Quantum Phase Transitions*. Cambridge University Press, April 2001.
- [33] J. W. Negele and Henri Orland. *Quantum Many-Particle Systems*. Perseus Books (Sd), January 1988.
- [34] F. E. A. dos Santos and A. Pelster. Quantum phase diagram of bosons in optical lattices. *Physical Review A*, 79(1):013614, January 2009.
- [35] E. T. Whittaker and G. N. Watson. *A Course of Modern Analysis*. Cambridge University Press, 4 edition, January 1927.
- [36] J. K. Freericks and H. Monien. Strong-coupling expansions for the pure and disordered Bose-Hubbard model. *Physical Review B*, 53(5):2691, February 1996.
- [37] J M Kosterlitz and D J Thouless. Ordering, metastability and phase transitions in two-dimensional systems. *Journal of Physics C: Solid State Physics*, 6(7):1181, 1973.

- [38] Till D. Kühner, Steven R. White, and H. Monien. One-dimensional Bose-Hubbard model with nearest-neighbor interaction. *Physical Review B*, 61(18):12474, May 2000.
- [39] E. T. Jaynes and F.W. Cummings. Comparison of quantum and semi-classical radiation theories with application to the beam maser. *Proceedings of the IEEE*, 51(1):89–109, January 1963.
- [40] Serge Haroche, Jean-Michel Raimond, and S. Haroche. *Exploring the Quantum: Atoms, Cavities, and Photons*. Oxford University Press, October 2006.
- [41] V. Hussin and L. M. Nieto. Ladder operators and coherent states for the Jaynes-Cummings model in the rotating-wave approximation. *Journal of Mathematical Physics*, 46(12):122102, 2005.
- [42] Jens Koch and Karyn Le Hur. Superfluid-Mott-insulator transition of light in the Jaynes-Cummings lattice. *Physical Review A*, 80(2), 2009.